Optimization and Comparative Analysis of a GC-FID Method using Nitrogen as Carrier gas: Investigating Dynamic Changes in Pilot-Scale Production of *Nannochloropsis*

Sofie Stenseth Stette

Department of Chemistry

University of Bergen

A thesis submitted for the degree of

Master of Science

October 20

Optimization and Comparative Analysis of a GC-FID Method using Nitrogen as Carrier gas: Investigating Dynamic Changes in Pilot-Scale Production of *Nannochloropsis*

Sofie Stenseth Stette

Department of Chemistry

University of Bergen

Supervisor

Prof. Svein Are Mjøs, PhD

Department of chemistry, University of Bergen

A thesis submitted for the degree of

Master of Science

October 2023

Acknowledgements

The work presented in this thesis was performed at the Department of Chemistry, University of Bergen, from January 2023 to October 2023.

First and foremost, I would like to express my sincere gratitude to my supervisor, Professor Svein A. Mjøs, for his invaluable guidance and patience throughout the course of this project. His assistance in the realms of chemometrics and chemical analysis have been of great importance. I also want to thank Svein for teaching me the MATLAB based software, Chrombox C and O, by providing me with different tutorials and giving me clarifications whenever I needed. Svein, this year has been more challenging than I expected, but whenever I've been stressed, your calm being and relaxed tone have contributed to calming me down, so thank you. I am grateful for the opportunity to work with this project; it has fed my curiosity about chemometrics and microalgae. I will remember this year with gratitude.

I also extend my appreciation to Egil Nodland for his invaluable support in the processing of data within the pattern recognition system, SIRIUS. Thank you for patiently answering my questions and for refreshing my skills in SIRIUS. I would also like to express my gratitude to Olav M. Kvalheim. He may not know, but his dedication and passion for chemometrics inspired my chosen path in chemistry. Additionally, I would like to give thanks to Mathias Brevik for his valuable guidance in statistics and his contributions to my understanding of validation parameters. Additionally, special thanks goes to Pia Steinrücken at NORCE for providing crucial samples and assisting with my inquiries.

To my dear friends who have been pillars of support over the past five years – Julie, Hadi, Joar, Adrian, Pauline, Piraveen, Victoria and Nora – your friendship and camaraderie have been invaluable during my time in Bergen.

Finally, my heartfelt thanks go to my family, my mother, father, brother, aunt, uncle, grandparents and cousins. Your unwavering support and close-knit bond have been a source of strength. To my parents, your love and support have been instrumental. Thank you for always telling me that hard work pays off.

To each and every one of you, I convey my deepest appreciation and thanks.

Abstract

The decreased reliance on marine resources has led to reduced levels of long chain ω-3 fatty acids in farmed salmon feed, impacting the nutritional quality of the meat. Microalgae offer a sustainable alternative for enriching fish feed with essential marine nutrients. However, economic challenges hinder large-scale cultivation of microalgae. Therefore, optimizing the production is crucial. This requires a reliable, less expensive, and available analytical method for quantifying and identifying fatty acids in microalgae. Gas chromatography with flame ionization detector using helium as carrier gas is the most common choice. However, a helium shortage has led to increased prices and reduced availability. This has lead researchers to search for an alternative.

This thesis aims to optimize a gas chromatographic method with flame ionization detector using nitrogen as carrier gas and compare it with an original helium-based method, developed for fatty acid analysis in microalgae. Attention is also given to a pilot-scale experiment involving *Nannochloropsis* microalgae cultivation for fish feed production. This experiment aimed to investigate dynamic changes within the cultivation, providing a basis for optimizing production.

To optimize the method, response surface methodology and experimental design were employed. The experimental design was used to screen for optimal carrier gas velocity and temperature rate. The optimized method had a temperature rate of 1 °C/min and a carrier gas velocity of 12 cm/s. It provided a similar retention pattern (selectivity) and slightly higher efficiency compared with the original He method. However, this came at the cost of increased analysis time.

Comparative analysis was done by analysing samples with the optimized method and the original helium method. The comparative study included parameters such as linearity, bias, precision, accuracy and selectivity. The results showed that the method could accurately quantify most fatty acids in the studied concentration range. However there were systematic bias and significant variations between the methods.

The optimized method was used to analyse samples from the *Nannochloropsis* pilot-scale experiment for fish feed production. The results showed that the *Nannochloropsis* biomass had dynamic changes in eicosapentaenoic acid (EPA) and polyunsaturated fatty acid content,

positively correlated with the optical density of the culture. Additionally, significant changes in the fatty acid profile were established during cultivation where the fatty acid profile moved towards being more polyunsaturated before harvesting. Variations between reactors were investigated, revealing dissimilarities in the production of EPA over time, even for reactors possessing the same volume. Further investigation is needed to determine the cause.

The optimized method proved to give reliable results in quantifying fatty acids in microalgae, suggesting nitrogen as carrier gas as a reliable alternative to helium. However, as an alternative to the original helium method it should be investigated further due to significant differences in variation, accuracy and bias. Although some further work may be necessary, the work performed in this thesis demonstrated that the optimized method has great potential for accurate and precise quantitative analysis of fatty acids in the microalgae *Nannochloropsis*.

Sammendrag

Redusert tilgang til pelagiske marine ressurser har ført til lavere nivåer av omega-3 fettsyrer i fôret til oppdrettslaks, noe som påvirker ernæringskvaliteten til kjøttet. Mikroalger har vist seg som en bærekraftig løsning for å øke nivåene av essensielle marine næringsstoffer i fiskefôr. Imidlertid utfordres storskala dyrking av mikroalger av økonomiske faktorer. Derfor er optimalisering av produksjonen avgjørende. Dette krever en pålitelig, rimelig og tilgjengelig analytisk metode for kvantifisering og identifisering av fettsyrer i mikroalger. Det vanligste valget av metode er gasskromatografi med flammeioniseringsdetektor og helium som bæregass. Dessverre har helium mangel ført til økte prise og redusert tilgjengelighet. Dette har ført til at forskere leter etter alternativ.

Denne avhandlingen har som mål å optimalisere en gasskromatografisk metode med flammeioniseringsdetektor med nitrogen som bæregass og sammenligne den med en tradisjonell heliumbasert metode, utviklet for fettsyreanalyse i mikroalger. Det blir også viet oppmerksomhet til et piloteksperiment med mikroalger av typen *Nannokloropsis* for produksjon til fiskefôr for å undersøke dynamiske endringer innen dyrkning, og danne et grunnlag for produksjonsoptimalisering.

Analysemetoden ble optimalisert ved bruk av responsflate-metodikk og eksperimentelt design. Det eksperimentelle designet ble brukt til å undersøke optimal bæregasshastighet og temperaturstigningsrate. Den optimaliserte metoden hadde en temperaturstiginingsrate på 1°C/min og en bæregasshastighet på 12 cm/s. Den viste tilsvarende selektivitet og noe høyere effektivitet sammenlignet med den tradisjonelle helium metoden, men hadde lengre analyse tid. En sammenlignende analyse ble utført ved å analysere prøver med den optimaliserte metoden og den tradisjonelle helium metoden. Den sammenlignende studien inkluderte parametere som linearitet, bias, presisjon, nøyaktighet og selektivitet. Resultatene viste gode kvantifiseringsegenskaper for de fleste fettsyrene i det undersøkte konsentrasjonsområdet, men med systematisk bias og betydelige variasjoner mellom metodene.

Den optimaliserte metoden ble brukt til å analysere prøver fra piloteksperimentet med *Nannokloripsis* for produksjon av fiskefôr. Resultatene viste dynamiske endringer i EPA og polyumettet fettsyre innhold i løpet av dyrkingen, positivt korrelert med optisk tetthet i kulturene. I tillegg ble det etablert betydelige endringer i fettsyreprofilen under dyrking, der fettsyreprofilen beveget seg mot økt polyumettet fettsyreinnhold før høsting. Variasjoner

mellom reaktorene ble undersøkt, og avslørte ulikheter i EPA-produksjon over tid, selv for reaktorer med samme volum. Dette burde undersøkes videre for å fastslå årsaken.

Den optimaliserte metoden viste seg å gi pålitelige resultater ved kvantifisering av fettsyrer i mikroalger, og antyder at nitrogen som bæregass er et pålitelig alternativ til helium. Imidlertid bør dette alternativet undersøkes nærmere på grunn av betydelig forskjeller i variasjon, nøyaktighet og bias. Selv om noe ytterligere arbeid kan være nødvendig, viste arbeidet utført i denne avhandlingen at den optimaliserte metoden har godt potensial for presise og nøyaktige resultater ved identifisering og kvantifisering av fettsyrer i mikroalgen *Nannokloropsis*.

Table of Contents

List of Tables

Appendix A.

Appendix B.

Appendix C.

List of Figures

2 Theory

4 Results and discussion

Abbreviations

FAME	Fatty acid methyl ester
DoE	Design of experiments
SN	Separation number
ECL	Equivalent chain lengths
GC	Gas Chromatography
FID	Flame ionization detector
TPGC	Temperature programmed gas chromatography
PPC	Peaks per carbon
IP	Intermediate precision
R	Repeatability
IR	Injection repeatability
RSD	Relative Standard Deviation
STD	Standard Deviation
I	Kovats Index
RSM	Response Surface Methodology
PUFA	Poly unsaturated fatty acid
MUFA	Monounsaturated fatty acid
MS	Mass spectrometry
FA	Fatty Acid
EPA	Eicosapentaenoic acid
TAG	Triacyl glycerides
PBR	Photo Bioreactor

DHA	Docosahexaenoic acid
ALA	Alfa linoleic acid
LA	Linoleic acid
ACP	Acyl carrier protein
TE	Thioesterase
PPTase	Phosphopanthetheinyl transferase
AA	Arachidonic acid
FAS	Fatty acid synthetase
N	Theoretical plate number
HETP (H)	Height Equivalent to theoretical plate
α	Selectivity
RI	Retention Index
HPLC	High Performance Liquid Chromatography
PCA	Principal component analysis
DW	Dry Weight
PC1	Principal component 1
PC2	Principal component 2
NAM	National Algae pilot Mongstad
CS	Culture start
BD	Before dilution and harvest
AD	After dilution and harvest

Symbols

ω	Omega
β	Beta
α	Alfa
γ	Gamma
Δ	Delta
k	Retention factor
t_r	Retention time
t_m	Hold-up time
w_b	Width at baseline
R_s	Resolution
α	Selectivity, ratio of retention factors
w_h	Width at half height
A	Multiple paths
B	Longitudinal diffusion
C	Mass transfer
u	Mobile phase velocity
u_{opt}	Optimal mobile phase velocity
L	Column length
d_c	Column diameter
d_f	Film thickness
i	Interacting effect

$\hat{y}$	Predicted ELC values
α_g	Type I error rate (probability of a false significance) for the multiple tests
α	Same rate for each individual test
q	Number of tests

1 Introduction

1.1 Background

In recent years, the global landscape of seafood production has undergone a significant transformation. The traditional reliance on pelagic fisheries to meet the increasing demand for seafood has paved the way for the rapid expansion of aquaculture. Among various farmed species, salmon has emerged as the top seafood product consumers prefer. Traditionally, salmon diets were enriched with marine sources, primarily derived from pelagic fish, rich in long-chain polyunsaturated fatty acids (LC-PUFAs), notably omega-3 (n-3) LC-PUFAs. These essential nutrients do not only contribute to the health and vitality of the salmon, but also enhance the nutritional value of the final product for human consumption (1).

However, a concerning decrease in fishery resources has emerged in the recent years. This has prompted a fundamental shift in the composition of farmed salmon diets. The modern salmon diet now relies heavily on plant-based ingredients, constituting up to 70% of the feed composition. While this shift has been necessary to address the resource constraints of marine fisheries, it has had significant repercussions. The decreased reliance on marine resources has led to a reduction in the levels of n-3 LC-PUFAs in farmed salmon meat, ultimately impacting its nutritional quality (1).

In response to these challenges, the spotlight has turned to the microalgae, a group of photosynthetic organisms with a long history in aquaculture and human food production. Microalgae, including the species *Nannochloropsis*, have been harnessed as a valuable food source for aquatic organisms and humans for the past three decades. What distinguishes microalgae and elevates their significance in modern aquaculture is their remarkable ability to produce a range of valuable products, such as PUFAs (2).

The appeal of microalgae doesn't only lie in their ability to synthesize essential nutrients, but also their simplicity and the sustainability of their cultivation (2), utilizing inorganic compounds such as CO_2, N, S, P, and light, converting captured solar energy into biomass through photosynthesis (3). As a natural additive, microalgae offer a promising solution to the challenges faced by the aquaculture industry. Algae oils, in particular, have gained attention as a rich source of essential LC-PUFAs, such as eicosapentaenoic acid (EPA) and docosahexaenoic acid (DHA). These oils have found their way into the diets of Atlantic Salmon, contributing to increasing the marine content of their diet, and thereby their nutritional profiles (1).

As the aquaculture industry continues to expand to meet the rising global demand for seafood, there is an urgent need for high-quality, sustainable ingredients in fish feed. The potential of microalgae, as natural sources of essential nutrients, makes them a compelling choice (2).

It is essential to acknowledge that the integration of microalgae as an ingredient in fish feed into aquaculture is not without challenges. One significant challenge lies in techno-economic factors. Several key barriers must be addressed to unlock the full potential of microalgae as a viable feed ingredient in aquaculture. These barriers include the high production costs associated with microalgal biomass, the risk of contamination in algal cultivation systems, and the fluctuations in the biochemical composition of microalgae, all of which continue to present hurdles for successful integration. Microalgae cultivation often demands specific and resource-intensive conditions, including precise control of environmental factors and energy-intensive processes for harvesting and dewatering the microalgal biomass. These factors can lead to increased production expenses, potentially impeding the cost efficiency of microalgae-based feeds (4).

To overcome challenges related to large-scale production of microalgae, NORCE has built a pilot-scale facility for biomass production of microalgae, called the National AlgaePilot Mongstad (NAM). The pilot-scale production in this facility is investigated to provide a deeper understanding of the dynamic changes of the fatty acid profiles during large scale cultivation of the microalgae, *Nannochloropsis*, in closed tubular photo bioreactors. More specifically, the LC-PUFA, EPA, is investigated more closely due to its importance in fish feed. This knowledge can contribute to the development of cost-effective and environmentally sustainable microalgae biomass production.

Quantification and characterisation of microalgal fatty acids are crucial for determining the nutritional quality of the microalgal biomass during the production process. By characterizing the types and quantities of fatty acids present, researchers can adjust cultivation conditions to maximize the production of specific fatty acids, such as EPA. This optimization can improve production efficiency, reduce costs, and enhance the economic viability of the microalgae-based aquaculture feed production. Additionally, quantification and characterization provide a basis for quality control in the biomass production, monitoring fatty acid composition to maintain product consistency, and meet regulatory requirements for reliability and safety of the feed.

Microalgal fatty acids are typically quantified and characterized using gas chromatography-flame ionization detection (GC-FID) and GC-mass spectrometry (MS) detection systems (5).

GC achieves separations through a sequence of interactions between a mobile gas phase (also known as the carrier gas) and a stationary phase contained within a tube with small diameter, referred to as the column. This process starts with the injection of a narrow band of a mixture into the column. A detector then tracks the composition of the gas stream as it emerges from the column, carrying with it the components that have been separated. The signals generated by this monitoring serves as the primary input for data acquisition purposes (6).

As detector, FID is the most common option, partially due to its inexpensive instrumentation, but also because FID has been shown to be more reliable for quantitative analysis, producing lower standard deviations (5). In addition to detector types, different types of GC columns exist. The most common column in modern GC is the capillary column. A capillary column is in most cases capable of greater separation at a faster speed than packed columns, and can be used to quantify analytes with a wide range in volatilities (5).

In GC, there are three gases that are commonly used as a carrier gas: nitrogen, helium and hydrogen. When selecting the right carrier gas, the user has to consider different parameters such as; price, performance, speed, analytical compatibility, or just availability (7).

Helium is produced as a byproduct from the extraction of natural gas, but due to increasing demand of growing economies worldwide, not all market demands can be covered. Unfortunately, this leads to helium shortages and results in increasing prices (7).

Helium is widely used in technology, science, medicine, and manufacturing, including MRI scanners, semiconductors, fibre optics, nuclear applications, rocket purging, leak detection, and welding etc. Global helium demand is estimated at 6 billion cubic feet (Bcf) per year, with China importing 1 Bcf annually. Demand is predicted to rise to 8.5 Bcf by 2030. The helium market has unique dynamics, causing continuous increase in price. Over the past decade, helium demand remained steady due to limited supply, resulting in an 8% annual price growth, reaching US$375/mcf in late 2022—much higher than US natural gas prices. In 2019, medical and industrial sectors had the highest demand, shifting towards electronics in 2021. A helium supply crisis emerged after the 2019 closure of the US federal reserve. Most helium is a by-product of hydrocarbon production, with concentrations of 0.04% to 0.35%. Increasing production is challenging due to its low-grade nature, causing an inelastic supply (8).

Helium has conventionally been the preferred choice as a carrier gas for GC (9). However, over the past decade, researchers have been searching for alternatives. Helium is non-renewable, increasingly rare and consequently pretty expensive. In fact, estimates suggest that reserves could run out altogether in the coming years (9). As a result, nitrogen and hydrogen have become the more common choice as a carrier gas due to their availability. Nitrogen makes up

around 78% of the Earth`s atmosphere, making it the most abundant gas and is therefore readily available (9). When using nitrogen as carrier gas, the disadvantage is increased analysis time, however it should be kept in mind that this is a highly efficient gas. A big advantage of nitrogen is that it can be directly generated from air, this means that it is readily available and inexpensive (7).

Hydrogen is considered as the most optimal choice of carrier gas, combining high efficiency separations with short analysis time, and on top of that it can be produced by a generator. The biggest issue using hydrogen gas is the safety risk, a 4 % concentration in air can lead to an explosion (7).

In the context of the increasingly rare and expensive helium gas, a GC-FID method with nitrogen as carrier gas and temperature-programming is developed and optimized as a potential alternative for an already functioning method with helium as carrier gas for fatty acid analysis. The work of Svein A.Mjøs and Habtewold D.Waktola (10) and Milan Chhanganlal and Liv K. Skartland (11) have significantly contributed to the methodology of optimizing the chromatographic efficiency and selectivity of the method.

The optimized method is used to quantify and characterize the fatty acids in samples taken throughout the course of pilot-scale biomass production of *Nannochloropsis* at NAM. By optimizing the method, the generated results regarding fatty acids profiles are more likely to be accurate and trustworthy. When assessing changes in microalgal fatty acids in response to several factors, it is essential to ensure that the analytical results obtained using the optimized method, are comparable to those obtained using the common method with helium as carrier gas. A method comparison is therefore executed. This comparison is crucial for validating the consistency and reliability of the findings, ensuring that any observed variations are not method-related but, instead, reflect actual changes in the microalgal composition. If the optimized method proves to produce comparable results to the original helium method, this can have economic benefits in the long run due to its low price and availability. This is particularly relevant in large-scale biomass production of microalgae, where cost-effective analytical methods can contribute to overall cost savings.

1.2 Objectives

The aim of this thesis is to apply response surface methodology and experimental design to optimize a GC-FID method with nitrogen as carrier gas for the analysis of fatty acids in microalgae. Additional emphasis is put on the ability of the method to provide similar results compared to a method using helium as carrier gas when analysing fatty acids in the microalgae *Nannochloropsis.* The optimized method is also used to analyse samples provided from a pilot-scale experiment at NAM for biomass production of *Nannochlorpsis* to investigate dynamic changes in the photobioreactors during cultivation.

The main objectives of the thesis are:

1. Optimizing efficiency and selectivity of the GC-FID method using nitrogen as carrier gas according to predefined target values obtained from an original method using helium as carrier gas. The optimization focus on determining optimal conditions in terms of carrier gas velocity and temperature rate.

2. Evaluate the comparability of the results obtained using the optimized method and the method using helium as carrier gas. Specifically evaluating accuracy, bias, and precision (intermediate precision, repeatability and injection repeatability) of the optimized method using the helium method as reference.

3. Investigate dynamic changes of EPA content, optical density, fatty acid profiles, and reactor variations related to pilot-scale biomass production of *Nannochloropsis* at NAM.

2 Theory

2.1 Microalgae

Microalgae are a group of eukaryotic, unicellular and multicellular photosynthetic microorganisms thriving in both saline and freshwater ecosystems (3, 12, 13). These remarkable organisms possesses the ability to harness sunlight, water, and carbon dioxide, transforming these elemental components into valuable algal biomass (12). Microalgae are broadly classified into diatoms (Bacillariophyta), green algae (Chlorophyta) and red algae (Rhodophyta) (3). Although cyanobacteria, commonly referred to as blue-green algae, are procaryotic and not true algae, they share physiological and ecological characteristics with eukaryotic microalgae, and offers numerous biotechnological applications (13).

Microalgae can be autotrophic or heterotrophic. Autotrophic microalgae utilize inorganic compounds such as CO_2, N, S, $and\ P$ for growth, converting captured solar energy into biomass through photosynthesis. This process is essential for generating reducing power, adenosine triphosphate (ATP), O_2 and 3-phosphoglycerate, supporting their growth (3). In contrast, heterotrophic microalgae can grow in the absence of light, by utilizing organic carbon sources dissolved in culture media, bypassing atmospheric CO_2 fixation (14). In this study, the microalgae *Nannochloropsis* is cultivated autotrophically.

One distinctive feature of microalgae is their ability to synthesize storage lipids, primarily in the form of triacylglycerols (TAGs) (12), in addition to proteins and carbohydrate (3). Microalgae`s exceptional growth rate and productivity, often exceeding 60% of their dry biomass, distinguishes them from higher plants (12). This high productivity offers promising environmentally friendly alternatives to the current consumer products (3).

2.2 Nannochloropsis

Nannochloropsis holds particular industrial significance. Commercially, *Nannochloropsis* is used in production of animal feeds, health foods, biofuels and serves as live prey in the aquaculture for shrimp and fish juveniles etc. (15). *Nannochloropsis* species are unicellular microalgae known for their high photoautotrophic biomass productivity, natural ability to accumulate high lipid content, and successful industrial scale cultivation. These simple, non-flagellates, spherical to slightly ovoid cells, typically measuring 2-4 μm in size, exhibit high lipid productivity, and abundance of polyunsaturated fatty acids (PUFA), and robust growth. The availability of genome sequences and molecular-genetic tools for various *Nannochloropsis*

strains makes this genus an attractive cell platform for producing lipid molecules of industrial interest (15).

Nannochloropsis species offer great potential as sustainable sources of biofuels and nutritionally valuable oils, including long chain omega-3 fatty acids. However, to make these products economically viable and competitive, there is a need for biological enhancements in strains used, and the development of cost-effective and energy-efficient bioprocessing technologies encompassing cultivation, harvesting, and product preparation, especially in the high-volume, low-value context of biofuels (15).

Nannochloropsis is also utilized in aquafeeds for marine fish, molluscs and shrimps, thanks to its favourable fatty acid composition, including relatively high content of eicosapentaenoic acid (EPA), a highly unsaturated omega-3 fatty acid. Expanding beyond aquaculture, there is growing interest in incorporating *Nannochloropsis* PUFA-rich feed into other animal diets to enhance the nutritional value of farmed foods (15).

Moreover, *Nannochloropsis* holds promise for direct use in human diets. Extensive toxicology studies have confirmed the safety of both *Nannochloropsis* oil and whole algae cells as dietary supplements. These products provide EPA sources that mitigate concerns related to depleting fish stocks and potentially heavy metal contaminants in fish oils (15).

The development of *Nannochloropsis* as a biofuel feedstock has garnered substantial research attention. However, several key challenges remain to be addressed to make algal biofuel production cost-effective and competitive with conventional fuel sources. These challenges encompass the development of strains producing high quantities of TAGs with desired chain lengths and degrees of saturation, understanding the link between growth conditions and lipid productivity, establishing large-scale cultivation facilities, and refining oil extraction techniques (15).

2.3 Cultivation of microalgae

Microalgae have gained significant interest due to their potential as a sustainable source of food, feed, fuel, and other value-added products. Cultivation of microalgae can be performed at both laboratory and industrial scales, using different cultivation systems and culturing conditions (16, 17, 18, 19).

Laboratory scale production of microalgae is typically done using small-scale cultivation systems, such as test tubes, flasks, or small-scale photobioreactors. These systems provide a controlled environment for growing microalgae and can be used to evaluate different nutritional and environmental conditions. In contrast, industrial scale production of microalgae is typically

done using large-scale open ponds or closed photobioreactors. Open ponds are low-cost, low-maintenance systems that use natural sunlight and CO_2 sources, but they are more susceptible to contamination and variability in environmental conditions. Photobioreactors, on the other hand, provide a more controlled environment for growing microalgae, but they require high capital and operating costs (16, 17, 18, 19).

The nutritional mode of microalgal cultivation is a crucial factor that determines the productivity and quality of microalgal biomass. In photoautotrophic cultivation, microalgae use light as their energy source and inorganic carbon as their carbon source. Photoautotrophic cultivation is typically used in closed systems, such as photobioreactors, where environmental factors can be controlled to maximize productivity. In contrast, heterotrophic cultivation uses organic carbon sources, such as glucose or acetate, and organic nitrogen sources for growth. Heterotrophic cultivation is commonly used in large-scale open ponds or fermenters, where high cell density and growth rates can be achieved (16, 17, 18, 19).

Several parameters play a crucial role in regulating algal growth, including temperature, light intensity, CO_2 concentration, pH, and nutrient availability. These parameters can be optimized to maximize microalgal biomass productivity and quality. For example, temperature is a key factor that affects the growth rate of microalgae, with optimal temperatures ranging from 20-30 ℃ for most species. Light intensity and CO_2 concentration are also important factors that can be controlled in closed systems to maximize productivity (16, 17, 18, 19).

2.4 Photobioreactor

To achieve high productivity during mass cultivation of microalgae, it is essential to have high biomass concentrations of the culture. This requires a non-limiting supply of nutrients and CO_2. However, as the culture density increases, shading between cells occurs, reducing light penetration into the culture. When the temperature is maintained in the optimal range, light becomes the major limiting factor for growth. Culture mixing can help overcome this limitation by circulating the biomass between illuminated and dark zones. The frequency of intermittent illumination depends on the optical path of the cultivation system, cell density, and the extent of culture mixing. Several systems for large-scale microalgal cultivation have been established, including open pond systems and closed photobioreactors (PBRs). Enclosed PBRs offer better control of growth conditions and protection against contamination, with tubular and flat panel PBRs being the two major types (20).

Tubular PBRs, which consist of long transparent glass or plastic pipes where the culture circulates using pumps, are the most common reactor types. Tubular PBR is often arranged in

straight tubes, connected by U-bends to form a loop. These can be either vertically or horizontally oriented (20). To ensure high performance of the photobioreactor, tubing diameter, tube length, and mixing are factors that should be optimized for the specific microalgae being cultivated (21). Challenges when using tubular PBR is usually gradients of pH, oxygen and CO_2 along the tubes, and fouling. Another challenge is some degree of wall growth that will limit irradiance, making the cultivation less efficient. Additionally, large scale cultivation of microalgae requires large land and space (22).

Irradiance in enclosed PBRs can be natural sunlight, artificial light, or a combination of both. Temperature-control systems are crucial for maintaining cultures at tolerable or favourable temperatures but contribute significantly to production costs. Closed PBRs protect cultures from the environment, resulting in a higher quality of the microalgal biomass. Furthermore, the narrower optical path and culture mixing allow for improved light exploitation, leading to higher biomass concentrations and volumetric productivities. However, the high capital investment and energy costs during operation, as well as poor system scalability, are major limitations. The most optimal PBR design depends on the location, microalgal species, and the final product of interest. Ongoing improvements to classical designs and the proposal of new PBR concepts offer hope for maximizing productivity while minimizing operation costs (20).

2.5 Health benefits of PUFAs

Polyunsaturated fatty acids (PUFAs) are vital components of a healthy diet, sourced from various organisms, such as marine organisms. PUFAs play a crucial role in maintaining overall health by offering protection from several diseases, such as osteoarthritis, cancer, and autoimmune disorders (23).

Considered the most important fatty acids, are the omega-3 (ω-3) and omega-6 (ω -6) fatty acids, available in both terrestrial and marine environment. These PUFAs are known for their contribution to cellular fluidity and their role as building blocks for essential molecules within the body. Additionally, they have been shown to reduce the risk of heart disease by preventing blood clotting (23).

Growing interest surrounds the potential health benefits of omega-3 fatty acids, particularly regarding their effect on the immune system, mental health, and preventing conditions like Chron`s disease, ADHD, and anorexia. While conclusive evidence is still emerging, omega-3 fatty acids have demonstrated the most substantial benefits in relation to heart disease and rheumatoid arthritis (24).

Western societies often face an imbalance, characterized by low marine omega-3 intake, resulting in adverse health effects. Despite their significance, many individuals do not obtain an adequate intake of omega-3 fatty acids through their diet. Omega-3 fatty acids are essential fatty acids and must be obtained through the food we eat, or through supplements. The most common omega-3 fatty acids are α-linolenic acid (ALA), eicosapentaenoic acid (EPA) and docosahexaenoic acid (DHA) and can be found in both plant-based and marine sources (24).

2.6 Fatty acid structure and nomenclature

Fatty acids are organic molecules that consist of a carbon chain with a methyl group at one terminal end (designated as the omega or "ω" carbon) and a carboxyl group at the other end. The carbon atom immediately adjacent to the carboxyl group is referred to as the alpha (α) carbon, while the subsequent carbon atom is referred to as the beta (β) carbon. Additionally, the notation "n" may be utilized instead of the Greek letter "ω" to designate the location of the double bond closest to the methyl end. The systematic nomenclature for fatty acids may also indicate the position of the double bonds relative to the carboxyl group, using the symbol "Δ". The structures of several types of naturally occurring fatty acids are depicted in *Figure 2. 1* (26).

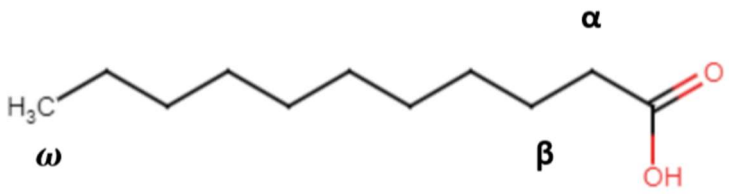

Figure 2. 1 Nomenclature for fatty acids. The methyl group at the terminal end is denoted by "ω", the carbon atom adjacent to the carboxyl group is denoted by "α", and the subsequent carbon atom is denoted by "β". Figure developed in chem-space.com.

Fatty acids can be either saturated or unsaturated. Saturated fatty acids are characterized by the presence of a full complement of hydrogen atoms along the carbon chain. This saturation results in a linear hydrocarbon structure, typically containing an even number of carbon atoms. Within the class of saturated fatty acids, those that are most prevalent are those containing a carbon chain length ranging from 12 to 22 carbon atoms (26).

Unsaturated fatty acids, on the other hand, can be distinguished into monounsaturated or polyunsaturated fatty acids. Monounsaturated fatty acids (MUFAs) possess a single carbon-

carbon double bond, which can be located at varying positions along the carbon chain. The most prevalent form of MUFAs contains a chain length ranging from 16 to 22 carbon atoms, with the double bond having a cis-configuration. Cis-configuration is characterized by hydrogen atoms located on either side of the double bond, aligned in the same direction (*Figure 2. 2*). Trans-configuration is characterized by hydrogen atoms located on opposite side of the double bond. Trans-isomers can be formed through industrial hydrogenation processes, heating of unsaturated oils and in the gastrointestinal tracts of ruminants (26).

The presence of a double bond restricts the mobility of the carbon chain, and the kink in the molecular shape caused by the cis-configuration results in reduced thermal stability compared to its trans-configuration. This is why cis-configurations have lower melting points compared to both trans-isomers and their saturated counterparts (26).

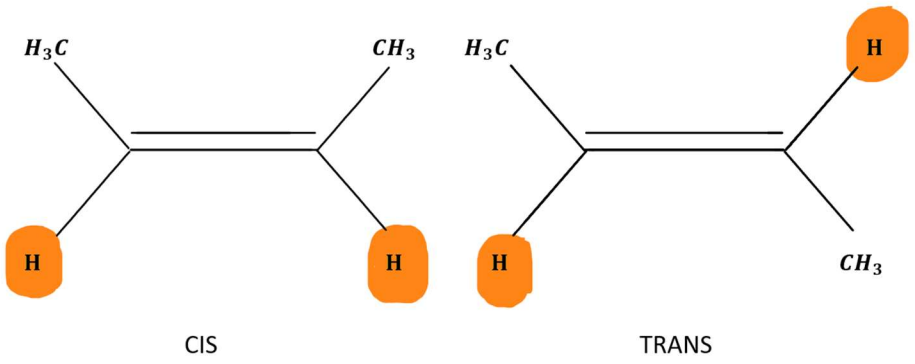

Figure 2. 2 Cis and trans configuration. Cis-configuration, the hydrogen atoms are located at the same side of the double bond (left). Trans-configuration, the hydrogen atoms are located on opposite sides of the double bond (right).

Polyunsaturated fatty acids (PUFAs) contain multiple double bonds along their carbon chain. The first double bond in PUFAs can occur between the third and fourth carbon atom from the omega carbon (ω -3 fatty acids), or between the sixth and seventh carbon atom (ω -6 fatty acids). The double bonds in PUFAs are separated by a methylene group. The ω -3 and ω -6 fatty acids cannot be interconverted and are both considered essential nutrients. The metabolic processes in the body further modify PUFAs by adding carbon atoms and through desaturation (removal of hydrogen). Mammals possesses desaturases that are only capable of removing hydrogens from carbon atoms located between an existing double bond and the carboxyl group. LC-PUFAs are therefore essential for higher organisms and have to be consumed through the diet (26).

2.7 Fatty acid biosynthesis

The biosynthesis of fatty acids in microalgae occurs in the chloroplast and endoplasmic reticulum (ER). The chloroplast is a cellular organelle where photosynthesis happen. Microalgae make their own fatty acids via a complex process using a type II fatty acid synthase (FAS). This modular, multi-domain enzymatic complex is comprised of separate proteins that each encode a specific activity. The process begins with a post-translational modification of an acyl carrier protein (ACP) catalysed by a phosphopantetheinyl transferase (PPTase). This modification activates the ACP, which then begins to attach fatty acids via thioester linkage. The ACP is loaded with an acyl starter unit, and then fatty acid synthesis occurs by sequential action of various enzymes, each resulting in a net addition of two carbons to the growing chain. During chain elongation, the ACP protects the growing fatty acid by burying it in its hydrophobic core. As the mature fatty acid is assembled on the ACP, a thioesterase (TE) receives the acyl chain, priming it for hydrolysis. In algal fatty acid biosynthesis, the TE must functionally interact with ACP to mediate the hydrolysis of fatty acids, and significant protein-protein interactions between ACP and TE are required (25).

Biosynthesis of LC-PUFAs in microalgae starts with the production of stearic acid (18:0) in the chloroplasts (*Figure 2. 3*). This is followed by a series of desaturation and chain elongation processes that occur in the endoplasmic reticulum, which are catalysed by a group of specific fatty acid desaturases and elongases. These processes add double bonds to the molecule and introduce new carbon atoms to it. After desaturation of stearic acid to oleic acid (18:1 n-9) and linoleic acid (LA, 18:2 n-6), fatty acid desaturation can take two different metabolomic paths: the n-3 and the n-6 routes. The n-3 route results in the production of α-linoleic acid (ALA, 18:3 n-9) through the introduction of a double bond toward the methyl end of the molecule. Further chain elongation and desaturation reactions produce EPA and DHA. On the other hand, the n-6 route results in the production of γ-linoleic acid (18:3 n-6) and arachidonic acid (AA, 20:4 n-6) through the introduction of a double bond toward the carboxyl end of the molecule (20).

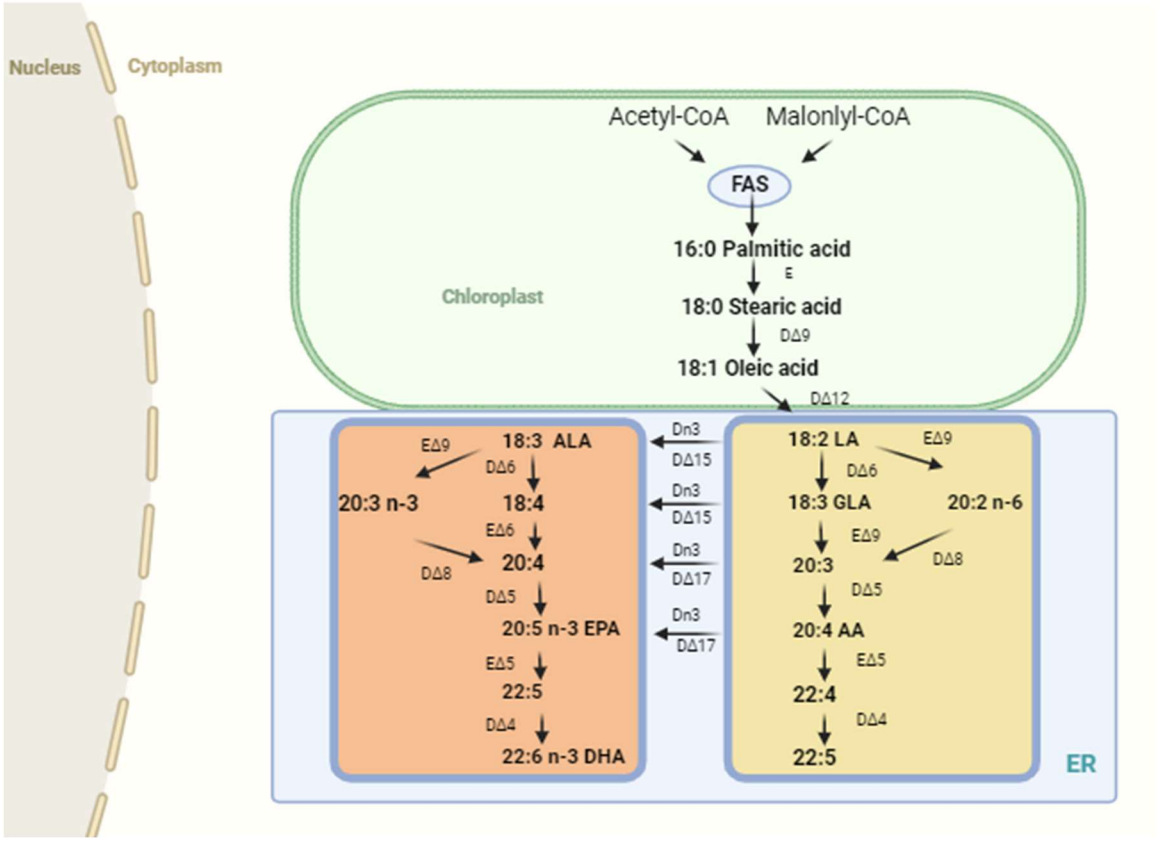

Figure 2. 3: Pathway for biosynthesis of LC-PUFAs in microalgae. Left (orange): synthesis of omega-3 fatty acids. Right (yellow): synthesis of omega-6 fatty acids. AA: arachidonic acid, ALA: α-linoleic acid, LA: linoleic acid, GLA: γ-linoleic acid, D: desaturase, E: elongase, FAS: fatty acid synthetase, CoA: Coenzyme A, n: location of double-bond closest to the methyl end (omega), Δ: location of double bond closest to the carboxyl group. Figure developed from (20) in biorender.com.

Human cannot synthesise LA and ALA from oleic acid due to a lack of a specific desaturase. However, these fatty acids are present in higher plant seeds and nuts, and if consumed in appropriate amounts, can be converted to EPA and DHA in the body (20).

2.8 Chromatography

The chromatographic analytical technique is powerful and versatile, widely used in the separation and analysis of complex mixtures. One of the most common applications of chromatography is the separation of derivates of fatty acids, fatty acid methyl esters (FAME), which are found in many biological and industrial samples. The principle behind chromatographic separation is based on the difference in migration velocity of various components within a two-phase system, with the goal of maximizing mass-transfer rate between these phases (6, 27).

Chromatographic separation is achieved by introducing a mixture of molecules onto surfaces or within solids or liquids, known as the stationary phase, which are then separated from one another by a mobile phase, typically a liquid or gas. The molecular characteristics of the compounds within the mixture, including adsorption, partition, and differences in molecular weight, play a significant role in the separation process. Some components within the mixture tend to spend more time in the stationary phase and migrate through the chromatographic system at a slower rate, while others quickly pass into the mobile phase and are rapidly eluted from the system (28). The different characteristics results in separation, enabling characterization and/or quantification of specific compounds in a mixture.

The chromatographic technique is composed of three main components: a stationary phase, a mobile phase, and separated molecules. The stationary phase may consist of a solid phase, or a layer of liquid absorbed onto a solid support. The mobile phase, on the other hand, can be a liquid or gaseous component (28).

2.8.1 Gas Chromatography

A gas chromatograph is an instrument used for the separation and analysis of volatile chemical compounds within a sample. It typically includes three key components: an injection system through which the sample is introduced, a column in which the separation of the sample's components is conducted, and a detector that produces a signal corresponding to the mass or concentrations of the eluted components (*Figure 2. 4*) (29).

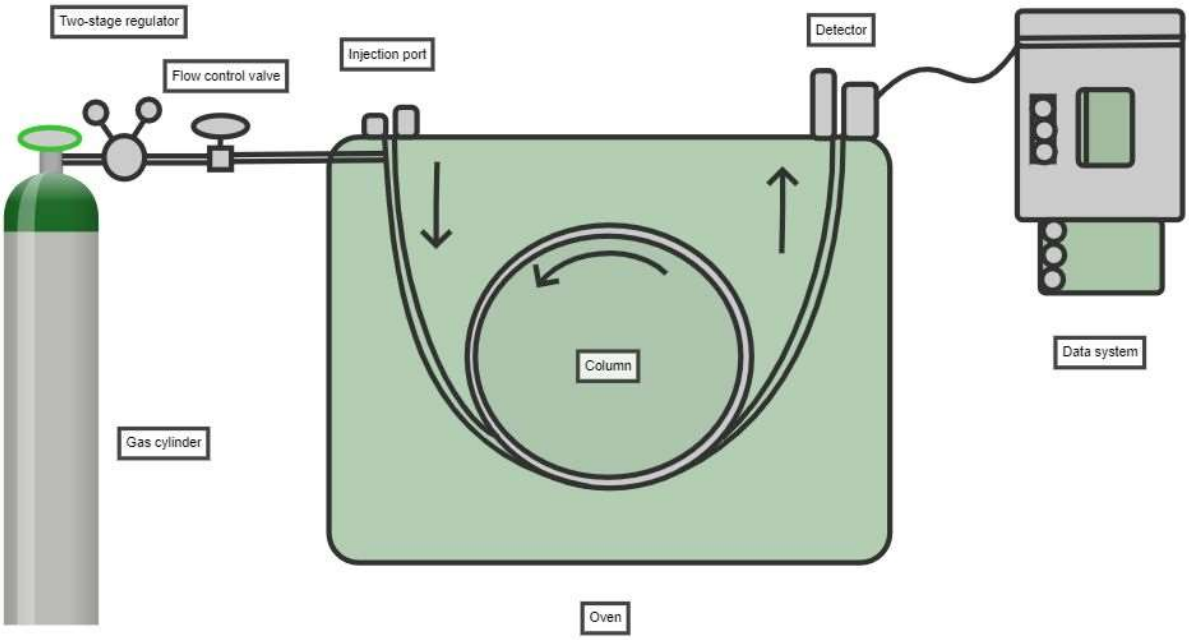

Figure 2. 4: Gas chromatographic system. A gas chromatographic system consisting of several key components that work together to separate and analyse chemical compounds within a sample. Figure developed from (29) in chemix.org.

When a volatile sample is introduced into the gas chromatograph, the solutes within the sample rapidly partition between a stationary phase and a gaseous mobile phase, also known as a carrier gas. The choice of carrier gas is critical as it can impact the separation efficiency and detection sensitivity. Commonly used carrier gases include helium, hydrogen and nitrogen. The sample is then conveyed through the column, where the components within the sample are separated based on their distributional characteristics between the stationary phase and mobile phase (30, 31, 32, 45). The partitioning of solutes between the stationary phase and mobile phase in a gas chromatograph is quantitatively described by the retention factor, denoted by "*k*", of the solute, as expressed by Equation 1 (31).

Equation 1: $$k = \frac{amount\ of\ analy \quad in\ stationary\ phase}{amount\ of\ analyte\ in\ mobile\ phase}$$

All molecules spend an equivalent amount of time in the mobile phase, and separate based on how much they interact with the stationary phase. The difference in how long each molecule sticks to the stationary phase determines when they elute from the column and how they are separated. The retention factor is affected by several factors, such as temperature, the type of stationary phase utilized, stationary phase thickness, and column diameter (31, 45). In

isothermal gas chromatography, where the temperature is maintained constant throughout the analysis, the retention factor can also be represented in terms of retention times (32, 45).

Equation 2: $$k = \frac{t_R - t_M}{t_M} = \frac{t'_R}{t_M}$$

The retention time, t_R, of a compound in a gas chromatograph is a fundamental parameter that represents the time elapsed from the introduction of the sample to the GC instrument until the peak maximum of the respective compound is observed in the chromatographic output. The holdup time, denoted by, t_M, also referred to as the "dead time," represents the duration of time required for a non-retained compound to traverse the column. The difference between the retention time (t_R) of a specific compound and the holdup time (t_M) is defined as the adjusted retention time, denoted by the symbol t'_R, and represents the duration of time the compound spends in the stationary phase. This relationship is depicted in *Figure 2. 5* (32, 45).

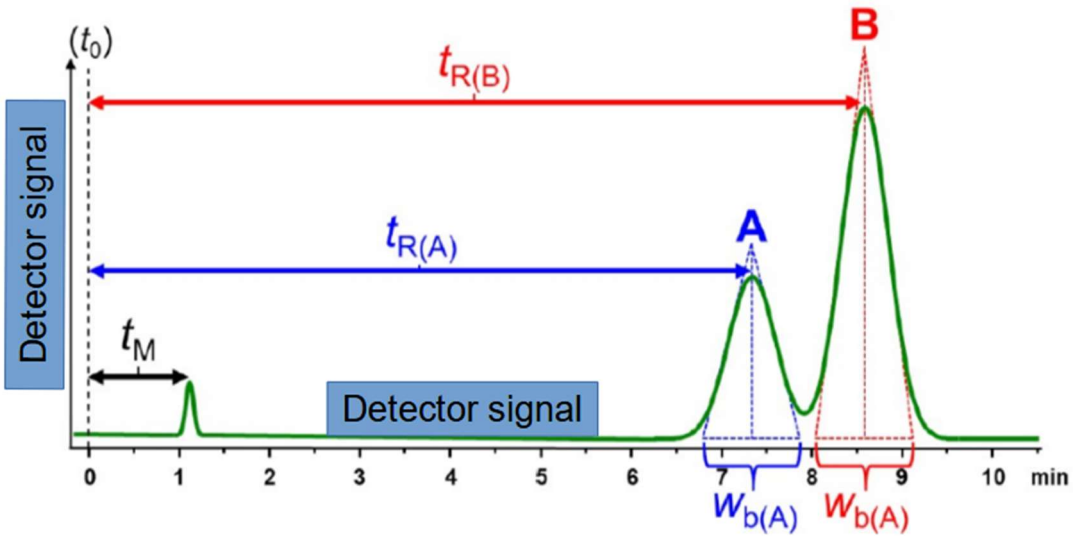

Figure 2. 5: Relationship between retention time and holdup time is the adjusted retention time. Two peaks representing compounds A and B, which are closely eluted and exhibit slight overlap in their elution profiles (24).

The primary objective of chromatography is to separate the individual components of a sample mixture into a series of chromatographic peaks, each of which corresponds to a unique component of the sample. A commonly used metric to quantify the degree of separation between two chromatographic peaks, A and B, is the resolution (R_s), which is mathematically defined by the equation below (32, 45).

Equation 3: $$R_s = \frac{t_{R(A)} - t_{R(B)}}{\frac{1}{2}(w_{b(A)} + w_{b(B)})} = \frac{\Delta t_R}{\bar{w}_b}$$

Where R_s is the resolution, t_R is the retention time and w_b is the width of the peak at baseline. This equation represents the ratio of the difference in retention times of the two peaks to the average of the corresponding peak widths at baseline. The equation is based on the assumption that the shape of the peaks follows a normal distribution curve (24).

The separation between two peaks in a chromatographic output can be improved by increasing the distance between the peaks or decreasing the peak width. By increasing the difference in retention (k) between the solutes, the selectivity is increased. The selectivity of a chromatographic system can be quantitatively expressed by the ratio of retention factors of two different compounds, denoted as α, given by Equation 4 (33):

Equation 4: $$\alpha = \frac{k_B}{k_A}$$

Where k_A and k_B are the retention factors of the compounds A and B, respectively.

Another alternative for increasing the resolution in GC is by increasing the chromatographic efficiency (33). Chromatographic efficiency is typically measured by the number of theoretical plates (N). The relationship between the number of theoretical plates (N) and the efficiency of a chromatographic separation is well established, as demonstrated by Equation 5:

Equation 5: $$N = 16(\frac{t_R}{w_b})^2$$

Where N is the ratio of retention time (t_R) to the width of a peak (w_b). As N increases, the peak width decreases, indicating an improvement in the separation power of the column. Improving efficiency can be done by decreasing the column diameter leading to a smaller diffusion path, and thereby a narrower peak. Additionally, by increasing the column length, the compounds can partition between the mobile phase and stationary phase more thoroughly. This increases the number of theoretical plates, which results in better separation and narrower peaks. However, it should be noted that improving efficiency in GC often increases the analysis time, and a balance must be struck between the resolution and speed (33).

The number of theoretical plates are also linked to the length of the column, *L*. The relationship between *N* and *L* can be represented by Equation 6, highlighting the independence of these two factors on the overall efficiency of the chromatographic separation.

Equation 6: $$H = \frac{N}{L}$$

Where *H* is the height equivalent to the theoretical plate (HETP). HEPT is a measure of the efficiency of a chromatographic column, where a low value indicates a higher efficiency per meter of column length. In the process of optimizing the efficiency of chromatographic separation, it is widespread practice to minimize the value of HETP.

The Purnell equation summarizes the three key factors that determine the efficiency, selectivity, and retention of a chromatographic separation. These factors are encapsulated in a single equation, providing a comprehensive understanding of the underlying mechanism that governs chromatographic separation (34, 45).

Equation 7: $$R_s = \frac{\sqrt{N}}{4} \cdot \frac{\alpha - 1}{\alpha} \cdot \frac{k_B}{1 + k_B}$$

The first term in the Purnell equation accounts for efficiency, the second term accounts for selectivity and the third term accounts for retention, respectively. The Purnell equation can be used to improve the resolution of a chromatographic separation by manipulating the variables in the equation. Generally, a resolution of at least 1.5 is considered necessary to ensure good separation, while higher resolution may be desirable in some cases. Alternative ways to improve resolution include (34):

1. Increasing the column length, which increase the number of theoretical plates (*N*) and improves the resolution, according to the first factor in Equation 7.
2. Decreasing the particle size of the column, or the column diameter in capillary column, also results in higher *N*. The same is the case for reduced stationary phase thickness in both capillary and packed columns.
3. Decreasing the column temperature increases the retention factors (*k*), which leads to increased resolution according to Equation 7.
4. Using a column with a different stationary phase can change the selectivity of the column (α in Equations 4 and 7) and improve the resolution of certain solutes.

Note that improvement of resolution should be balanced against the analysis time and sample properties (34).

2.9 Temperature Programmed Gas Chromatography

Temperature programmed gas chromatography (TPGC) is a technique that enables precise separation and identification of compounds in a mixture. The technique takes advantage of the different boiling points of the compounds, which results in varying rates of vaporization and migration through the column. As the temperature of the column is progressively increased, the vapour pressure of the compounds also increases, facilitating their vaporization and subsequent migration through the column, resulting in separation of the compounds based on their boiling points. To achieve optimal separation, TPGC often employs a constant heating rate, typically in the range of 1-10℃/min. The ideal heating rate will depend on the specific compounds being analysed and the desired level of separation. Furthermore, TPGC allows for dynamic interactions between the solute and both the stationary and mobile phase throughout the analysis, leading to variations in the retention factor (k). As a result, the equations based on "k" are no longer valid, and the concepts of selectivity and efficiency must be redefined to accurately reflect the unique characteristics of TPGC (35, 36).

2.9.1 Efficiency and Selectivity in Temperature Programmed GC

While the Purnell equation may not be directly applicable to the specific context of Temperature Programmed Gas Chromatography (TPGC), the fundamental principles of retention, efficiency, and selectivity that the equation represents, remain valid. To evaluate and compare the performance of TPGC separations, alternative metrics have been proposed, such as the separation number (SN) and retention indices (RI). These metrics provide a robust way of assessing the efficiency and selectivity of TPGC separations, allowing for deeper understanding of the underlying mechanisms and enabling the optimization of separation conditions (37, 45).

Selectivity

In GC, identifying components is typically done by comparing retention times. However, this method is prone to lack of reproducibility when experimental conditions such as column temperature or carrier gas flow are altered. To overcome this limitation, retention indices are employed, which express the retention of a compound relative to a reference series. The most widely used system is the Kovats retention index system, where n-alkanes are used as reference.

Equivalent chain lengths (ECL) are the most common method for identifying fatty acids, as they compare the retention time of a compound to that of a reference series of homologous compounds (38, 45).

In TPGC, the ECL of a compound is calculated using a modified version of the van den Dool and Kratz equation, originally developed for Kovats indices (*I*) (38). The equation considers the retention time ($t_{R(x)}$) of the compound (x), as well as retention times of saturated unbranched fatty acid methyl esters (FAMEs) eluting before and after the compound ($t_{R(z+n)}$). By comparing the number of carbons in the FAME chains of these reference compounds (z), the ECL of the target compound can be determined. The ideal difference in the number of carbons between the reference compound (n) is 1 (39, 40, 45).

Equation 8: $$ECL_x = n\frac{t_{R(x)}-t_{R(z)}}{t_{R(z+n)}-t_{R(z)}} + z$$

Retention indices are used in both isothermal GC and temperature programmed GC. In case of isothermal GC, the retention time of a sample component is interpolated using a logarithmic equation, in relation to the retention times of two n-alkanes that elute before and after the peak of the sample component. Kovats retention index (I) is represented by Equation 9, where x is the compound of interest, z is the n-alkane with z carbon atoms eluting before the compound of interest, and z+1 is the n-alkane with z+1 carbon atoms eluting after the compound of interest (39, 40, 41):

Equation 9: $$I_x = 100 \cdot \left(\frac{logt'_{R(x)}-logt'_{R(z)}}{logt'_{R(z+n)}-logt'_{R(z)}} + z\right)$$

In TPGC, the relationship between retention time and number of carbon atoms is linear. Therefore, logarithmic equations and plots are not necessary. As the temperature is increased, the partition coefficient decreases which eliminates the need for a logarithmic relationship (36). A value with the same purpose as Kovats retention index, referred to as the linear retention index, is calculated using the total retention times:

Equation 10: $$I_x = 100 \cdot \left(n \cdot \frac{t_{R(x)}-t_{R(z)}}{t_{R(z+n)}-t_{R(z)}} + z\right)$$

This simplified equation does not need to factor the dead time, as it is based on the total retention times (t_R) of the compounds, relative to the difference in carbon number (n) of the reference n-alkanes used (43).

Efficiency

In TPGC, the traditional measure of efficiency, *N*, is not valid. To overcome this limitation, L.S. Ettre (42) introduced the concept of separation numbers (*SN*) as an alternative method of expressing column performance in TPGC. *SN* describes the number of peaks that can be resolved between two members of a homologous series. It is calculated by using the difference in retention time between two homologs ($t_{R(z+1)} - t_{R(z)}$) and their peak width at half height ($w_{h(z+1)} + w_{h(z)}$) according to Equation 11 (42, 44).

Equation 11: $$SN = \frac{t_{R(z+1)} - t_{R(z)}}{w_{h(z+1)} + w_{h(z)}} - 1$$

The inverse of SN inverse is not a suitable replacement for the Height Equivalent to a Theoretical Plate (*H*). This is because even when *SN* is zero, the homologs are still separated, indicating some level of separation efficiency. As an alternative, the peak per carbon (*PPC*) metric is used, which is the number of peaks that can be separated with chromatographic resolution equal to one per compound in a homologous series (*Figure 2. 6*).

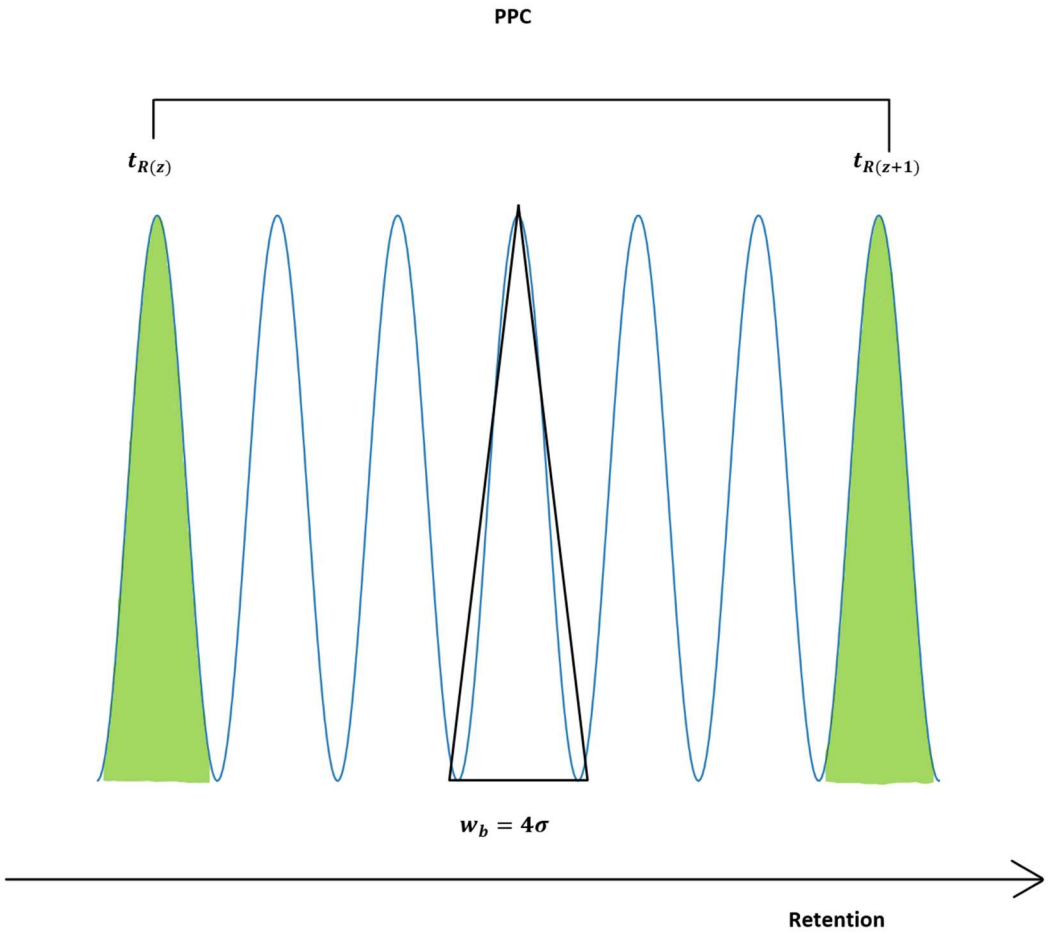

Figure 2. 6 Peaks per carbon. Two peaks, well separated, with narrow peak widths, belonging to two homologous series and separated by a chromatographic resolution of one. Figure developed in OneNote Office.

Mathematically, *PPC* can be expressed as the difference in retention time between the two homologous compounds ($t_{R(z+1)} - t_{R(z)}$) divided by the average peak width at baseline ($0.5(w_{b(z+1)}+w_{b(z)}$). This metric provides a more accurate representation of the separation efficiency in TPGC (41, 44, 45).

Equation 12: $$PPC = \frac{t_{R(z+1)}-t_{R(z)}}{0.5(w_{b(z+1)}+w_{b(z)})}$$

The equation for calculating *PPC* can be simplified by replacing the retention time scale with a retention index scale, where the difference in retention between homologous compounds is defined as 1 for equivalent chain length (*ECL*) and 100 for Kovats indices (*I*). This eliminates the need for measuring retention times and peak width separately, making the calculation more efficient (41, 44, 45).

Equation 13: $$PPC = \frac{1}{w_{b,RI}}$$

A similar equation to the one above connects *SN* to peak width in ECL units. To achieve maximum efficiency, it is important to minimize the peak width in retention index units in the same way that H is minimized in isothermal GC. An equation describing the relationship between resolution (R_s), PPC and ECL is presented by this simple equation (41, 44, 45):

Equation 14: $$R_s = \Delta ECL \cdot PPC$$

2.10 Models for efficiency

The van Deemter equation is the most known chromatographic equation. It describes the dependence of the column`s height equivalent to a theoretical plate (HEPT) on the linear mobile phase velocity (46).

To decrease the height of a theoretical plate (*H*), it is important to understand the experimental factors that cause peak broadening in a solute`s chromatographic peak. Van Deemter`s approach considers four contributions: multiple paths, longitudinal diffusion, mass transfer in stationary and mobile phase (32, 45).

Peak broadening by multiple paths (*A*) in chromatography occurs when solute molecules take different paths through the column, leading to variations in elution time. This occurs in packed columns, where large and irregularly shaped particles increase the effect (32, 45).

The second contribution to peak broadening is the solute's longitudinal diffusion (*B*) in the mobile phase. As solute molecules are constantly in motion, even when the mobile phase velocity is zero, they diffuse through the mobile phase, leading to an increase in the width of the peak. This is because the concentration of solute is greater at the centre of the peak, and more solute diffuses towards the peak`s forward and rear edges than towards the centre. The diffusion results in a spreading of the peak. To minimize longitudinal diffusion the mobile phase velocity should be high to minimize the time the analyte spends in the mobile phase. Mathematically, this can be described by the van Deemter equation. Longitudinal diffusion is

one of the key parameters that is considered when optimizing the separation of solutes in a sample (32, 45).

The final two contributors to peak broadening are a result of the time it takes for a solute molecule to diffuse through both the stationary and mobile phase. As solute molecules move between the two phases they must diffuse to the interface between them, a process called mass transfer (*C*). Due to the time required for this process, solute molecules in the mobile phase may travel further down the column than expected before entering the stationary phase, while solute molecules in the stationary phase may take longer than expected to cross into the mobile phase. The mass transfer contribution to peak broadening will therefore increase with mobile phase velocity. This slow movement of the solute to the interface between two phases is a crucial factor to consider when optimizing chromatographic separations (32, 45).

The van Deemter equation is and equation showing the effect of the mobile phase velocity on the height of a theoretical plate, putting all three terms together (A, B and C) expressing *H* as a function of carrier gas velocity (*u*) (32, 45):

Equation 15: $$H = A + \frac{B}{u} + Cu$$

A, accounts for multiple paths, B/u for longitudinal diffusion, and Cu for the solute`s mass transfer in the stationary and mobile phase. (32) The impacts of the three terms *A, B* and *C* are depicted in *Figure 2. 7*. The contribution of the *A* term is not influenced by the velocity of the mobile phase in GC. Conversely, the impact of the B term increases at low mobile phase velocities and subsequently diminishes rapidly with increasing mobile phase velocity. On the other hand, the contribution of the C term increases as the mobile phase velocity increase. The mobile phase velocity at which the sum of the three terms is at a minimum, is referred to as the optimal velocity (u_{opt}). The plate height, *H*, has its minimum at optimal velocity, therefore the partial derivate of the van Deemter equation with respect to the carrier gas velocity (*u*) is zero (45).

Equation 16: $$u_{opt} = \sqrt{\frac{B}{C}}$$

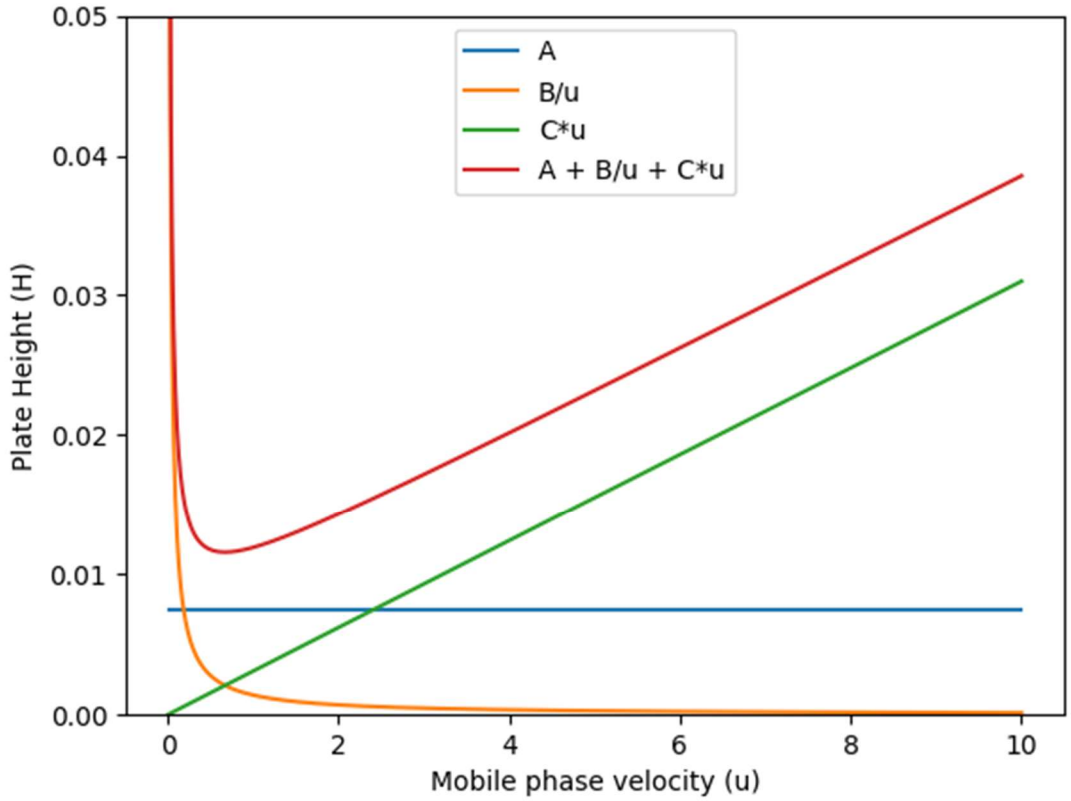

Figure 2. 7 Van Deemter Curve. Optimal mobile phase velocity is where the orange and green lines intersect. Figure developed in python from fictional data.

The van Deemter equation, originally developed to model plate height in packed columns, does not consider band broadening occurring in other chromatographic columns, such as open tubular (capillary) columns. These columns contain no packing material, instead, they have a thin film of stationary phase coating the interior wall. This absence of packing material allows the mobile phase to move through the column with less pressure, resulting in a reduction of plate height (*H*). This is due to the disappearance of the A term (multiple paths) leading to a new equation, the Golay equation (32, 45):

Equation 17: $$H = \frac{B}{u} + Cu$$

The van Deemter curve and Golay equation does not always fit well to experimental results due to column effects that are not accounted for, such as compressibility of the mobile phase. In addition, they cannot explain peak broadening happening outside of the column (i.e., in injector or detector). However, despite these limitations, the van Deemter and Golay equations remain

the most widely used models for explaining band broadening in chromatography. Additionally, there are several alternatives and variants of these equations that are better suited to certain conditions, which can be used to improve the accuracy of the model. (32, 45) Some examples of alternative equations are the Knox equation (47) and the Giddings equation (48).

2.10.1 Carrier gas

When performing GC, it is important to use a carrier gas that does not react with the compounds being analysed and the stationary phase. Inert gases like helium, hydrogen, nitrogen, and argon are the most common carrier gases. Among these, the most popular choices are helium and hydrogen. Helium is particularly preferred in capillary columns because it enables high resolution while maintaining a high linear velocity of the sample through the column (32, 45). The choice of carrier gas can influence the appearance of the chromatogram and plays a significant role in GC optimization. Two properties of gas play a role in the chromatographic process: diffusivity and viscosity (48). The diffusion speed of an analyte in the gas determines the speed of GC. Analytes need to spend time in both the stationary phase and mobile phase to separate. The diffusivity is higher in hydrogen than in helium, while nitrogen has a diffusivity three to four times lower than helium, which results in longer separation times (48). If the velocity of the flow rate with nitrogen as carrier gas is increased, then the van Deemter curve shows that the efficiency will fall off dramatically (*Figure 2. 8*) (48).

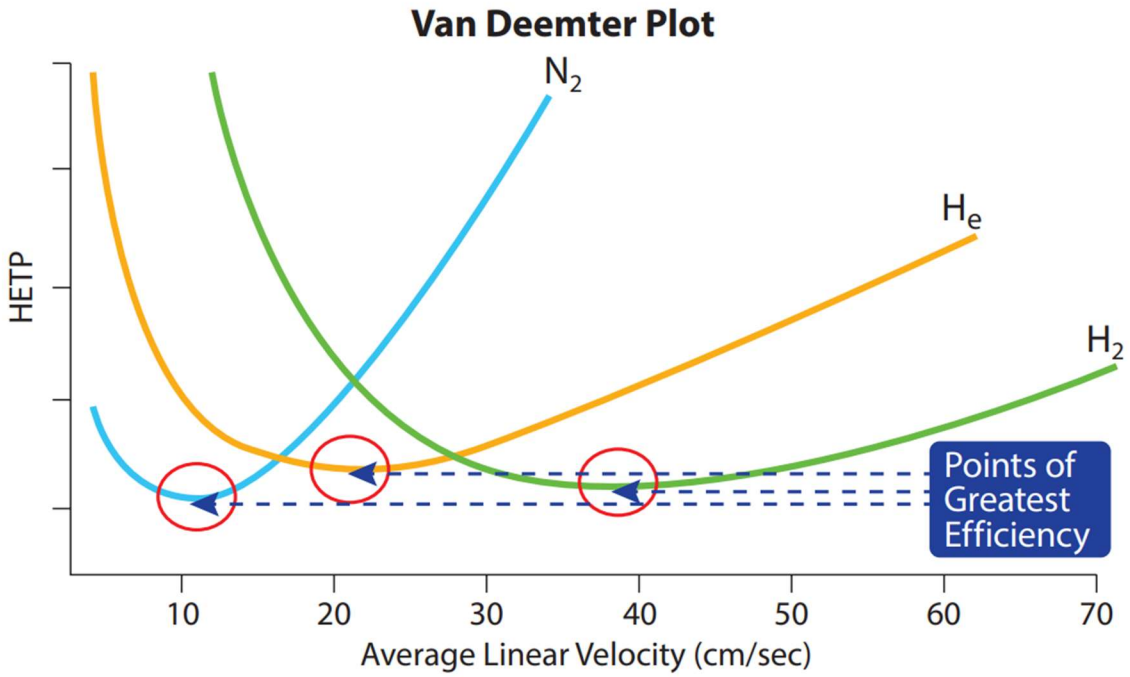

Figure 2. 8: Van Deemter curves for hydrogen, helium, and nitrogen as carrier gases. Optimum efficiency obtained at the linear velocity corresponding to the minimum point on each curve (50).

The viscosity of the carrier gas affects how much pressure is required for a certain gas velocity. If the pressure is high, the gas will be compressed at the start of the column and its velocity will change as it moves through the column. In capillary columns with helium as carrier gas, an average speed of 20 to 25 cm/s is typically desired. Hydrogen is less viscous than helium and nitrogen and the optimal velocity for hydrogen, the most efficient carrier gas, is at around 60 cm/s making the separations faster. Hydrogen has the most favourable properties and is less expensive than other carrier gases. At the same time, hydrogen is not endorsed universally by gas chromatographers due to it being highly explosive (49).

2.10.2 Column dimensions

The efficiency of gas chromatographic separations can be greatly impacted by the choice of column and column dimensions. These dimensions include column length, internal diameter and film thickness, each significantly affecting the resolution and separation of sample components. A comprehensive understanding of the relationships between resolution and these column dimension, as outlined in the Purnell equation (Equation 7), is crucial in making informed choices during method development (51).

Table 2. 1 provides an overview of the relationship between chromatographic variables and GC column dimensions. As the column length (L) increases, the efficiency and resolution increase but also results in longer analysis time and higher pressure. Decreasing column diameter (d_c) leads to faster analysis and lower pressure but decreased resolution and separation. Increasing the film thickness (d_f) results in improved separation, but at the cost of slower analysis time and increased column bleed. In summary, choosing appropriate column dimensions for a specific analysis requires a trade-off between separation efficiency and analysis time (51).

Table 2. 1 Relationship between chromatographic variables and GC column dimensions (52). L: column length, d_c:column diameter, d_f: film thickness.

Parameter	**Increasing L**	**Decreasing d_c**	**Increasing d_f**
Efficiency	Increase	Increase	Decrease
Resolution	Increase	Increase	(k<5) increase, (k>5) decrease
Analysis time	Increase	-	-
Pressure	Increase	Increase	-
Cost	Increase	-	-
Flow rate	-	Decrease	-
Capacity	-	Decrease	Increase
Bleed	-	-	Increase
Retention	-	-	Increase
Inertness	-	-	Increase

In GC, there are two main types of columns used, namely capillary columns and packed columns. Capillary columns, made of fused-silica material, provide higher resolution than packed columns, especially in fatty acid analysis. The inner diameter and film thickness of capillary columns greatly affect their efficiency, retention time, and capacity. Non-polar stationary phases, such as methyl silicone columns, are preferred due to their high thermal stability, chemical inertness and ability to separate most mixtures. However, careful column selection may be required for special applications. The polarity of the columns can be indicated by the column polarity index (CP) which ranges from 0 to 100 (53).

Capillary columns can be classified into three categories: PLOT, WCOT and SCOT columns (*Figure 2. 9*). WCOT columns feature a direct coating of the stationary phase on the wall with a film thickness of 0.05-3 μm. SCOT columns, on the other hand, have an adsorbed layer of fine solid support coated with the liquid phase. These columns have a higher sample capacity than WCOT columns due to the ability to hold more liquid phase. PLOT columns consist of a

porous layer of a solid adsorbent material such as alumina, molecular sieves, or Porapak. These columns are particularly suited for the analysis of light gases, other volatile compounds, and fixed gases (54).

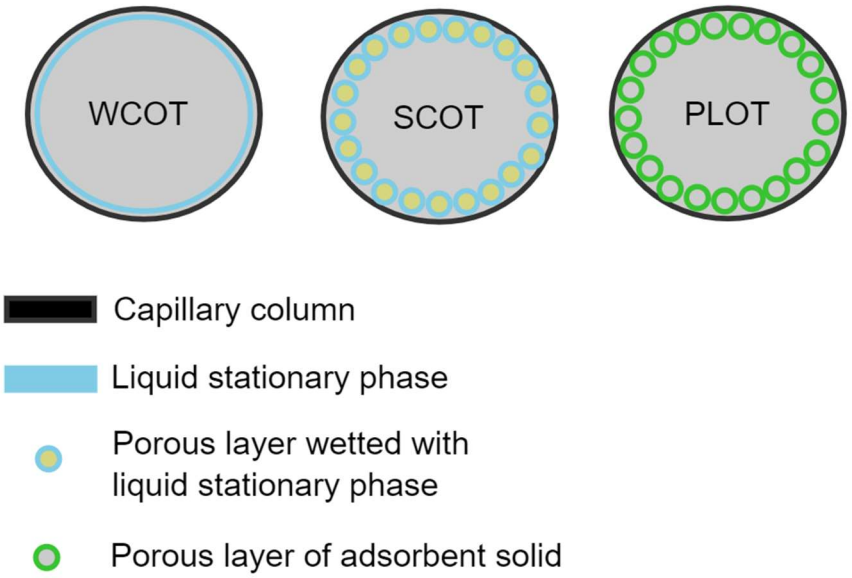

Figure 2. 9 Types of capillary columns. Figure developed in chemix.org from (55).

2.11.1 Split/Splitless injection

The most frequently used injector in GC is the split/splitless injector, typically featuring three flow lines: the septum purge, the split purge and the liner and septum (*Figure 2. 10*). The septum purge flow prevents the carrier gas in contact with the septum from entering the column. Meanwhile, the split flow plays a crucial role in the injector`s operational mode. When an open split valve is used, it divides the sample, allowing only a fraction to enter the column. Conversely, closing the split valve during injection results in the entire sample entering the column (56).

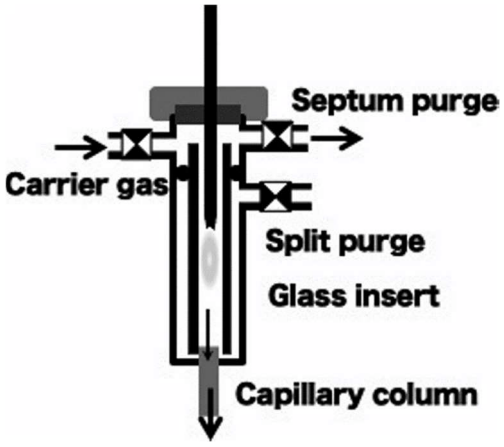

Figure 2. 10: Illustration of split/splitless injector. Figure from (56).

The liner and septum require frequent replacement. The liner serves multiple functions, including the capture of impurities and non-volatile compounds to prevent them entering the column. Over time, these compounds can accumulate and potentially disrupt the chromatographic performance. A plug of glass wool is often placed inside the liner to increase the surface area, facilitate rapid sample volatilization, and enhance impurity capture compared to an empty liner (56).

Maintaining the injector temperature within a specified range is important. If the temperature is too low, heavier analytes may be lost or produce tailing peaks. In splitless injection, it is common practice to open the split valve after a few minutes to allow compounds with lower volatility to exit through the valve rather than entering the column. Premature opening of the split valve can also result in the loss of heavier analytes (56).

2.11.2 FID

The Flame Ionization Detector (FID) is the most widely used detector in gas chromatography, offering a multitude of advantages. These encompass a universal responsiveness to organic compounds, low detection thresholds, sustained stability over time, user-friendly operation, minimal dead volume, and an exceptional liner response range (57).

Moreover, the FID demonstrates a strong response towards organic compounds, while displaying negligible responses to inert gases, specific nitrogen oxides, single-carbon compounds bound to oxygen or sulphur, inorganic gases, water, formamide, and formic acid. This selectivity enables precise calibration for intricate mixtures. The detector is often characterized as a carbon-selective detector, exhibiting a molar reaction proportional to

hydrocarbon based on their carbon atom number, with a relative response for carbon-containing compounds, regardless of molecular structure (57).

Operatively, the FID functions by combusting organic compounds within a hydrogen-air diffusion flame. Prior to combustion, the carrier gas from the chromatographic column mixes with hydrogen and, and possibly, makeup gas. Subsequently, charged particles produced during combustion are gathered by a collector electrode, and then the ion currents undergo conversion into voltage, followed by amplification. Any organic compound capable of oxidation (burning) within the flame generates ions, resulting an electric current within the detector circuit (57).

However, the FID's sensitivity encounters limitations from factors such as thermal noise, fluctuations in charged particle flux, and environmental electromagnetic interferences. Employing active filters serves to minimize background noise effectively. (57) Additionally, FID only detects carbon groups that can undergo oxidation, such as carbon-hydrogen bonds (C-H), excluding, for instance, the carbon in the carbonyl group of a FAME from contributing to the signal. As a result, FID response factors for FAMEs depend on both carbon number and degree of saturation (58).

The upper boundary of the response range is subject to influences from the flame dimensions, collector electrode bias voltage, and detector geometry. In contrast, the response speed is primarily limited by electronic components (57).

The detector's performance is primarily influenced by the ratios of carrier gas-to-hydrogen-to-air flow rates and the detector geometry. Conversely, the choice of carrier gas and detector temperature exerts a less significant impact. In practice, adhering to the manufacturer's recommended conditions, provided they have been correctly optimized, yields optimal FID performance (57).

2.12 Response surface methodology

Response surface methodology (RSM) is a comprehensive set of statistical and mathematical techniques employed for developing, improving, and optimizing processes. It holds significant important applications in the design, development, and formulation of new products, as well as in the improvement of established product designs (59). RSM has the advantage of functioning well in cases where there is partial knowledge about the state and behaviour of the studied

system, under the assumption of a stable system and rational correlation between set-points and actual conditions (10).

In RSM, a series of experiments are conducted while systematically adjusting various predictor variables (chromatographic conditions etc.) according to a predetermined experimental design plan. A model is employed to highlight the response variable as a function of two or more predictors, estimating the response surface. Typically, these models are constructed using polynomial equations, depicting responses in terms of linear and quadratic predictor terms, along with interactions among these predictors (10).

What is important to note is that RSM extends beyond the confines of polynomial models, as certain mathematical relationships are not adequately captured by polynomial response functions. These include inverse relationships and logarithmic functions (such as the "B" term in the van Deemter equation). As described below, models concerning efficiency and retention time in GC falls into this category (10).

2.12.1 Modelling efficiency and retention time

Similar to the van Deemter equation that explains the inverse efficiency as a function of mobile phase velocity in isothermal GC, a model explaining the inverse efficiency as a function of carrier gas velocity and the temperature rate in TPGC has been developed by Mjøs and Waktola (10). The developed model is based on the van Deemter equation and is expanded to account for the temperature rate, and is noted by (*i*), interacting effect. No equivalent to the van Deemter equation explains peak broadening as a function of carrier gas velocity in TPGC. However, longitudinal diffusion and resistance to mass transfer, is similar to isothermal GC. The model applied to model the inverse efficiency is described by Equation 18:

Equation 18: $$w_{b,ECL} = a + \frac{b}{u} + c \cdot u + d \cdot i + e\frac{i}{u} + f \cdot i \cdot u$$

The *a, b* and *c* terms in the equation are comparable to the A, B and C terms in the van Deemter equation (10). The next terms explain the effect of temperature rate. The *d*-term explains the linear effect of (*i*) on peak widths (in *RI*-units), *e* explains the effect of (*i*) on the *b*-term in the van Deemter equation, and *f* explains the effect of (*i*) on the van Deemter equation (45).

To find the optimal velocity at any temperature rate (within a valid range of the model Eq. 18) a partial derivative of Equation 16 can be used to estimate u_{opt} if the *b, c, e* and *f* terms are known:

Equation 19: $$u_{opt} = \sqrt{\frac{b+e \cdot i}{c+f \cdot i}}$$

When optimizing chromatographic efficiency in TPGC, a common approach is to choose a low temperature rate. However, this leads to longer retention times extending chromatographic runs. In practice, the aim is often to maximize efficiency within a specified time frame. A precise model is therefore needed to predict the retention time of the last eluting compound. This model is described in Equation 20 (10):

Equation 20: $$\ln(t_R) = D + E \ln(u) + F \ln(i) + G \ln(u) \ln(i)$$

This equation assumes a linear relationship between the logarithms of t_R and the two variable parameters, incorporating a constant (D) and an interaction term (G). After determining the regression coefficients, the exponent can be taken of the predicted values and the predictors, yielding a response surface that directly elucidates retention time as a function of *u* and *i* (10).

2.12.2 Modelling selectivity by transferring retention patterns

On polar stationary phases used in GC, transferring retention patterns can be challenging across different systems and column of varying ages. In the optimization in this study, the aim is to replicate a "target" pattern through the exploration of diverse chromatographic conditions using a response surface design (11, 60).

The elution pattern is determined by the retention indices (*RI*) of distinct peaks, specifically the *ECL* of FAME. To reproduce this retention pattern, each FAME should exhibit an *ECL* value closely mirroring that in the target chromatogram. For each FAME, a response surface model is calculated to elucidate how its *ECL* value changes with respect to two parameters. This is done by a polynomial model linking response to experimental settings and are obtained by regression (11, 60). The model looks like this:

Equation 21: $$\hat{y} = b_0 + b_1 u + b_2 i + b_3 ui + b_4 u^2 + b_5 i^2$$

Where $\hat{y}$ represents the ECL values to be predicted, u denotes the carrier gas velocity (cm/s), and i signifies its temperature rate ($℃/\mathrm{min}$). Since there are six b coefficients in the equation, at least six experiments has to be conducted to solve the equation by regression (11, 60).

2.13 Experimental design

Experimental design, also known as design of experiments (DoE), is a systematic approach used to plan, conduct, and analyse experiments in a structured and efficient manner. The goal of DoE is to maximize the information obtained from a limited number of experiments. In chromatography, researches can efficiently optimize methods, improve analytical performance, and gain valuable insights into the chromatographic process (39).

The most common design to determine response surfaces are the full and fractional designs and the more complex central composite, Box-Behnken, Doehlert and mixture designs. All methods require the user to supply minimum and maximum values for each factor that defines the experimental domain to be investigated during the optimization procedure. Depending on which multivariate technique is used, combination of different factor levels used to perform the actual experiments are determined (61).

In this study, experimental design was applied to provide the data necessary for finding the models described by Equation 18, 20 and 21. Two factors were varied; the carrier gas velocity (u) and the temperature rate (i). An *ad hoc* experimental design is used. In the *ad hoc* design the numbers of experiments are flexible and limited by the interest of the user (62). This design is applied in the method optimization with two factors containing 16 levels of carrier gas velocities, and 4 levels of temperature rate.

3 Materials and Methods

3.1 Chemicals and Reagents

3.1.1 Standards and Materials

Internal standard (23:0 FAME, 4. 176 mg/ml), reference mixture (GLC793), spike samples and "EFF mix" were purchased from Nu-Chek Prep (Elysian, MN, USA).

GLC793 reference mixture contains equal masses of the following unsaturated FAMEs: 14:1 n–5, 16:1 n–7, 17:1 n–7, 18:1 n–9, 18:2 n–6, 18:3 n–6, 18:3 n–3, 20:1 n–9, 20:2 n–6, 20:3 n–6, 20:4 n–6, 20:3 n–3, 22:1 n–9, 20:5 n–3, 22:4 n–6, 24:1 n–9, 22:5 n–3, and 22:6 n–3 in addition to the saturated FAMEs: 12:0, 14:0, 15:0, 16:0, 17:0, 18:0, 20:0, 22:0, 23:0 and 24:0.

The GLC793 reference mixture was used for calculation of the response factors in the quantitative analysis and to find the models described by Equation 21 (modelling selectivity).

The spike sample contained the saturated FAMEs 12:0, 14:0, 15:0, 16:0, 17:0, 18:0, 19:0, 20:0, 21:0, 22:0, 24:0, 25:0, 26:0, 27:0 and 28:0. The spike sample was used for calculating the ECL values in the quantitative analysis.

The "EFF-mix" sample contained the unsaturated FAMEs 16:1 n-7, 18:1 n-9, 18:2 n-6tt, 18:3 n-6, 20:3 n-6, 20:5 n-3, and 22:6 n-3. The EFF mix was used to find the models described by Equations 18 (model of inverse efficiency) and 20 (model of retention time).

The longest chain saturated FAMEs, used to model retention time, were purchased from Sigma Aldrich (25:0, 26:0, 27:0 and 28:0). All other individual FAMEs were purchased from Nu-Check Prep.

The Pavlova algal paste used as reference samples in were purchased from Reed Mariculture and contained the saturated FAMEs 12:0, 14:0, 15:0, 16:0, 18:0, 23:0 and the unsaturated FAMEs 14:1 n-5, 16:1 n-7, 16:1 n-5, 16:2 n-4, 16:3 n-4, 18:1 n-9, 18:1 n-7, 18:3 n-3, 18:4 n-3, 20:4 n-6, 20:5 n-3, 22:5 n-6, 22:6 n-3.

3.1.2 Sample Preparation

The following chemicals used for sample preparation were purchased: HPLC grade Isooctane from Sigma Aldrich. Methanolysis reagent (2M dry HCl in methanol) for conversion of fatty acids to FAMEs from Supleco. Nitrogen 5.0 ultra (50 l) gas from Nippon gases (Norway, Oslo). Ultra-pure water was obtained through a Milli-Q system from Merck KGaA (Darmstadt, Germany).

3.1.3 Chromatography

Two Agilent 7890A gas chromatographs were used, each featuring an autosampler, split-splitless injector, and flame ionization detector (FID). While both instruments shared identical setups, they operated with different carrier gases. Specifically, Nitrogen 5.0 Ultra and Helium 5.0 Ultra from Nippon gases. Hydrogen and synthetic air were used for the FID (Nippon gases, 5.0 Ultra).

Both instruments were equipped with a BPX70 (SGE Ringwood, Australia) capillary column composed of 70% Cyanopropyl polysilphenylene-siloxane. The instrument operating with nitrogen as carrier gas had a 30 m column with internal diameter of 0.22 mm and stationary phase thickness of 0.25 μm. The instrument operating with helium as carrier gas had a 60 m column with internal diameter of 0.25 mm and a stationary phase thickness of 0.25 μm.

3.2 Sample Preparation

Algal paste of the microalgae Pavlova was used as a reference sample and weighed in at approx. 0.17 g ww, filled with nitrogen and capped, ready for preparation when needed.

Frozen microalgae (*Nannochloropsis*) from NORCE were the samples provided for this study. During the sample preparation the algae samples were placed in a heating block for evaporation at 80 ℃ under nitrogen until dry. According to each sample`s dry weight, an appropriate volume of internal standard (23:0 FAME, 4.176 mg/ml) were added in the reaction tubes (Equation 3.1). The tubes were then added 1 ml of methanolysis reagent (2M dry HCl in methanol) with a variable volume pipette with glass tip, followed by 2 hours of incubation at 90 ℃ in a heating cabinet converting the fatty acids into their corresponding FAMEs.

After incubation, half of the reagent was evaporated at 70 ℃ under nitrogen at the heating block. 1 ml of Milli-Q water and 1 ml of isooctane were added, followed by vortex for 30 seconds and centrifugation at 3500 rpm at 5 min. The isooctane layer was transferred to a 2 ml vial. 1 ml of isooctane were added to the reaction tube again and vortex and centrifugation were repeated. The extracts were then combined. According to each sample IS volume, an appropriate volume

of the extracts was quantitatively added with a syringe to GC-vials that already contained 1 ml of isooctane (Equation 3.2).
Table of added volume of IS and extracts according to dry weight is provided in Appendix A (Table A. 1).

Equation 3.1 $$IS_V = DW \cdot 30$$

Where IS_V is the internal standard volume in µl and DW is the dry weight in mg.

Equation 3.2 $$V_E = \frac{12\ 000}{4 \cdot IS_V - 12}$$

Where V_E is the volume of extract in µl added to 1 ml isooctane in a GC-vial.

3.3 Quantitative fatty acid analysis

Quantitative analysis with nitrogen as carrier gas

Samples were injected 0.5 µl in splitless mode at 60°C and held for 3 minutes for proper analyte focusing. The temperature was then increased by 60°C/min to the start temperature ramp of 150°C, followed by 4 °C/min until the last compound had eluted.

Quantitative analysis with helium as carrier gas

Samples were injected 1 µl in splitless mode at 60°C and held for 3 minutes for proper analyte focusing. The temperature was then increased by 40°C/min to the start temperature ramp of 150°C, followed by 1.5 °C/min until the last compound had eluted.

The carrier gas velocity (u) is a nominal value estimated from the average carrier gas velocities at the injection temperature assuming nominal column dimensions. All experiments were conducted in constant flow mode.

3.4 Quantification and Treatment of Data

To allow for initial quantification, Agilent Chemstation raw data was processed by the Matlab-based software program Chrombox C. This software was applied for preliminary handling of GC-FID data, including integrating, identifying, and quantifying FAMEs based on retention indices. Chrombox C was used for quantification of all samples in this thesis.

The GLC793 reference mixture was applied for calculating the response factors. The raw areas of the peaks in the reference mixture were adjusted with the response factors. To determine the mass of the different analytes, their adjusted peak areas were divided by the adjusted area for the internal standard peak and multiped with the mass of internal standard added to the sample. In this study the absolute amounts are µg/sample where all samples of microalgae were 10 ml microalgae culture. The absolute amounts for the samples are therefore µg/10 ml of algae suspension. Additionally, relative amounts are discussed, which are the mass percentage of quantified fatty acids, the sum of these are always 100%.
To model efficiency, retention time, and selectivity Chromebox O was utilized. This software reads data from Chrombox C, enabling modelling of a large number of peaks in an efficient manner, creating response surface plots to illustrate optimal conditions for the separation of fatty acids, and corresponding retention pattern.
Complete procedure using both Chrombox C and O is outlined in this tutorial (63) .

3.5 Statistical calculations

Microsoft® Excel® for Microsoft 365 MSO (Version 2307 Build 16.0.16626.20170) was used for organizing, processing, plotting and running statistical analysis on collected raw data for this thesis. The results are presented as RSD%, differences, slopes and intercepts.

Differences between means and variances, slopes, and intercepts, were considered significant at $p \leq \alpha$. The significance level (α) was corrected by Bonferroni`s correction: If $\alpha_g$ is the Type I error rate (probability of a false significance) for the multiple tests and $\alpha$ is the same rate for each individual test, Bonferroni`s inequality tells us that (64):

Equation 3.3 $$\alpha_g \leq \alpha \cdot q$$

Where q is the number of tests.
This correction may be overly conservative in some cases (64).
A significance level of 0.05% was applied. All significance tests had the same number of tests (FAs) and α was calculated to $\alpha = 0.00454$ where $q = 11$. If $p \leq \alpha$ (significant) it is denoted by * in the tables.

For preliminary visualization of the similarity or dissimilarity of the reference method and the optimized method, a PCA in Python was conducted between the samples derived from each method.

For the precision study, all FAMEs representing less than 1% of the total amount of FAME were removed. The FAMEs investigated are summarized in the tables along with their RSD% and significance in the results and discussion section.

Preliminary handling of the *Nannochloropsis* samples from NORCE, like standardization and block normalization, were conducted in the pattern recognition system, SIRUS 13.0. This system was also used to conduct PCA on the pilot-scale experiment (NORCE) to visually detect patterns and correlations.

3.6 Accuracy study

All samples were analysed two times, one with the optimized method, using nitrogen as carrier gas, and one method, using helium as carrier gas, as reference method. The reference samples (Pavlova, R1-R9).

3.6.1 Precision

Intermediate precision, repeatability and injection repeatability of the instrument (GC-FID) with nitrogen as carrier gas was estimated.

Intermediate precision was estimated by analysing nine reference samples (R1-R9). The reference samples contained an algal paste of the microalgae, Pavlova, weighed in at about 0.17 g ww. for each sample. The samples were prepared and analysed at different days over a period of about 2 months, covering sample preparation and instrument variation. The relative standard deviation (RSD%) were calculated for absolute amounts of each FAME as an estimate of the intermediate precision of the optimized method.

Repeatability was estimated by analysing 10 vials prepared from the same sample. Sample 61 was used in this estimation, carefully selected from the samples provided by NORCE. Sample 61 had a DW of 6.88 mg and was one of the most concentrated samples. The 10 vials were analysed at the same day and time, two times, once with nitrogen as carrier gas and once with helium as carrier gas. The RSD% was calculated for absolute amounts of each FAME as an

estimate of the repeatability of the optimized method. F-test was conducted to check for any significant differences in variation of absolute amounts between the methods for each fatty acid.

Injection repeatability was estimated by doing 10 injections from the same vial. The vial was prepared from sample 61 and was analysed at the same day and time. 10 injections from the same vial were conducted for the two methods, one with nitrogen as carrier gas and one with helium as carrier gas. The RSD% was calculated for the absolute amounts of each FAME as an estimate of the injection repeatability for the optimized method. F-test was conducted to check for any significant differences in variation in absolute amount between the methods for each fatty acid.

Additionally, F-test was performed to compare injections made from different vials with those made from the same vial for both methods. This analysis aimed to determine whether there was statistical significance in terms of variation in absolute amounts when injecting from different vials as opposed to the same vial.

3.6.2 Accuracy

Careful selection of 31 samples (algal samples from NORCE) with different dry weights (concentration levels) were conducted to evaluate the linearity of relative amounts and absolute amounts of FAME. The samples were prepared at different times over a period of 2 months. Amounts of each FAME and sum of quantified FAMEs for both methods were plotted against each other. Correlation coefficients, R-squared values, slopes and intercepts for the linear relationship were derived from the plots and evaluated. To confirm linearity, the residuals were checked for heteroscedasticity.

Using the equations for the linear relationships in the plots from the linearity study, the accuracy was assessed by comparing the slopes of the FAs against 1, and the intercepts against 0, for estimating bias. Python was used for visualizing the percentage difference (relative bias) between the methods and any occurring trends for the sum of FAMEs and the sum of each individual FAME. The p-values were also calculated and compared to α to determine any significant differences. Significant differences are indicative of bias.

3.6.3 Selectivity

To determine if the selectivity of the method was satisfactory, retention patterns of the reference mixture (GLC793) was compared to a target retention pattern of the same reference mixture

(GLC793) acquired with the original He method. Differences between the RI units of the target pattern and optimized pattern were calculated.

3.6.4 Method application

The optimized and studied method was applied to 245 samples obtained from different pilot-scale tubular PBRs at different days in cultivation in NORCE`s research facilities at Mongstad and Marineholmen. The experiment consisted of three production lines. Only one production line was investigated since the other two had a limited number of samples.

3.7 Method Optimization

The GC-FID method with nitrogen as carrier gas was optimized through and *ad hoc* experimental design (described in section 2.13) investigating 16 different carrier gas velocities and 4 different temperature rates. Other conditions were as explained for the N_2 program in Section 3.3. The results obtained with experimental design were analysed using Chrombox O for the development of response surface plots for efficiency (Equation 18), selectivity (Equation 21) and retention time (Equation 20). A table for the experimental conditions used are presented in *Table 3. 1*.

Table 3. 1 Experimental conditions for optimizing efficiency and selectivity.

Experiment no.	Velocity (cm/s)	Temperature Rate(°C/min)
1	8	1
2	9	2
3	10	3
4	11	4
5	12	1
6	13	2
7	14	3
8	15	4
9	16	1
10	17	2
11	18	3
12	19	4
13	20	1
14	21	2
15	22	3
16	23	4

3.8 Significant figures

To determine the appropriate number of significant figures for reporting results, the precision of the internal standard utilized during sample preparation was evaluated. In this study, the internal standard contained 4.176 mg/ml of 23:0 FAME. Consequently, it is advisable to limit the results to no more than four significant figures.

Furthermore, it is crucial to consider any disparities in peak widths at baseline when analysing chromatograms. In the case of sample 35 and 36, both possessing identical dry weights and being subjected to the same analytical method, the investigation is focused on the 16:0 and 16:2 n-4 peaks. While the 16:0 peak is automatically integrated in the chromatograms, the 16:2 n-4 peaks typically require manual integration due to the presence of a shoulder, indicative of impurity within the peak.

For both peaks, the uncertainties extended to the fourth decimal place. Consequently, four significant figures are chosen to report the results, ensuring accuracy while avoiding excessive precision.

4 Results and Discussion

4.1 Method Optimization

The following section presents the results and discussion of the optimization of a GC-FID method with nitrogen as carrier gas conducted on a 30 m BPX70 column with and internal diameter of 0.22 mm, phase thickness of 0.25 µm, and a start temperature of 150℃. A method with helium as carrier gas is used as target for efficiency and selectivity. Models of efficiency, retention time and selectivity were developed and combined to optimize temperature rate and carrier gas velocity for the method using Chrombox O. The models are calculated based on Equations 18, 20 and 21. The method is optimized according to the fatty acid profile of the reference sample, GLC793 mix and EFF mix. A temperature rate of 1 ℃/min and a carrier gas velocity of 12 cm/s resulted in the optimal efficiency and selectivity with an analysis time of about 65 min. These conditions provided similar selectivity and slightly higher efficiency compared with the helium method, but with the cost of increased analysis time.

4.1.1 Model of efficiency

The response surface depicted in *Figure 4. 1* illustrates the relationship between the average peak widths in retention index units (w_b, ECL) and the interplay of carrier gas velocity and temperature rate of the analysed fatty acids in the EFF mix sample. The model of efficiency is calculated based on Equation 18.

The surface plot showcases the aggregated outcomes of individual models, originally established for each compound. Notably, a consistent pattern emerges across all sixteen experiments. The influence of temperature rate on efficiency outweighs that of carrier gas velocity. This trend is present in both *Figure 4. 1* and *Figure 4. 2*, where the efficiency decreases (increased w_b, ECL) with higher temperature rates at any given carrier gas velocity. When transitioning from higher to lower carrier gas velocities a minimum in w_b, ECL at various temperature rates is exposed. This minimum signifies the optimal carrier gas velocity, denoted as u_{opt}, and is calculated using Equation 19.

The grey line traversing the isolines on the graph intersects u_{opt} at different temperature rates.

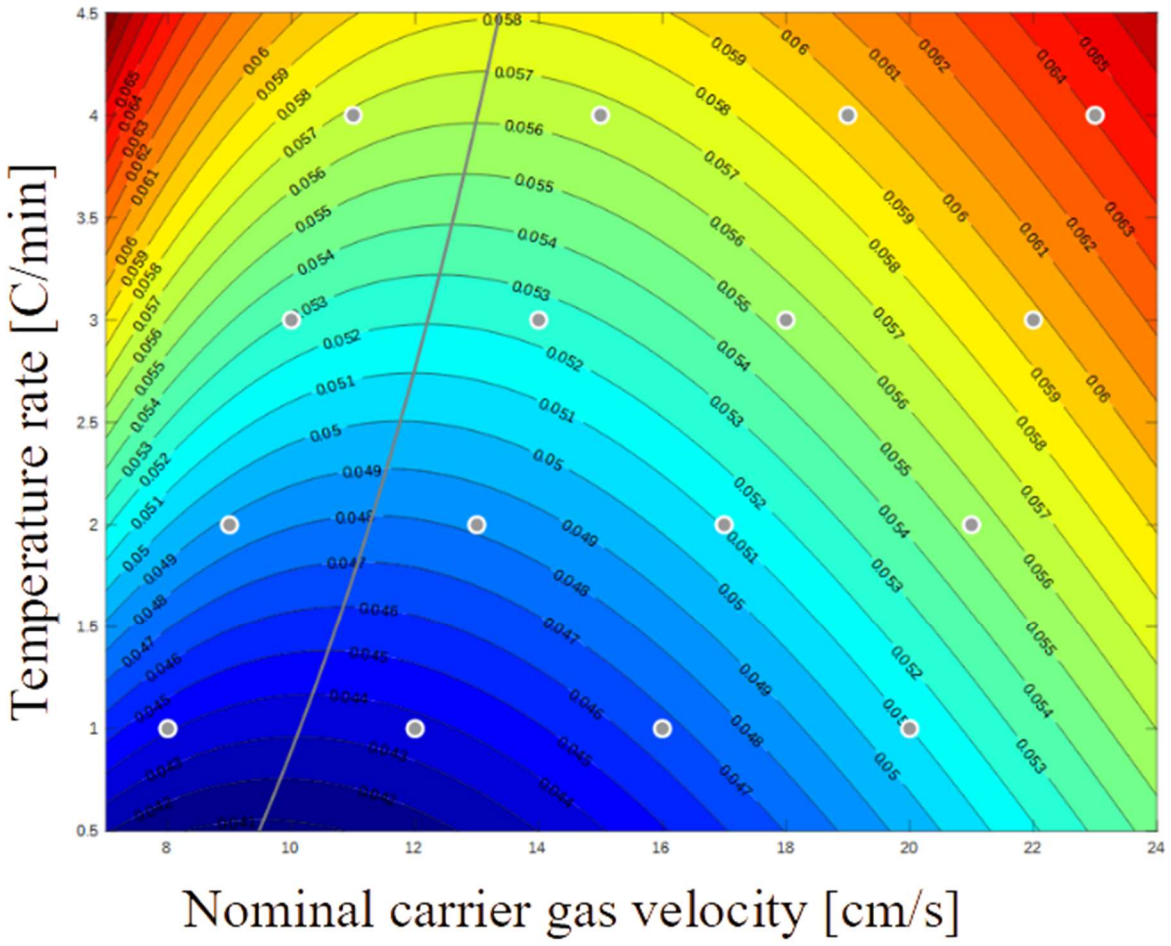

Figure 4. 1 Model of efficiency. Response surface plot for peak widths in retention index units (w_b, ECL). The experimental conditions are indicated by dots, and the optimal velocities (u_{opt}) are represented by a grey curve. C12 and C26 are excluded.

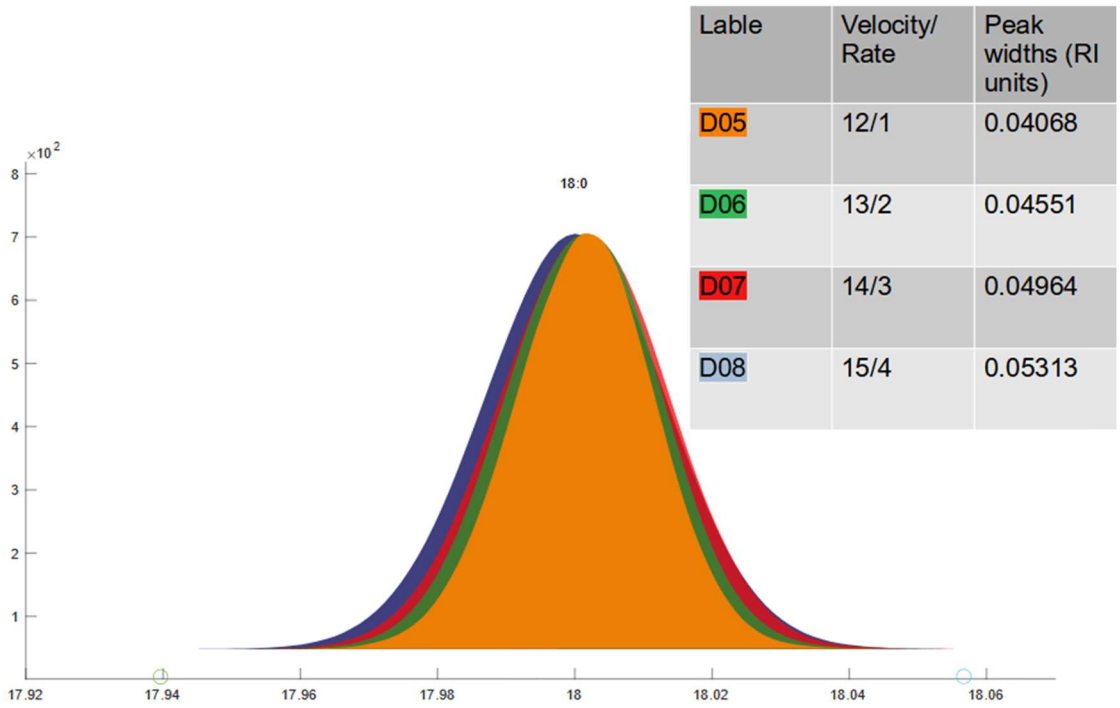

Lable	Velocity/ Rate	Peak widths (RI units)
D05	12/1	0.04068
D06	13/2	0.04551
D07	14/3	0.04964
D08	15/4	0.05313

Figure 4. 2: Stacked representation of FAME 18:0 peaks, corresponding to distinct temperature rates and carrier gas velocities illustrating that the peak widths increase with increasing temperature rate and carrier gas velocity.

Narrower peak widths are indicative of increased chromatographic efficiency. Consequently, lower temperature rates and mobile phase velocities results in enhanced efficiency due to narrower peaks. While elevated temperature rates expedite analysis time, they correspondingly compromise efficiency.

In the context of temperature-programmed GC, as temperature rises, column efficiency in compound separation diminishes, particularly pronounced at higher temperature ramp rates. Nonetheless, if carrier gas flow is accelerated, compounds traverse a longer column stretch before experiencing this effect. This explains the higher optimal carrier gas velocity observed at elevated temperature rates (10).

4.1.2 Model of retention time

Figure 4. 3, shows a response surface plot for the retention time of the last eluting compound, 26:0, calculated from Equation 20. From the figure it is obvious that increasing the temperature rate results in a significant decrease in retention times, whereas higher carrier gas velocities have a minor effect on this parameter. In optimizing a GC method, there is usually a balance

between efficiency and time. Combining the models of w_b, ECL (efficiency), and retention time gives valuable insights for selecting the best chromatographic conditions (Figure 4. 4).

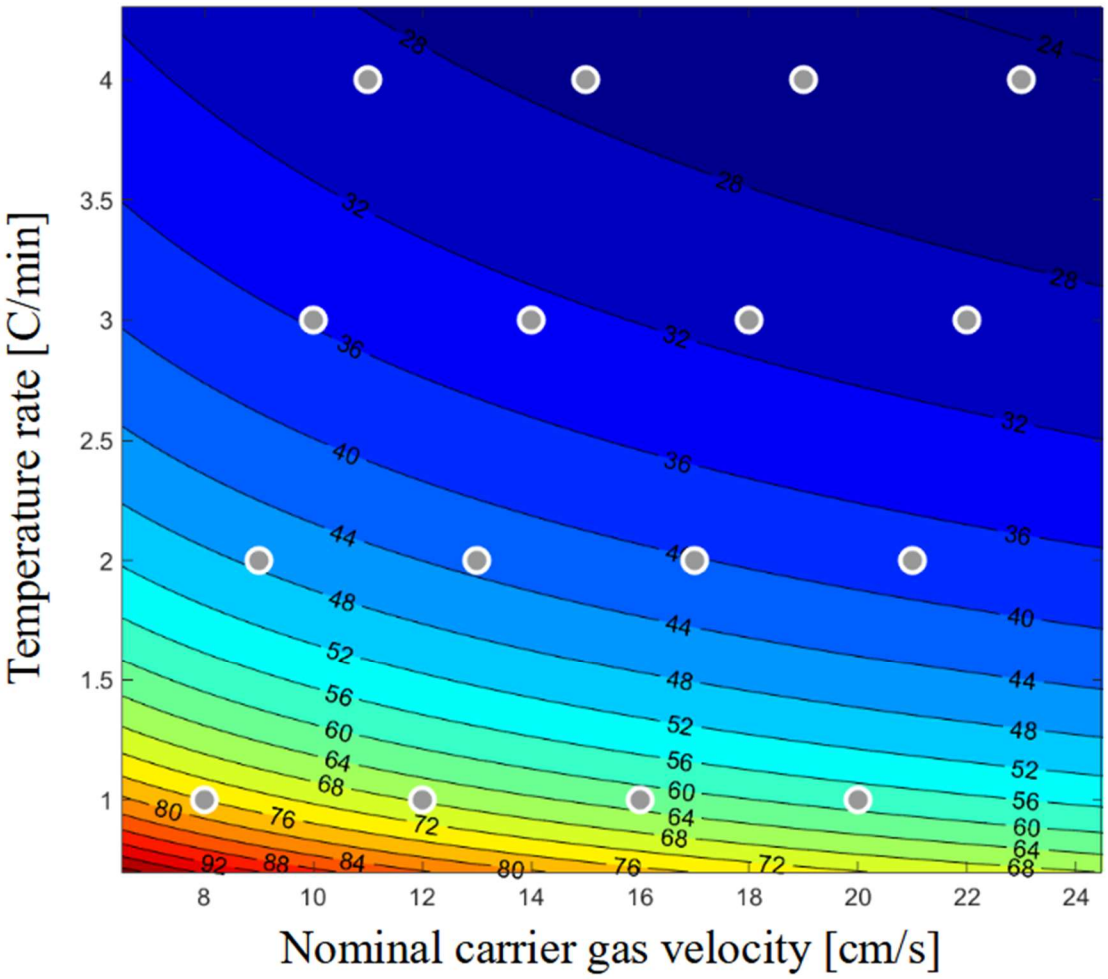

Figure 4. 3: Response surface plot for retention time of 26:0, grey dots indicate experimental conditions. The retention time decreases with increasing temperature rate.

4.1.3 Combined model of retention time and efficiency

The response surface plot depicted in *Figure 4. 4* illustrates how both retention time of the last compound and efficiency depend on carrier gas velocity and temperature ramp rate. The line that marks the optimal carrier gas velocity (u_{opt}) and the isolines from *Figure 4. 1* (white) are combined with the retention time response surface from *Figure 4. 3*. The black dots on these isolines are where the retention time model predicts a minimum by following each of the white isolines. These conditions were found by an iterative procedure in Chrombox O. The black curve fitted through these points by a spline function represents optimal conditions with respect

to time and chromatographic efficiency. For any combination of velocity and temperature rate that is not on the black curve it is possible to find conditions that are equally fast but more efficient, or equally efficient but faster.

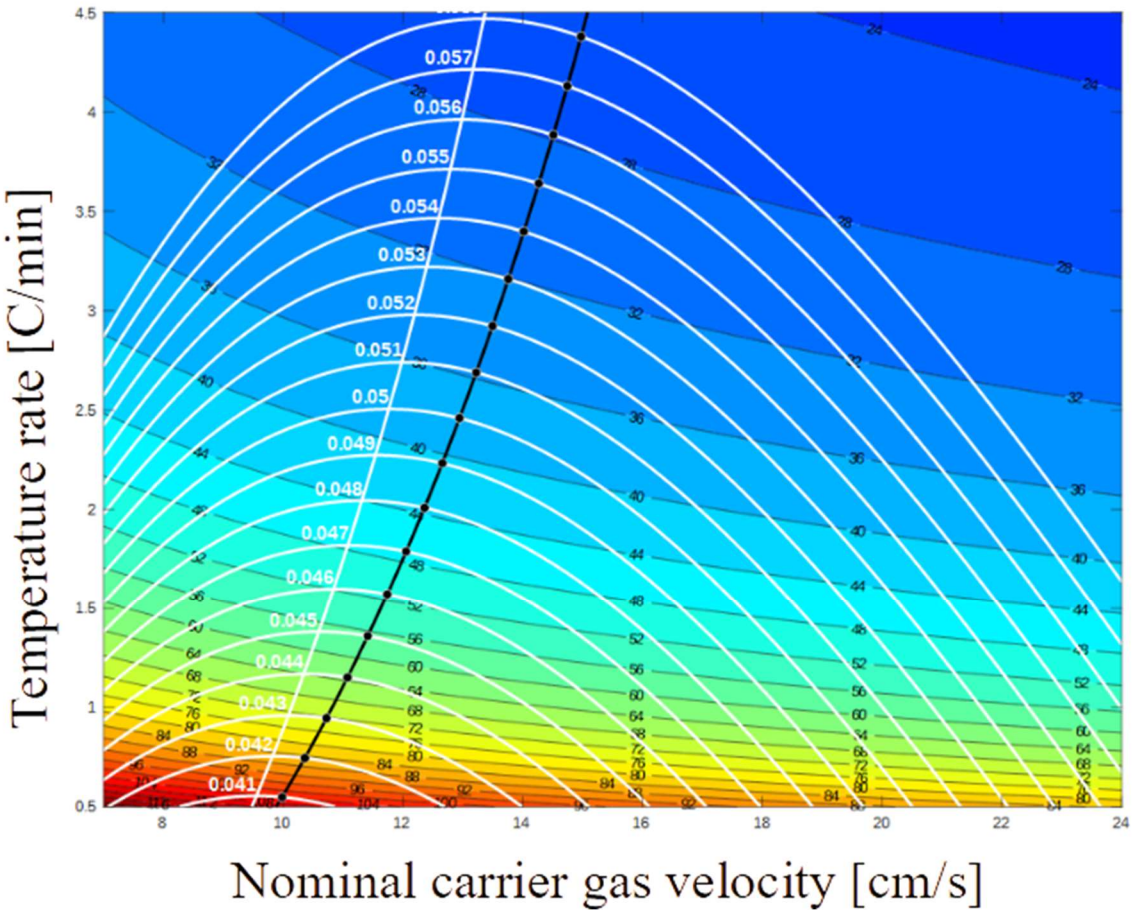

*Figure 4. 4: Most relevant isolines from (*Figure 4. 1 Model of efficiency*) superimposed on the response surface of retention time (Figure 4. 3). The minimum isolines from the average efficiency model of the response surface for the retention time are denoted by black dots. The x-axis values of these points correspond to the time optimal velocities (u_{opt}), and the conditions along the black curve are deemed optimal.*

4.1.4 Model of selectivity

To model the selectivity, a model was made for each of the fatty acids in the GLC793 sample based on Equation 21. The target values were then subtracted from the models, where the target values are equivalent ECL values for a GLC793 chromatogram obtained with the helium method. The response surface depicts the average absolute deviation from the target for each of the models. The same procedure as in Chhaganlal et al. (11) was used to model selectivity, but

in this study the carrier gas velocity was varied instead of the start temperature. The response surface plot in Figure 4. 5 provides insight into how the selectivity is influenced by both the temperature rate and carrier gas velocity. Along the dark blue area, the highest level of separation occurs, where the green dot represents the optimal selectivity. According to the selectivity model, the optimal selectivity is achieved with a carrier gas velocity of 18.86 cm/s and a temperature rate of 1.702 °C/min. The differences between the target selectivity and optimal selectivity is summarised in *Table B. 1, Appendix B.*

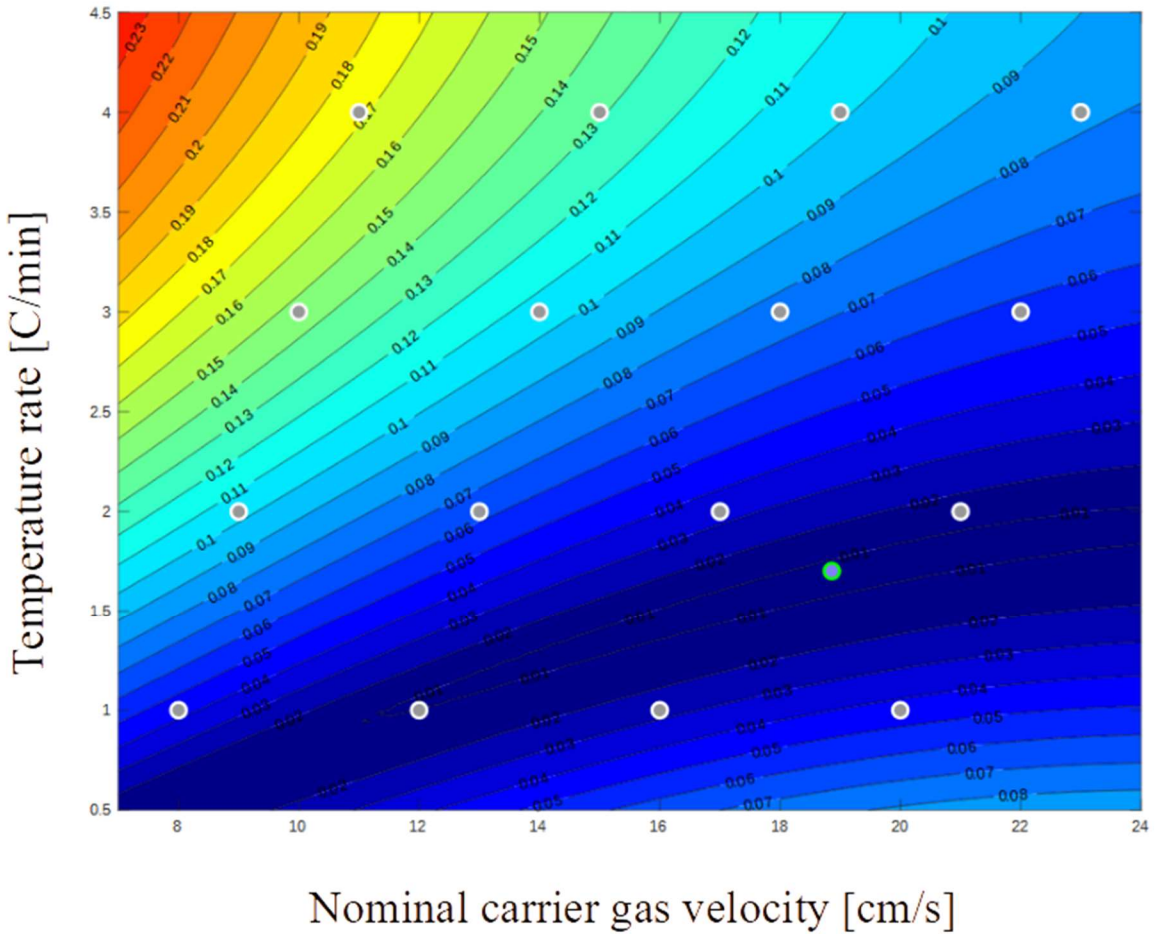

Figure 4. 5 Model of selectivity. Response surface plot of selectivity. The selectivity is mainly influenced by temperature rate. 14:1 n-5, 20:3 n-3, 20:4 n-6, 22:4 n-6 are excluded because they overlap.

In the same way as efficiency, the selectivity is mainly influenced by the temperature rate. The surface plot above illustrates that with higher temperature rates the selectivity becomes more different from the target, while the carrier gas velocity has less impact. This is also illustrated in Figure B. 2 *(Appendix B)* where the separation between the closely eluting peaks decreases as the temperature rate increases. This becomes clearer for late eluting compounds, where some

of the peaks elutes so close to one another that they are registered as one peak (for example at 14 cm/s and 2 °C/min). In all chromatograms in Figure B. 2 *(Appendix B),* the poorest separation is located around 22 RI units, where the peaks elute extremely close. As the temperature rate increases, the peaks elute closer and closer to each other, resulting in poor separation between the FAMEs.

It is important to note that optimal selectivity might not result in the best efficiency, therefore the ideal balance between optimal selectivity and efficiency proves to be the best solution. This aspect is investigated in the subsequent sections.

4.1.5 Combination of models of efficiency and selectivity

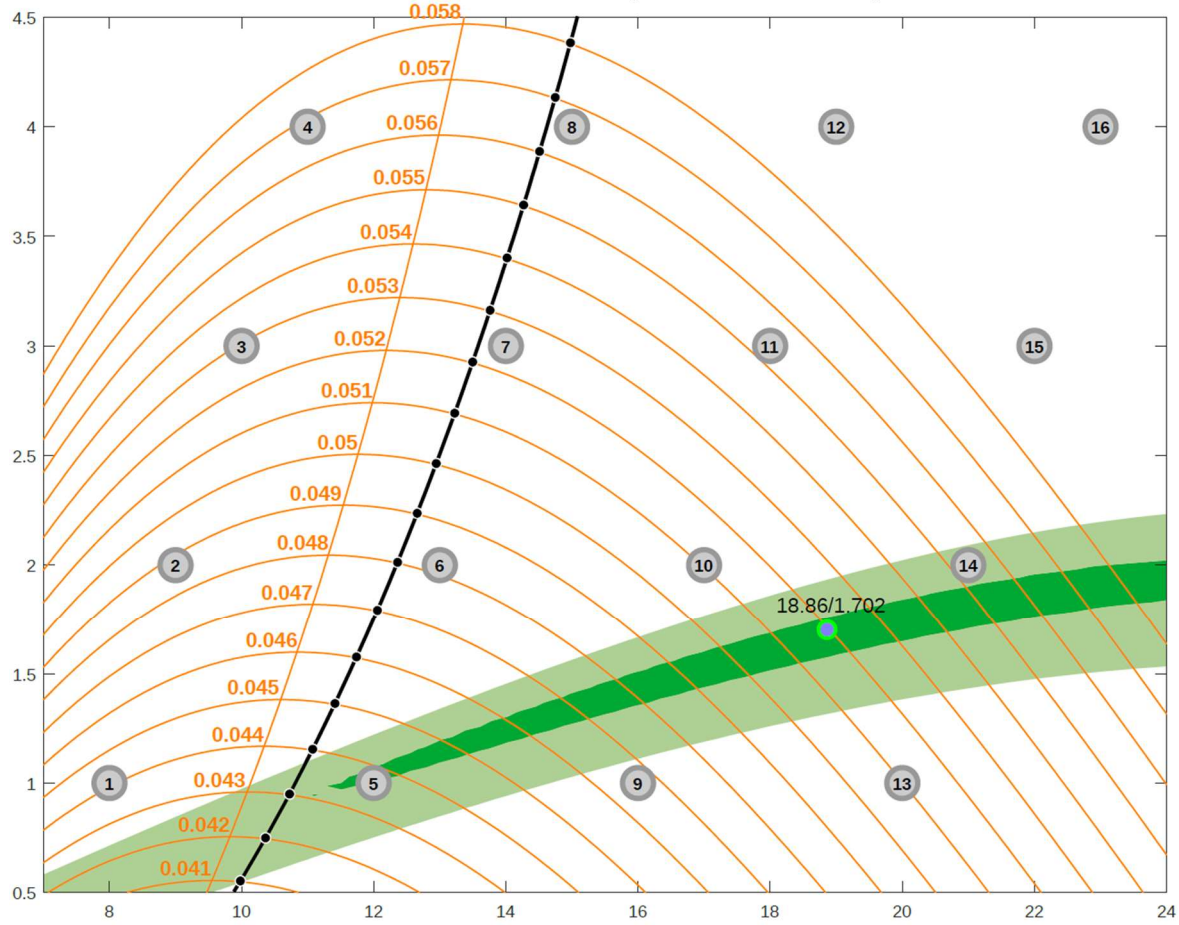

*Figure 4. 6: Combination plot of efficiency (*Figure 4. 1*) and selectivity (*Figure 4. 5*). The two green areas in the plot represents the areas in* Figure 4. 5 *where the average deviation in ECL values is less than 0.02 (light green) and less than 0.01 (dark green).*

In this section, the insights from Figure 4. 1 and Figure 4. 5 are united. This merge provides a robust foundation for suggesting new experiments aimed at method optimization. The green

field illustrates the optimal selectivity, whereas the black line illustrates the optimal efficiency at different temperature rates. The combined plot clearly states that optimal selectivity does not inherently lead to good efficiency, and vice a versa. Instead, a compromise between optimal selectivity and efficiency yields a solution that strikes a balance between these two factors.

In the quest for method optimization, the information obtained from Figure 4. 6 is leveraged to design four new experiments. The selection of temperature rates and carrier gas velocities are given in Table 4. 1.

Table 4. 1: Additional experiments selected from Figure 4. 6, where experiment 5 in Figure 4. 6 *corresponds to the carrier gas velocity of 12 cm/s and temperature rate of 1* ℃ */min.*

Temperature rate (cm/s)	**Velocity (℃/min)**
1.351	15.43
1.3	14
1.702	18.86
1	12

The selected experimental conditions above cluster along the distinct dark green belt in the combined plot. It's important to remain relatively close to the black line where the efficiency is optimal while also staying close to the dark green belt, where the selectivity is at its best. The light blue dot in the plot marks the point of optimal selectivity at 18.86 cm/s and 1.702 ℃/min. Despite its significant distance to the optimal efficiency (black line), it is investigated to assess the extent of efficiency loss when moving closer to the selectivity optimum. The loss of efficiency comes from higher temperature rates and carrier gas velocities when moving closer to the selectivity optimum. (Figure 4. 6*, blue point*)

4.1.6 Optimized method

4.1.6.1 Evaluation of efficiency

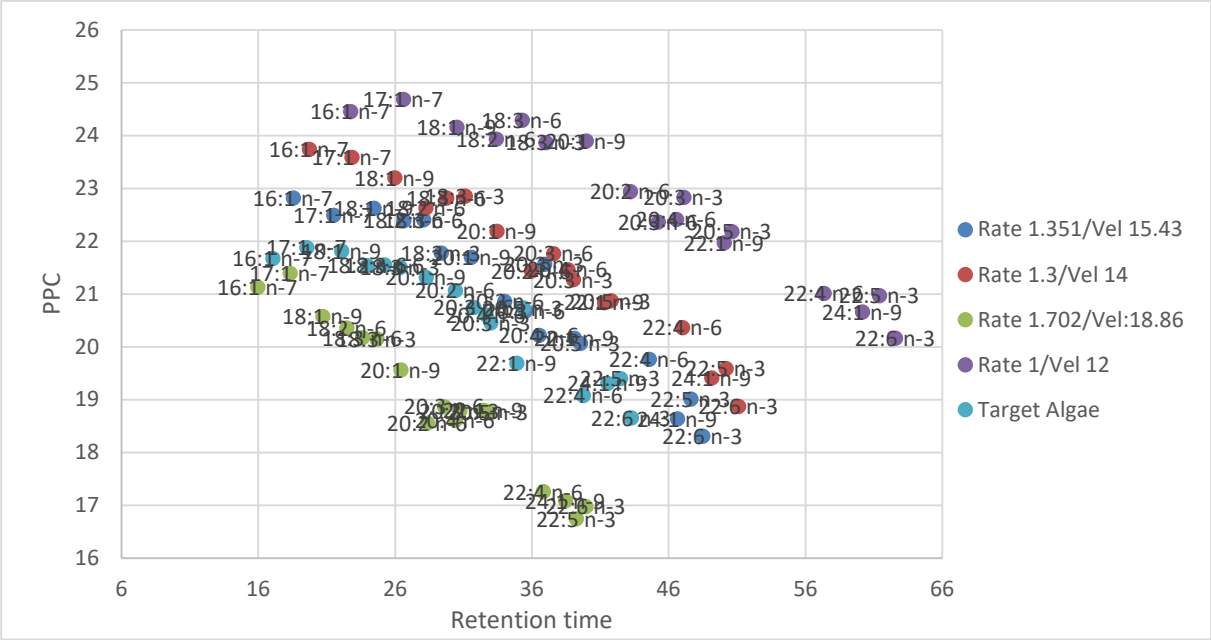

Figure 4. 7 Evaluation of efficiency. Retention time and PPC plotted against each other for different temperature rates and carrier gas velocities for a collection of FAMEs. All saturated FAMEs and 14:1 n-5 are removed. (Full plot in Appendix, Figure B. 1).

In Figure 4. 7, retention time and PPC of FAMEs for the experimental conditions in *Table 4. 1* are plotted against each other. In the plot, a trend announces itself. The first eluting FAMEs has the highest PPC, meaning they are well separated. With increasing retention time, the PPC decreases and thereby the efficiency decreases. For a temperature rate of 1 °C/min and a carrier gas velocity of 12 cm/s, the PPC is highest for all FAMEs compared to the other conditions, and therefore has the highest efficiency. What was aimed for in this test was to come closest to the target method (helium). A temperature rate of 1.351 and a velocity of 15.43 gave the closest fit to the target method (helium) with a slightly higher average PPC, meaning that it is more efficient than what was aimed for. The slightly higher PPC in the optimized method can also be explained by the state of the column in the target method used in the analysis, which is starting to get old.

The next step is to conclude with an optimized temperature rate and mobile phase velocity considering the selectivity and efficiency. From the combination plot above (*Figure 4. 6*) the experiment with a temperature rate of 1°C/min and a carrier gas velocity of 12 cm/s is closest to the black line and is also located on the dark green belt. This means that the efficiency is close to its optimum and the selectivity is close to the optimum. This is also shown in the plot

above where the PPC is highest for all the FAMEs compared to the other conditions, indicating a higher efficiency. However, the optimal conditions is more time consuming. With a carrier gas velocity of 12 cm/s and a temperature rate of 1 ℃/min, it takes about 65 minutes for all the FAMEs to elute.

If time is of the essence, it is possible to apply the operational conditions closest to the target method (helium) with a carrier gas velocity of 15.43 cm/s and a temperature ramp rate of 1.351℃/min. Applying these conditions will save about 20 minutes but will result in loss of efficiency as one moves further from the black line in the summary plot (*Figure 4. 6*).

For the next experiments in this thesis a temperature rate of 1 ℃/min and a mobile phase velocity of 12 cm/s is used since keeping the efficiency was regarded most critical.

4.1.6.2 Evaluation of separation

The chromatograms below (Figure 4. 8) are chromatograms of the target retention pattern and the retention pattern of the optimized method (12 cm/s and 1 ℃/min). The chromatograms show minor difference in their retention pattern, indicating that the optimized method (12 cm/s and 1 ℃/min) provides good separation between the FAMEs. The optimized method actually shows slightly better separation between some of the peaks than for the target retention pattern. This is most likely due to the state of the column of the target method. An old column can result in reduced separation due to peak tailing.

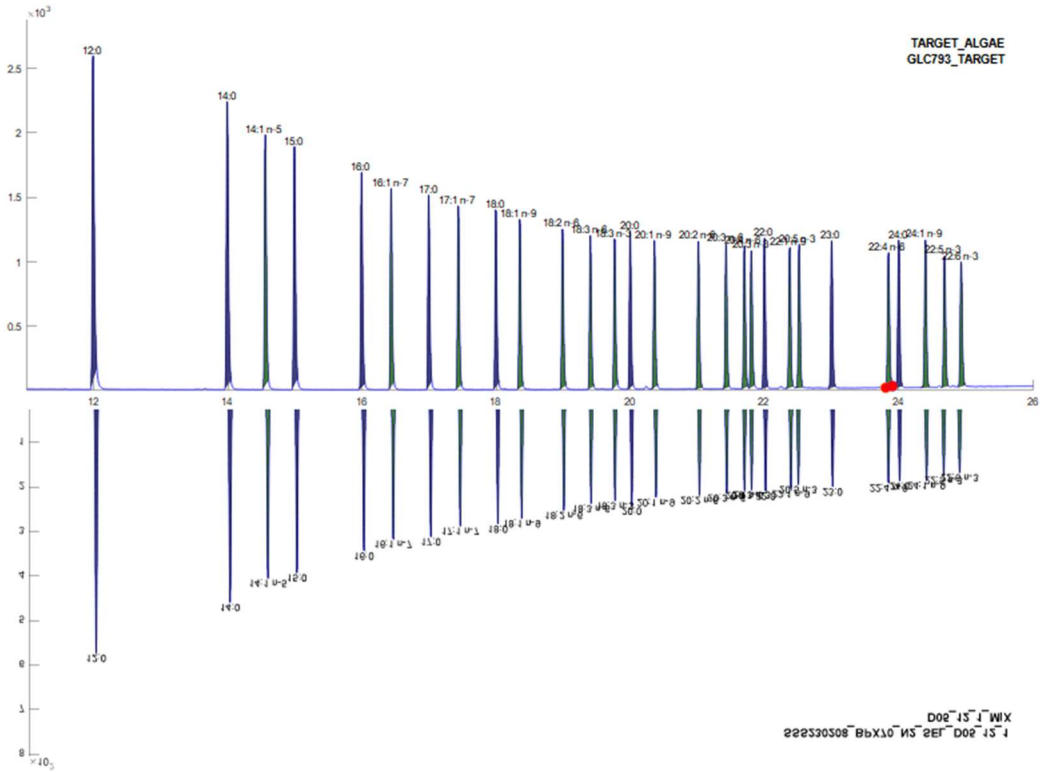

Figure 4. 8: Comparison of retention pattern of the target pattern and the optimized pattern. The optimized pattern is rotated 180° and placed below the target pattern for visual comparison.

The separation of the optimized method (12 cm/s and 1 ℃/min) is satisfactory when compared to the target pattern`s RI units. The difference between the target RI units and optimized RI units (*Table 4. 2*), as well as the difference between the target RI units and the optimal selectivity RI units, does not deviate with more than 0.1 for any FAME. This indicates minimal loss of separation for the optimized method.

Table 4. 2 Differences between target method`s RI units and optimized method`s RI units.

FAME	Target He	Opt N_2	Diff
16:1 n-7	16.48	16.44	0.04
17:1 n-7	17.48	17.44	0.04
18:1 n-9	18.40	18.36	0.04
18:2 n-6	19.05	18.99	0.06
18:3 n-3	19.83	19.75	0.08
18:3 n-6	19.47	19.39	0.08
20:1 n-9	20.40	20.36	0.04
20:2 n-6	21.06	21.01	0.05
20:3 n-6	21.49	21.42	0.07
20:5 n-3	22.59	22.49	0.10
22:1 n-9	22.41	22.38	0.03
22:5 n-3	24.74	24.66	0.08
22:6 n-3	24.99	24.90	0.09
24:1 n-9	24.43	24.40	0.03

4.2 Comparative analysis of quantitative data for microalgal samples analysed by the original He method and the optimized N2 method

The following section presents the results and discussion of the comparison of the optimized N_2 method to the original He method. Multiple statistical analyses were conducted to evaluate the optimized N_2 method in comparison to the original He method, including PCA, univariate plots, etc. A score plot of the samples analysed with both methods indicated that the methods provided similar results, except for two samples. These samples were investigated further to identify their difference, revealing problems with integration of some peaks, and adjacent peaks causing interferences. Accuracy and bias were also evaluated, revealing adequate accuracy with a systematic bias of under 10% for most of the fatty acids The fatty acids with low concentrations in the samples were highly biased. Additionally, the precision was estimated for intermediate precision, repeatability and injection repeatability and provided good results with precision below 6% for all estimates. The methods were investigated for significant differences in variation of absolute amounts where most of the fatty acids had significant variation. The cause of these variations are investigated in section 4.3 Troubleshooting.

In the following sections, the original He method and optimized N_2 method will be referred to as the He-method and the N_2-method, respectively.

4.2.1 Principal component analysis

Figure 4. 9 shows the principal component analysis (PCA) of two groups of samples; samples analysed with the He-method, and samples analysed with the N_2-method. The groups are organized in different colours to match their respective methods. Blue is the He-method, and green is the N_2-method. Short names for the respective fatty acids are depicted in the loadings plot with a red point showing their loadings.

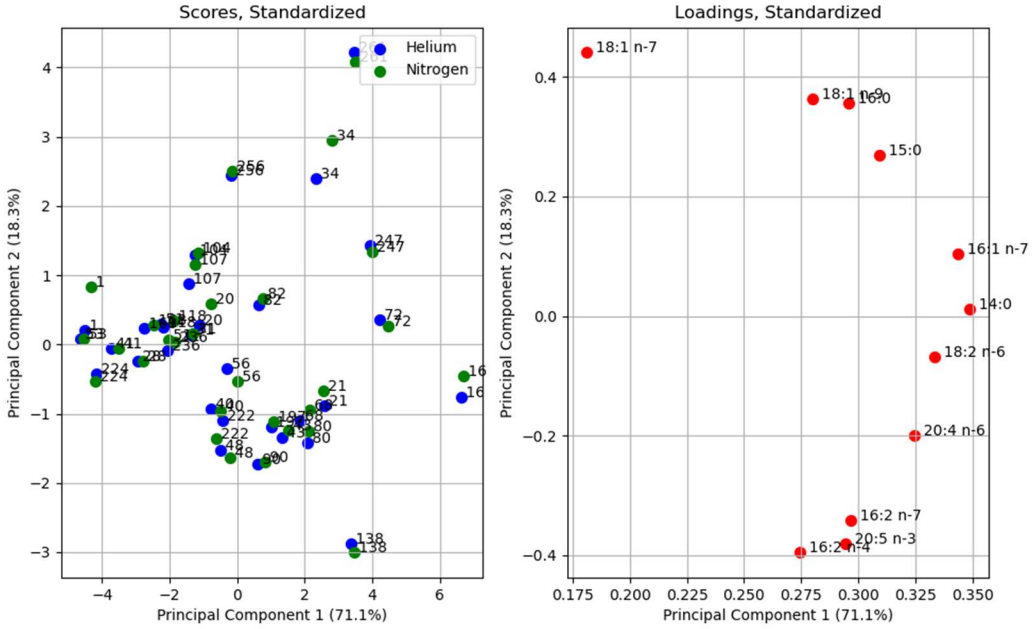

Figure 4. 9: PCA analysis of GC-FID method with helium and nitrogen as carrier gas. Amounts of fatty acids are standardized, score and loading plots are depicted above.

In the score and loading plot (*Figure 4. 9*), PC1 accounts for about 70 % of the total variance, establishing it as the most important component in these plots, and PC2 explaining about 18% of the total variance. Within the loading plot, the variables are distributed far from origo, which shows that they are well explained by the principal components.

In the scores plot, the majority of the samples from the two methods are placed close or on top of each other, indicating that the methods yield relatively similar quantities for the same sample. However, there are notable exceptions. Samples 1 and 34 exhibits a greater distance between them, suggesting a dissimilarity beyond the desired level. In the rest of this section sample 1 is excluded due to an error in sample preparation.

Figure 4. 10 depicts a bar chart comparing sample 34 analysed using the He-method and the N_2-method. The bar chart provides a quantitative representation of the variations within the same sample analysed using the He-method and the N_2-method.

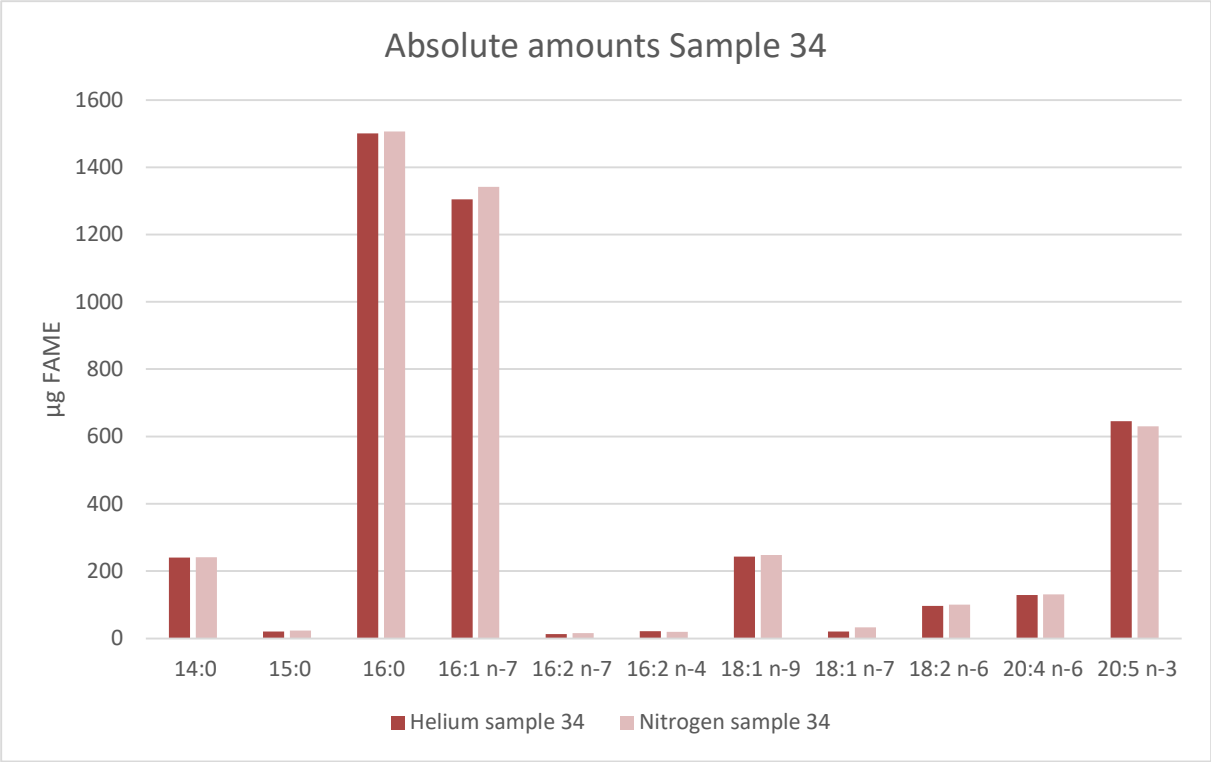

Figure 4. 10: Bar chart for the comparison of sample 34 analysed with the He-method and the N_2-method in absolute amounts.

Differences are visually observed in the absolute amounts of 16:1 n-7 and 18:1 n-7 when comparing sample 34 analysed for both methods (*Figure 4. 10*). A strong linear relationship (both absolute and relative amounts) in 16:1 n-7 is present when plotting the amounts quantified for both methods (*Appendix C,* Figure C. 1 *and Figure C. 3*), with a correlation coefficient of 0.999 and a R-squared value of 0.997 for the absolute amounts (*Table C. 1*, *Appendix C*). The difference for sample 34 is not that big and is most likely due to a close eluting compound interfering with the integration and thereby quantification.

The R-squared value of 18:1 n-7 is lower, $R^2 = 0.922$ (*see Appendix C*, *Figure C. 3),* indicating variations in quantification for all samples due to its low concentration. This is also the case for 15:0 and 16:2 n-7. The fatty acids in low concentrations have smaller peaks, leading to greater variation in the quantification. This is likely due to manual integration, closely eluting compounds interfering with quantification and baseline noise.

4.2.2 Accuracy

When estimating accuracy, bias is also determined. When bias is established, it is common practice to correct the data obtained from the method. Correcting the data for bias is not conducted in this case, because the true value is unknown. The He-method was used as reference method when estimating accuracy but is not a certified reference method. Nor was certified reference material applied. Additionally, the samples were not analysed on the same instrument, and the columns were different both in length and age. Correcting for bias in this case would lead to results with high uncertainty, because the correction would be based on assumptions and estimates containing uncertainty as well. In this study the accuracy is defined as the degree of agreement between results of the N_2-method and reference method (He-method), while bias is defined as the systematic difference between the results from the N_2-method and He-method. The accuracy and bias of the N_2-method is therefore a rough estimate since the true value is unknown.

Figure 4. 11 illustrates a strong linear relationship and correlation between the sum of absolute amounts of fatty acids between the He-method and the N_2-method. Similar plots for each FA in absolute amounts and relative amounts can be found in *Appendix C,* Figure C. 1 *and Figure C. 3*. R-squared values, slopes and intercepts for the linear relationships of the FAs are summarised in and *Table C. 1*, *Appendix C* for relative amounts and absolute amounts, respectively. The data points follow a straight line suggesting that there is a consistent proportional change in the total absolute amount of fatty acids for the methods. A linear relationship can imply that the choice of carrier gas (nitrogen or helium) does not significantly affect the sum of absolute amount of fatty acids being measured. This could be a positive outcome, indicating that the methods are comparable and produce consistent results regardless of the carrier gas being used. However, it is important to confirm linearity by checking the residuals. All residuals of the individual fatty acids show minimal heteroscedasticity (*Figure C. 4, Appendix C*). This means that the linearity plots (which also provide information about bias) should not be affected by heteroscedasticity. Therefore, there is no evidence to suggest that the estimates of accuracy and bias (slope and intercept) are unreliable.

The equation in *Figure 4. 11* has a slope of about 0.97 and estimates the accuracy of the method. The N_2-method therefore quantifies the total amount of fatty acids with about 97% accuracy. The intercept in the equation is approx. 108 and estimates the bias. This means that the results from the N_2-method is systematically higher than the results from the He-method with an

average of 108 µg. This is no more than about 10% bias for the lowest concentrations gradually decreasing as the concentration increases.

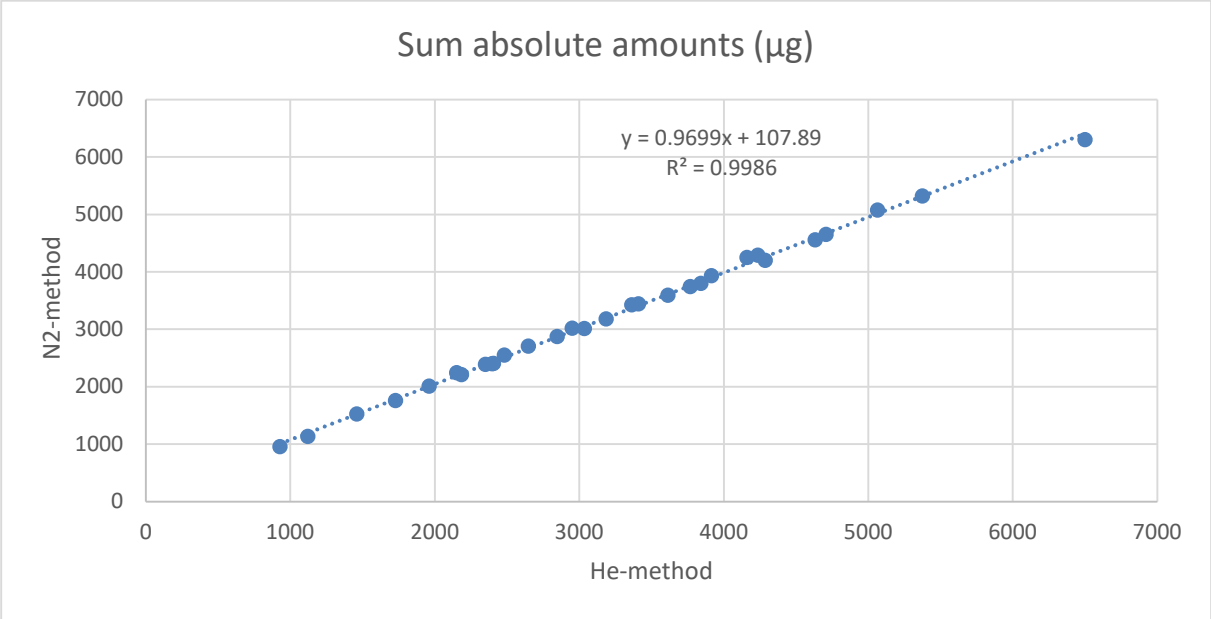

Figure 4. 11 Sum of absolute amounts of fatty acids plotted against each other for each method. The plot describes the accuracy and bias of the N_2-method where the He-method is used as reference.

Table 4. 3 summarizes the detailed statistics of the method comparison for each fatty acid in relative amounts. In *Table 4. 3*, the differences between the methods appear. The fatty acids 15:0, 16:2 n-7, 16:2 n-4 and 18:1 n-7 all have R-squared values below 0.99. These fatty acids provide small peaks in the chromatograms for all samples, indicating that the N_2-method provides less accuracy for quantification of low concentrations of fatty acids.

For quantification of fatty acids with higher concentrations, the N_2-method provides correlation coefficients and R-squared values close to 1, indicating that the N_2-method could be used as an appropriate alternative to the He-method for samples with high concentrations of fatty acids. However, the bias of these indications must be investigated.
Detailed statistics for the method comparison for each FAs in absolute amounts can be found in the appendix *(Table C. 1, Appendix C).*

Table 4. 3 Detailed statistics of relative amounts of FAMEs. Correlation coefficients (r), R^2 and equations for relative amounts for each method plotted against each other.

FAME	r	R^2	Slope	Intercept
14:0	0.9955	0.9910	1.013	-0.0490
15:0	0.8457	0.7153	1.089	0.0046
16:0	0.9997	0.9994	0.9735	0.5696
16:1 n-7	0.9978	0.9956	1.014	-0.0091
16:2 n-7	0.9547	0.9114	1.002	0.0428
16:2 n-4	0.9813	0.9630	1.039	-0.0195
18:1 n-9	0.9995	0.9990	1.012	0.0196
18:1 n-7	0.9601	0.9217	1.145	0.0360
18:2 n-6	0.9917	0.9835	0.9725	0.1287
20:4 n-6	0.9982	0.9964	0.9914	0.0484
20:5 n-3	0.9996	0.9991	0.9770	-0.0967

Figure 4. 12 depicts a scatter plot of the sum of absolute amounts of FAs of the He-method plotted against the relative difference between the sum of absolute amounts of FAs for both methods. The plot illustrates the relative bias. The x-axis indicates the total quantity of FAs detected using the He-method. The y-axis indicates how much the sum of absolute amounts of FAs for the He-method deviates from the sum of absolute amounts for the N_2-method.

From the plot, low total concentration of total fatty acids results in a higher relative difference between the methods. As the concentration of total fatty acid content increases, the relative difference decreases, eventually moving towards the direction of being negative. The magnitude of the bias changes significantly when moving from about 1000 µg FAs to 7000 µg FAs. This suggests that a constant bias with a considerable magnitude is present at 1000 µg FAs but becomes negligible around 3500 µg FAs and then moving in the negative direction. This confirms systematic bias in one or both methods, being more pronounced when the concentrations are low. The systematic bias is observed for most of the individual FAs (*Figure C. 1*).

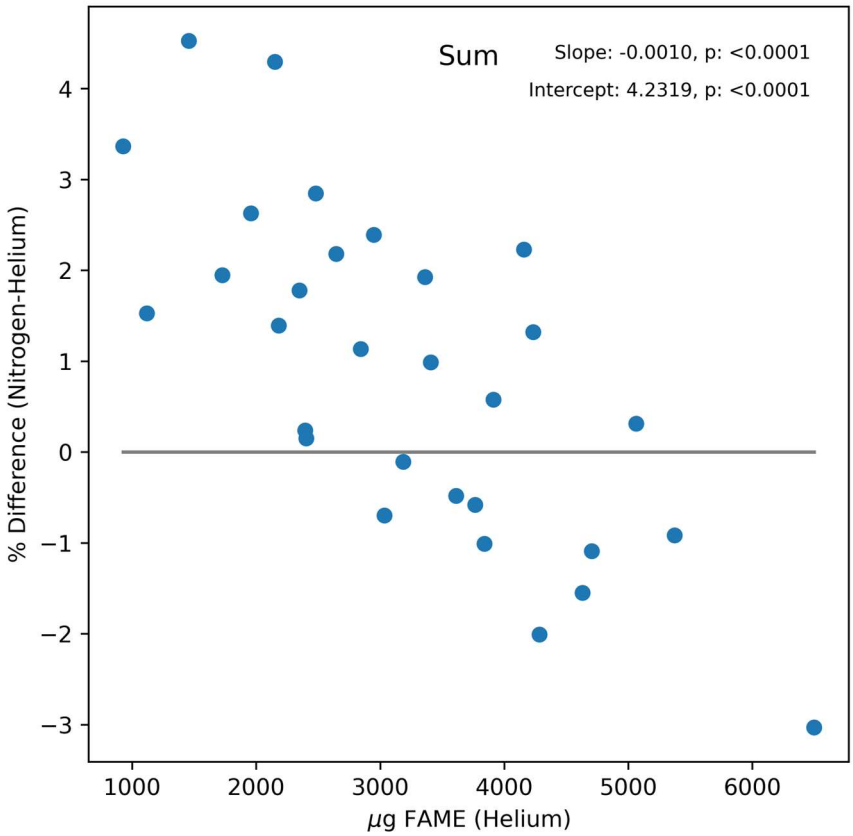

Figure 4. 12: Relative bias. Scatterplot of the sum of absolute amounts of fatty acids of the helium method plotted against the percentage difference between the sum of absolute amounts for both methods. A decreasing trend is revealed.

The relative bias between the methods is not remarkably high, where the highest percentage difference is about 5% and the lowest being about -3%. To investigate if the difference is significant a t-test was conducted. From the plot, the p-values for the slope and the intercept are depicted in the upper right corner. The p-value is 0.0001 for both the slope and intercept. Given a significance level of 5% (Bonferroni corrected α=0.00454) there is significant difference between the methods. A significance test was executed for each individual FA where most of the models were significant for both the slopes and the intercepts. These plots are summarised in *Appendix C,* Figure C. 2. The bias between the methods for the fatty acids are not high and may not be relevant regardless of their significance. However, it should be emphasized that the methods are applied on two separate instruments (with identical configurations). The bias may also be explained by this. The fatty acids 15:0, 16:2 n-7 and 18:1 n-7 has relative biases of 40 to -60%, 25 to -10% and 80 to -1 %, respectively. These are high biases, likely explained by

their small peaks in the chromatograms, manual integration and closely eluting peaks causing interferences. The plots of relative bias do not say anything about the bias being acceptable or not. Acceptable limits must be defined *a priori*, based on biological considerations or other goals (65).

4.2.3 Precision

To estimate the intermediate precision (IP), 9 reference samples (approx. 0.17 g w.w algal paste) of the microalgae "Pavlova" were analysed with the N_2-method. This is a different algae than for the previous experiments. Each sample was prepared and analysed at different days and thereby covering IP for sample preparation and instrument variation.

Repeatability was estimated analysing sample 61 (DW=6.88 mg) of the microalgae *Nannochloropsis,* 10 times in different vials at the same time and day, covering the repeatability of the instrument. The injection repeatability was estimated by analysing the same sample, 10 times from the same vial at the same time and day, covering the repeatability of the injections. Sample 61 was analysed with both the He-method and N_2-method.

4.2.3.1 Intermediate precision

For the results of the reference samples R1-R9, the intermediate precision (RSD_{IP}) varied from 2.387 to 3.260% (*Table 4. 4*). To estimate the intermediate precision, RSD% was calculated for each FA. For the sum of absolute amounts of FAs, a bar chart was created for visual investigation of the data and detection of any obvious outliers. A major outlier was detected in sample R1, with a total amount of FAs twice as large as the other samples. An error in the sample preparation caused this major outlier. Instead of adding 100 µl of internal standard in the sample, 50 µl of IS was added. This resulted in a total quantified amount of FAs twice as large as the rest of the samples. A correction was made for sample R1 by dividing the absolute amounts by 2. A new bar chart was made, and no outliers were detected. Additionally, Grubb`s test was conducted to check for other outliers. No outliers were detected.

An RSD_{IP} of approx. 3% for each FA is low and indicates that the method`s IP is a satisfactory. The IP indicates that the N_2-method is robust, when preparing and analysing samples at different days for the same type of samples. The RSD_{IP}% of the method is quite low. A possible explanation could be the use of nitrogen as carrier gas, contributing to a more stable flame in the FID, leading to less variation in the signal intensity, contributing to enhanced precision in the analytical results (66).

Table 4. 4: Intermediate precision. Average, standard deviation (SD) and relative standard deviation (RSD) for the respective fatty acids for the reference samples R1-R9 analysed with the N_2-method.

FAME	Average µg	SD µg	RSD_{IP}%
12:0	119.7	3.903	3.260
14:0	727.4	20.98	2.884
16:0	664.6	18.45	2.776
16:1 n-7	187.8	5.302	2.824
16:1 n-5	67.73	1.872	2.763
18:1 n-9	292.3	7.401	2.532
18:4 n-3	190.0	5.300	2.789
20:5 n-3	361.3	9.995	2.766
22:5 n-6	112.6	3.286	2.917
22:6 n-3	1316	41.11	3.123
Sum of FAME	4040	111.6	2.762

4.2.3.2 Repeatability

For the results of sample 61 analysed 10 times from different vials, the repeatability (RSD_R) varied from 0.6523 to 4.648% (*Table 4. 5*). The precision of the measurements conducted by the same operator, the same instrument, under the same conditions, over a brief period is satisfactory. For the He-method the repeatability ranges from 0.3272 to 11.02% giving a poorer repeatability than the N_2-method. The He method showed some peak tailing, probably due to column ageing. This may have affected the accuracy of integration and could explain the higher RSD_R for some of the peaks within this method. The He-method provides a generally lower RSD_R than for the N_2-method indicating that the repeatability of this method is better for most FAMEs.

Table 4. 5 Repeatability in vials. Average, standard deviation (SD) and relative standard deviation (RSD) for the respective fatty acids for the N_2-method and RSD for the He-method.

FAME	Average µg (N_2)	SD µg (N_2)	RSD_R% (N_2)	RSD_R% (He)
14:0	136.9	6.363	4.648	0.4283
15:0	5.051	0.2151	4.259	11.02
16:0	425.7	19.50	4.581	0.3272
16:1 n-7	646.9	28.26	4.369	0.5435
16:2 n-7	16.51	0.6474	3.921	5.891
16:2 n-4	16.16	0.6618	4.095	3.656
18:1 n-9	38.86	1.526	3.927	0.8303
18:1 n-7	6.187	0.2923	4.724	7.428
18:2 n-6	38.79	1.284	3.310	0.8363
20:4 n-6	99.08	0.6463	0.6523	0.7249
20:5 n-3	605.0	5.035	0.8321	1.029
Sum of FAME	2035	54.11	2.659	0.5055

An F-test was conducted between the amounts of FAMEs quantified by He-method and the N_2-method. The F-test tests the relationship between the variances of the two methods. If the difference in variance of the two methods is greater than what would be expected by chance, there is a statistically significant difference between the methods where the p-value is smaller than "α". This is denoted by "*" in *Table 4. 6* and *Table 4. 8*. The FAMEs 14:0, 15:0, 16:0, 16:1 n-7, 18:1 n-9 and 18:2 n-6 shows significant variations in repeatability.

The N_2-method gives significant variations in the results for samples that should be the same (because they are prepared from the same sample) when they are analysed and compared with the He-method. Significant differences indicates that there is variation between or within the methods when analysing the same sample multiple times. This can be due to instrumental problems, procedure variation or other factors influencing the repeatability of the method, like the column.

Table 4. 6 Significance test repeatability. Significance test for variance of respective fatty acids with F-test between the methods.

FAME	**F-test**	**p-value**
14:0	147.6	2.185e-08*
15:0	8.219	4.369e-03*
16:0	234.5	2.771e-09*
16:1 n-7	78.58	3.570e-07*
16:2 n-7	1.504	0.5530
16:2 n-4	1.230	0.7629
18:1 n-9	26.96	3.694e-05*
18:1 n-7	2.142	0.2720
18:2 n-6	18.66	1.725e-04*
20:4 n-6	1.067	0.9243
20:5 n-3	1.353	0.6599

4.2.3.3 Injection Repeatability

The injection repeatability (RSD_{IR}) for the N_2-method displayed an RSD ranging from 0.4952 to 5.431% (*Table 4. 7*). This indicates that repeated injection of the same sample from the same vial by the N_2-method gives similar results. The injection repeatability for the He-method ranges from 0.5454 to 7.756%, giving a slightly poorer result than the N_2-method. However, the He-method has lower RSD_{IR} than the N2-method for most fatty acids, except from 15:0. The 15:0 FAME also has the highest RSD in the N2-method. This could be explained by the small peak in the chromatograms and a branched alcohol eluting closely, interfering with the quantification.

Table 4. 7 Injection repeatability in vial. Average, standard deviation (SD) and relative standard deviation (RSD) for the respective fatty acids for the N_2-method and RSD for the He-method.

FAME	Average µg (N_2)	SD µg (N_2)	RSD_{IR}% N_2	RSD_{IR}% He
14:0	135.8	6.148	4.527	0.7815
15:0	4.949	0.2688	5.431	7.765
16:0	422.3	18.92	4.480	0.6022
16:1 n-7	642.3	27.42	4.269	0.5993
16:2 n-7	16.18	0.7756	4.794	3.411
16:2 n-4	15.93	0.8620	5.411	3.129
18:1 n-9	38.64	1.615	4.180	0.8050
18:1 n-7	6.058	0.2797	4.617	3.552
18:2 n-6	38.43	1.243	3.235	0.8733
20:4 n-6	99.01	0.4903	0.4952	0.6996
20:5 n-3	605.1	4.246	0.7017	1.012
Sum FAME	2024	53.66	2.651	0.5454

An F-test was conducted between the amounts of FAMEs quantified by He-method and the N_2-method. The FAMEs 14:0, 16:0, 16:1 n-7, 18:1 n-9 and 18:2 n-6 are significantly different in variance, again emphasizing that the N_2-method produce significantly different results compared to the He-method. The same FAMEs as in the repeatability study are significant in this case as well, except for 15:0.

Table 4. 8 Significance test injection repeatability. Significance test for variance of respective fatty acids with F-test between methods.

FAME	F-test	p-value
14:0	41.62	5.745e-06*
15:0	2.451	0.1978
16:0	65.57	7.919e-07*
16:1 n-7	61.14	1.076e-06*
16:2 n-7	2.953	0.1224
16:2 n-4	2.830	0.1372
18:1 n-9	32.63	1.639e-05*
18:1 n-7	2.003	0.3155
18:2 n-6	16.29	3.009e-04*
20:4 n-6	1.731	0.4264
20:5 n-3	1.849	0.3735

An F-test was also conducted between the repeatability sequence and injection repeatability sequence to establish any significant differences in injecting from different vials vs the same

vial when analysing with the same method. The tests resulted in no significant differences in injecting from different vials vs the same vial for the methods.

From the results presented above, significant differences between the methods are established. This is most likely due to instrument variation since the two methods were run on separate instruments. The He-method also have high RSD% in repeatability for the fatty acids with low concentrations (15:0 and 18:1 n-7) compared to the N_2-method. The column in the He-method is older than the one in the N_2-method, likely contributing to the differences in variation of 15:0 and 18:1 n-7.

4.3 Troubleshooting

In the precision study, significant variations between the methods were established. This is investigated further in this section. For the repeatability and injection repeatability study, the sum of each individual fatty acid and the sum of fatty acid content revealed a trend when plotted in a bar graph for the N_2-method. The trend shows that the amount of fatty acids decreases in the sample sequence (*Figure 4. 13*). Where the samples contain the same amount of analyte.

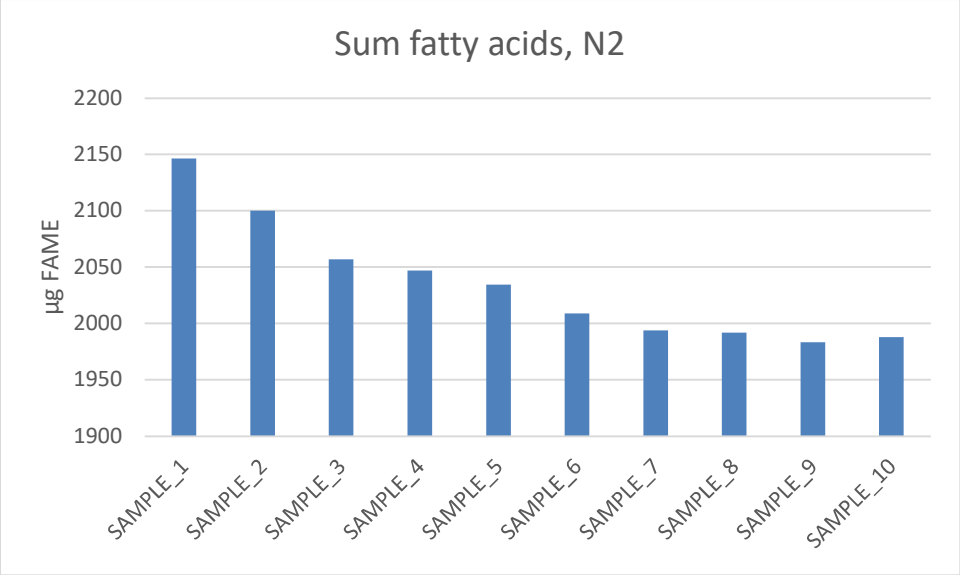

Figure 4. 13: Sum of total fatty acid content in the injection repeatability sample sequence of the N_2-method. A trend where the total amount of fatty acid content decreases reveals itself.

To find the cause of this trend, the raw areas of the N_2-method are investigated. The cause of the decrease moving further down the sequence could be due to the increase in raw areas. They increase more for the heavy fatty acids than for the light fatty acids. Some increase will always be present due to evaporation of solvent when injecting multiple times from the same vial (injection repeatability) due to increase in concentration. However, the change is over 20% for the heaviest fatty acids, which is more than what can be explained by evaporation. Additionally, there were no visually observable change in the volume of the vials. Evaporation of the solvent should also affect all FAMEs in the mixture equally, which it does not. The effect is also present when injecting from different vials (repeatability), but not as clearly. This cannot be explained by evaporation. The effect is also shown in the GCL793 mix (reference samples) analysed within the sequence runs of the repeatability and injection repeatability.

To account for instrument malfunctions, the instrument (N_2) was checked for leaks, the septum was replaced, and the samples in the repeatability and injection repeatability study were analysed again for the N_2-method. The repeatability for the new test had an RSD_R ranging from 0.38 to 7.43% (*Table C. 2*, *Appendix C*). This is a slightly poorer result than the first test but is still satisfactory. An F-test was also conducted and showed less significant variations in the fatty acids between the methods than the first test (*Table C. 3*, *Appendix C*).
The injection repeatability for the new test had an RSD_{IR} ranging from 0.31 to 5.49% (

Table C. 4, *Appendix C*). This provided a slightly better result than the first test. The same F-test was conducted between the methods and revealed that the variation between the methods were quite similar to the first test. (*Table C. 5*, *Appendix C*). The new test provided similar results to the first test and also exhibited the same trend. Leaks and old septum were probably not the cause of the observed trend.

To establish the effect of this trend on the *Nannochloropsis* samples analysed with the N_2-method, GLC793 samples from the sample sequence in the accuracy study (He-method) were compared to GLC793 samples from a long sequence of *Nannochloropsis* samples (N_2-method). Each GLC793 sample were analysed between five regular samples. The samples are labelled alphabetically where A is the first sample and G is the last. The effects on the raw area and stability in response factor are investigated in *Figure 4. 14* and *Figure 4. 15*.

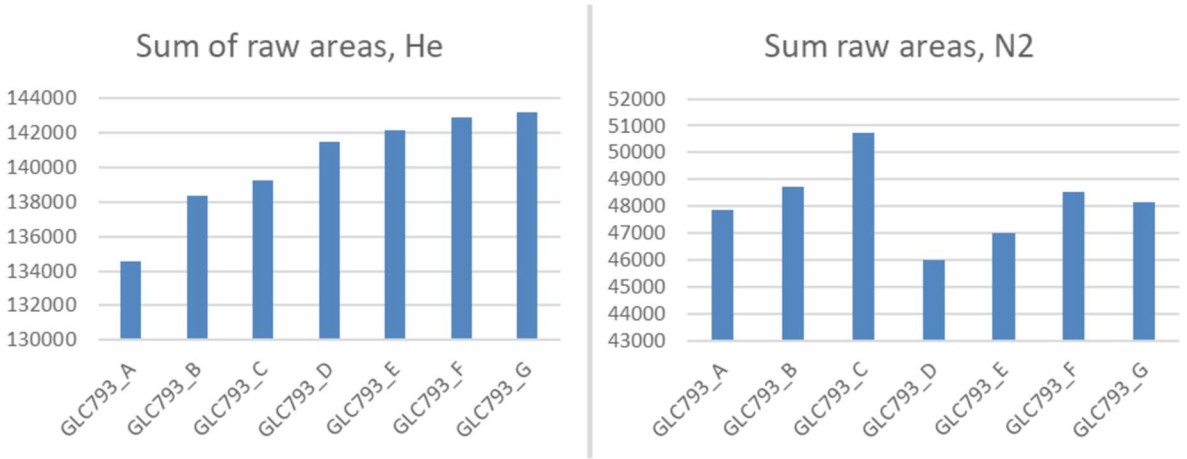

Figure 4. 14: GLC793 samples analysed with both methods. Raw areas for He are derived from the accuracy sample sequence, while raw areas for the N_2-method are derived from a long sequence of algal samples. The samples are labelled alphabetically, where A is the first sample, and G the last. Between each sample, five regular samples were analysed.

The sum of raw area for each GLC793 sample in the sequence run with the He-method now shows the same trend as in the first and second tests (injection repeatability and repeatability) for the N_2-method. What`s interesting is that the GLC793 samples (*Nannochloropsis* sequence) analysed with the N_2-method, does not have this trend. The raw areas vary in a more random manner than the sequence run with the He-method. Also, the raw areas of the fatty acids do not increase gradually like in the first and second test for the N_2-method (repeatability, injection repeatability).

When investigating the response factors, an interesting observation occurs. The response factors for heavier unsaturated fatty acids, such as 22-6 n-3 analysed with both methods increases (*Figure 4. 15).* The root of this trend is not established. Possible causes may for instance be instabilities in the detector (sensitivity for saturated vs unsaturated compounds), or the presence of active sites in the system becoming saturated after the first injections. Unsaturated fatty acids may be sensitive to oxidation or decomposition during analysis, but this should typically give the opposite trend.

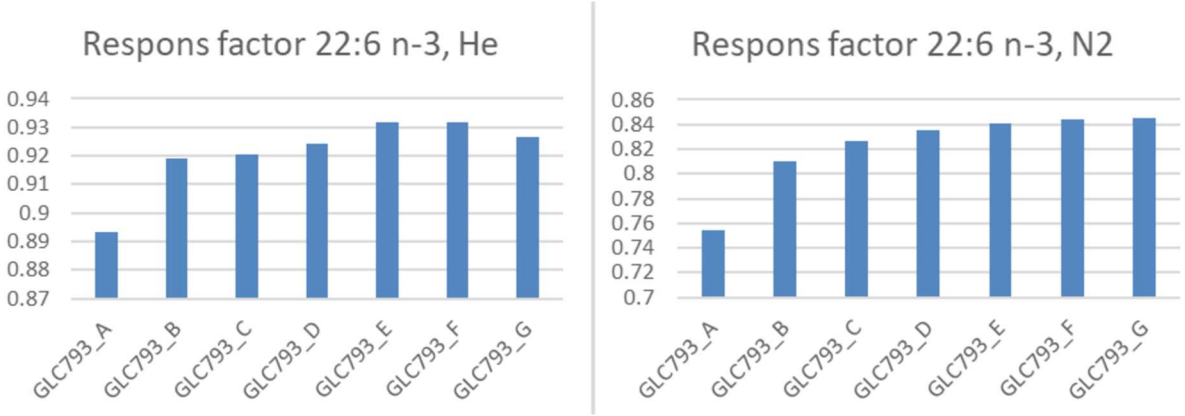

Figure 4. 15: Response factors for 22-6 n-3 in both methods. Response factors for He are derived from the accuracy sample sequence, while response factors for the N_2-method are derived from a long sequence of algal samples. The samples are labelled alphabetically, where A is the first sample, and G the last. Between each sample, five regular samples were analysed. An increasing trend in the response factor is present.

In summary, the differences may be due to the method and the instrument. Most likely, it is the instruments that are different, since the sequences are analysed on different instruments. Luckily, it does not seem to have affected the analysis of the *Nannochloropsis* samples from NORCE in a considerable extent. This could be due to the variation in concentration of the samples, while the samples from the repeatability and injection repeatability tests had the same

concentration. Additionally, it may seem that the variation in the N_2-method is overestimated. When using the Bonferroni correction, this is can contribute to overly conservative significance (64). The RSD_{IP}% (intermediate precision) is also lower than the RSD_R (repeatability), this is unusual, and indicates that the precision study does not give a correct image of the repeatability. The repeatability tests were conducted after the instruments had been idle for approximately two months during summer. This may have contributed to the trends observed in the methods, since the *Nannochloropsis* samples were analysed before summer, and the precision sequences, after summer.

4.4 Application on Nannochloropsis samples

4.4.1 The National Algae Pilot Mongstad

The National Algae pilot Mongstad (NAM) is a research and development facility located in Mongstad, at the west coast of Norway, near Bergen. This R&D facility is dedicated to the cultivation and study of microalgae, particularly for industrial and commercial applications. It`s close location to the sea is favourable, providing access to seawater for microalgae cultivation, and benefitting from the natural light in the region. One of the key aspects of NAM is its capability to conduct industrial-scale testing, focusing on practical applications and up-scaling of microalgae production for commercial use. NAM collaborates with the University of Bergen, and industrial partners to advance the field of microalgal research and explore innovative applications, closing the gap between laboratory-scale experiments and real-world industrial practices. The facility is committed to exploring sustainable solutions using microalgae, including their potential in carbon capture and utilization, providing an eco-friendly approach to reducing greenhouse gas emissions. Additionally, the facility forms a basis for developing more knowledge about the full value chain in the sea, from the choice of the right kind of microalgae, to the production of omega-3 fatty acids (67, 68, 69). In this study, PUFAs and the omega-3 fatty acid, EPA, is investigated in the microalgae *Nannochloropsis*, cultivated in pilot-scale at the NAM.

4.4.2 Outline of experiment for pilot-scale biomass production at NAM

The microalgae *Nannochloropsis* was upscaled from a start culture, via 200 mL Erlenmeyer flasks, and introduced to 300 ml bubble columns followed by inoculation in a 25 L photobioreactor for pilot-scale cultivation at NAM in one 250 L reactor and two 750 L reactors for biomass production in a fish feed trial.

Figure 4. 16: The microalgae Nannochloropsis is cultivated in bubble columns before inoculation in 25 L photobioreactor (left) ultimately reaching the NAM750 reactors (right). Photo: Jeroen de Vree.

4.4.2.1 Photobioreactor design

In this experiment, two distinct closed, vertically stacked tubular photobioreactor (PBR) systems known as LGem were employed. These systems encompassed one 250 L unit, and two 750 L units. Each of these reactor types are equipped with pH and temperature sensors and operated utilizing the innovative Wavywind™ and Bubblebrush™ technologies. This involves circulating 0.2 µm filtered air through the tubes in conjunction with the culture. In the two systems, a controlled injection of CO_2 is used to ensure an adequate carbon supply.

The 250 L (GemTube™ RD1-250) and 750 L (GemTube™ MK1-750) PBRs were used for pilot-scale biomass production and are situated within a greenhouse at NAM. These PBRs incorporate glass pipes measuring 65 x 2.2 mm, connected to a 70 L collection vessel. The culture is circulated through the tubes using both air and a liquid pump. Irradiance is primarily provided by sunlight, supplemented by LED lamps when natural irradiance within the greenhouse falls below 1000 µmol m-2s-1. Temperature regulation is automated through heat exchangers located in the collection tanks of the PBRs, using circulating tap water for cooling and heaters within the greenhouse for heating. Before cultivation, the PBRs undergo chemical cleaning and sterilization using hypochlorite and hydrogen peroxide.

4.4.2.2 Pilot-Scale Cultivation

The 250 L reactor was initially inoculated with biomass from the 25L reactor during the upscaling process, while two 750 L reactors were inoculated with biomass from the 250 L reactor (see *Figure 4. 17*). The production of *Nannochloropsis* spanned a period of three months through repeated batch cultivation. Once a high biomass concentration was attained, 80% of the culture was harvested, and the remaining culture was diluted with fresh growth medium. Across all systems, the pH was maintained within the range of 7.5 to 7 through automated injection of pure CO_2, and culture temperatures were regulated between 18 and 35℃. Irradiance was supplied by natural sunlight and/or LED lamps. For the preparation of growth medium, seawater from the fjord was collected in a tank, chlorinated with Sodium hypochlorite (15 ppm), and passed through several filter cartridges, including active coal filters (to remove chlorine) and filters with pore sizes ranging from 10 to 0.2 µm, before being introduced into the reactors. NORCE stock solution was also added to the medium.

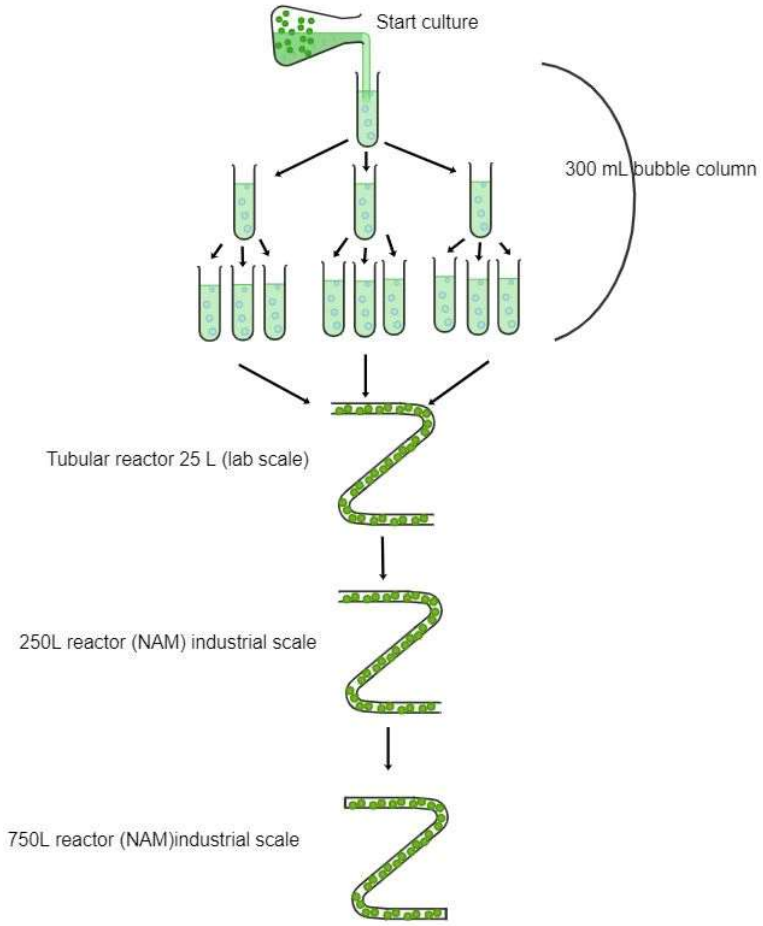

Figure 4. 17: Illustration of upscaling from laboratory scale to pilot-scale (industrial scale) at the NAM. Figure developed in chemix.org.

4.4.2.3 Sampling

Throughout the pilot-scale cultivation, samples were collected for optical density (OD) measurements at 750 nm (in duplicate). The tubular PBRs (NAM) were sampled regularly during the cultivation process (in duplicate), typically before and after each dilution and harvest, denoted by BD and AD, respectively. Some sampling was conducted at culture start (CS), and in some cases, a certain number of days into cultivation (Dx). The sample names in this study are organized based on the format "Batch number - Reactor name - what," where "what" indicates whether it is CS, Dx, BD, or AD. Example: “9-R-730-3-BD”. To distinguish between the NAM750 reactors, the names of the reactor was used, R-750-3 and R-750-4. The NAM250 reactor was named R-250. (R-250: 34 samplings, R-750-3: 26 samplings, R-750-4: 34 samplings).

4.4.3 Pilot-scale biomass production: culture start to full harvest

To provide a comprehensive picture of the pilot-scale biomass production, a PCA of all samples are conducted. The data points are averages of two replicates of the same sample. This is done to be able to visualize patterns in the biplots more accurately. Including each replicate of the same sample would provide a large number of data points and make a messy biplot. The replicates were located quite close when visualizing them in a biplot confirming their similarity.

All data is block normalized and standardized before conducting the PCA. The fatty acids contain block specific effects, block normalizing removes this effect, enabling detection of underlying patterns in the data. The disadvantage by block normalizing the data is potential loss of information leading to loss of block specific patterns. The benefit of standardizing the data is that the PCA is sensitive to the scale of the variables, and these are removed when standardized. The disadvantage is that standardizing, like normalization, removes the absolute values, these can be valuable if the original units are important for the interpretation of the results. Standardization also amplifies the effects of outliers, especially if the dataset is small or contains extreme values.

Figure 4. 18 displays a biplot featuring both scores (samples) and loadings (fatty acids) in the context of pilot-scale biomass production of *Nannochloropsis*. PC1 accounts for 41.5 % of the variance in the samples, while PC2 accounts for 27.5 %, collectively contributing to a total approx. 70%, which is sufficient for biological samples. The biplot readily distinguishes

between before harvest and dilution (BD, green), and after dilution and harvest (AD, blue). This distinction suggests a significant change in the dataset associated with the process of harvest and dilution. Notably, the 20:5 n-3 fatty acid, EPA, and the PUFAs, are located far to the right along PC1. Samples taken before dilution and harvest (BD), are located further to the right compared to those after dilution and harvest (AD), closer to EPA and the PUFAs. This signifies that the harvest is performed when the algae is rich in EPA and PUFAs, and that after dilution the EPA and PUFA content decreases.

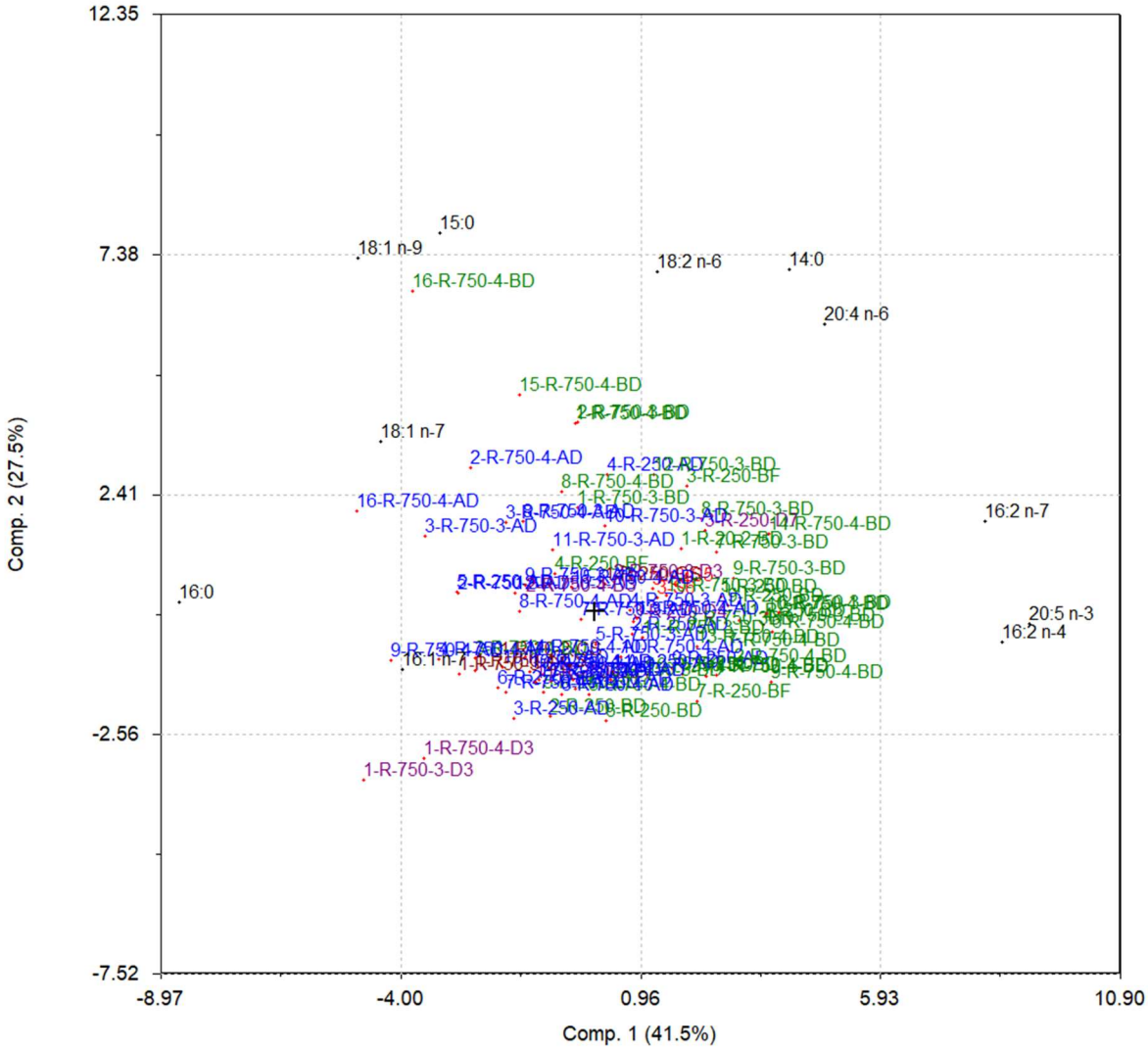

Figure 4. 18: Biplot with scores(samples) and loadings (fatty acid) of pilot-scale production. The colour green denotes before harvest and dilution (BD), while the colour blue denotes after harvest and dilution (AD). Purple denotes number of days in cultivation after dilution and harvest (Dx). Red denotes the laboratory scale and brown denotes culture start (CS). The fatty acids are named with their short names, where EPA is 20:5 n-3.

In (*Figure 4. 19*), the cultures BD has higher optical density compared to the optical density AD. This disparity results in reduced light exposure per cell BD, which is likely positively correlated with the increased EPA and PUFA content. Additionally, other parameters in the bioreactors probably contribute as well, but no data were available for these in the experiment.

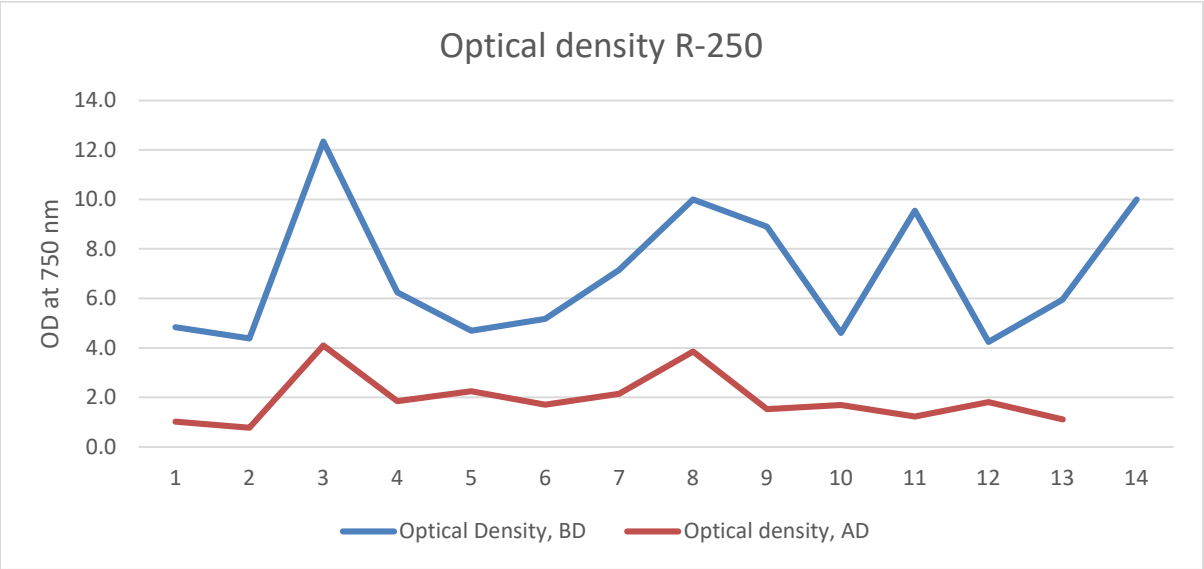

Figure 4. 19: Development of optical density over time (x-axis) in NAM250 for BD (blue) and AD (red).

Based on a study monitoring the EPA production in *Nannochloropsis*, it was found that nitrogen depletion increased the EPA content within the cell, and lower temperature or reduced light per cell increased the EPA content in the cell membrane of the algae (70). The positive correlation observed between the optical density and EPA and PUFA content can be explained by the stress imposed by the reduced light per cell (71). Low light conditions are often reported as a factor increasing the PUFA contents, possibly due to an increase in the number of thylakoid membranes to compensate for the reduced light availability (72). The higher optical density before harvest may explain the observed increase in EPA and other PUFAs.

To gain insights into the evolution of fatty acids within each reactor, biplots were created for each reactor (*Figure 4. 20, Figure 4. 21, Figure 4. 22*). These biplots exhibit a consistent pattern like that seen *Figure 4. 18*. The BD-samples are located further to the right, closer to the PUFAs and EPA, while the AD-samples are located further to the left.

In *Figure 4. 20*, it is evident that EPA and the fatty acids 18:1 n-9 and 15:0 show no significant correlation; they appear to be independent of each other. The fatty acid 16:0 and EPA is anti-correlated, meaning that as the EPA content increases, the 16:0 content decreases. Additionally,

EPA, 16:2 n-7 and 16:2-4 is positively correlated, implying that an increase in one of them is associated to an increase in the others.

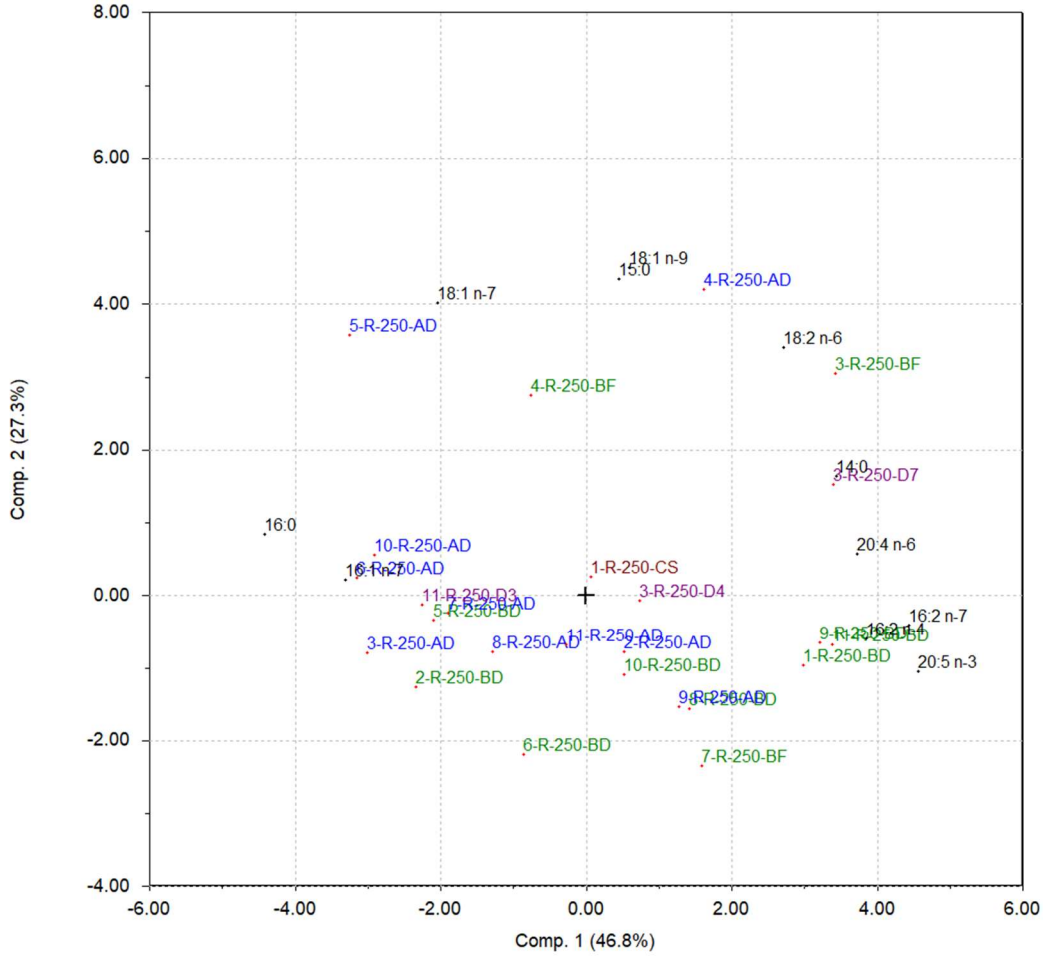

Figure 4. 20: Biplot with scores(samples) and loadings (fatty acid) in pilot-scale production, reactor R-250. The colour green denotes before harvest and dilution (BD), while the colour blue denotes after harvest and dilution (AD). Purple denotes number of days in cultivation after dilution and harvest (Dx). Brown denotes culture start (CS). The fatty acids are named with their short names, where EPA is 20:5 n-3.

When investigating all the loadings of the fatty acids, a consistent pattern emerges, with PUFAs are located to the right, and MUFAs and saturated FA are situated to the left. This pattern indicated that as cultivation progresses from after harvest and dilution to before harvest and dilution, the FA profile becomes more unsaturated. This observation applies for all the pilot-scale reactors.

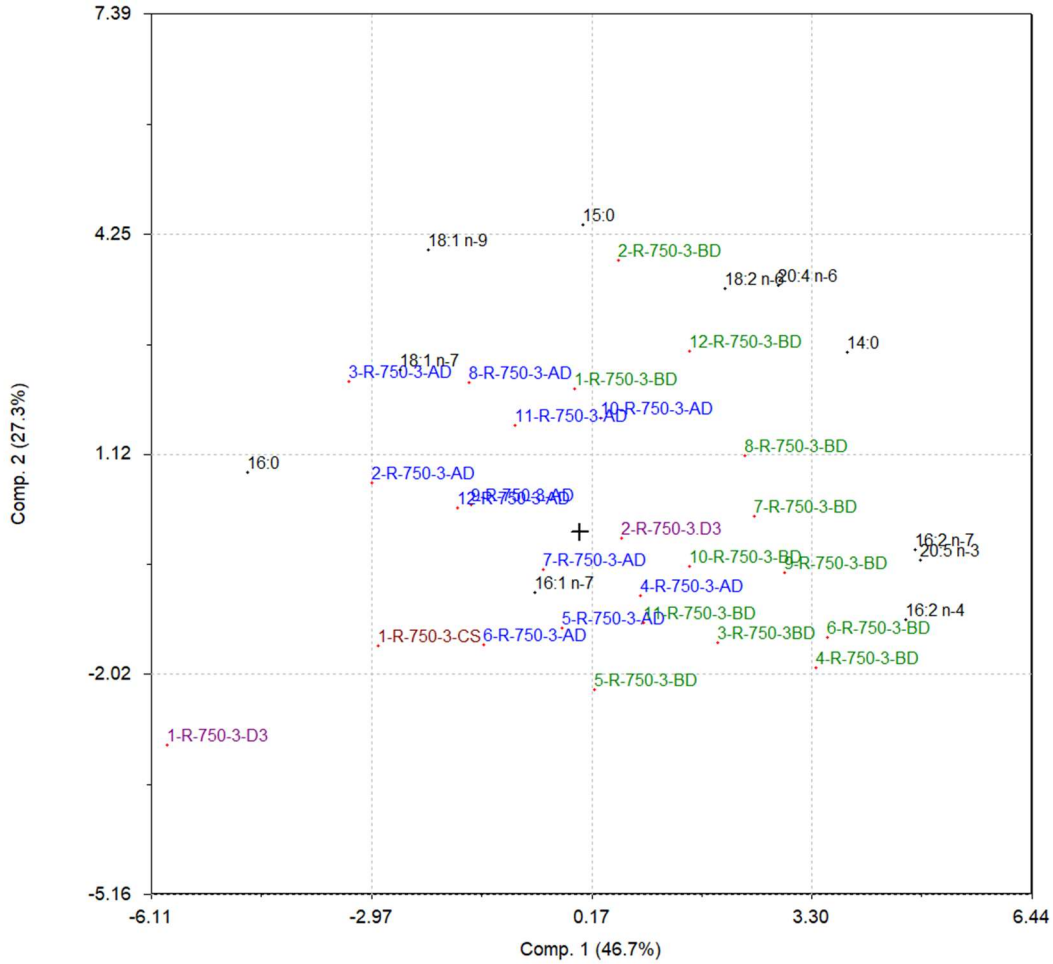

Figure 4. 21: Biplot with scores(samples) and loadings (fatty acid) of the samples in pilot-scale production, reactor R-750-3. The colour green denotes before harvest and dilution (BD), while the colour blue denotes after harvest and dilution (AD). Purple denotes number of days in cultivation after harvest and dilution (Dx). Brown denotes culture start (CS). The fatty acids are named with their short names, where EPA is 20:5 n-3.

In reactor R-750-4 (*Figure 4. 22*), some of the samples from BD are located far to the left with greater distance to EPA. As illustrated in *Figure 4. 19*, the optical density is at its highest before dilution and harvest, and is also when the EPA content reaches its peak. It is logical to assume that higher optical densities yield higher EPA contents, but this trend appears to reverse beyond a certain threshold. In R-750-4 two of the final batches, batch 15 and 16, stand out as prominent outliers.

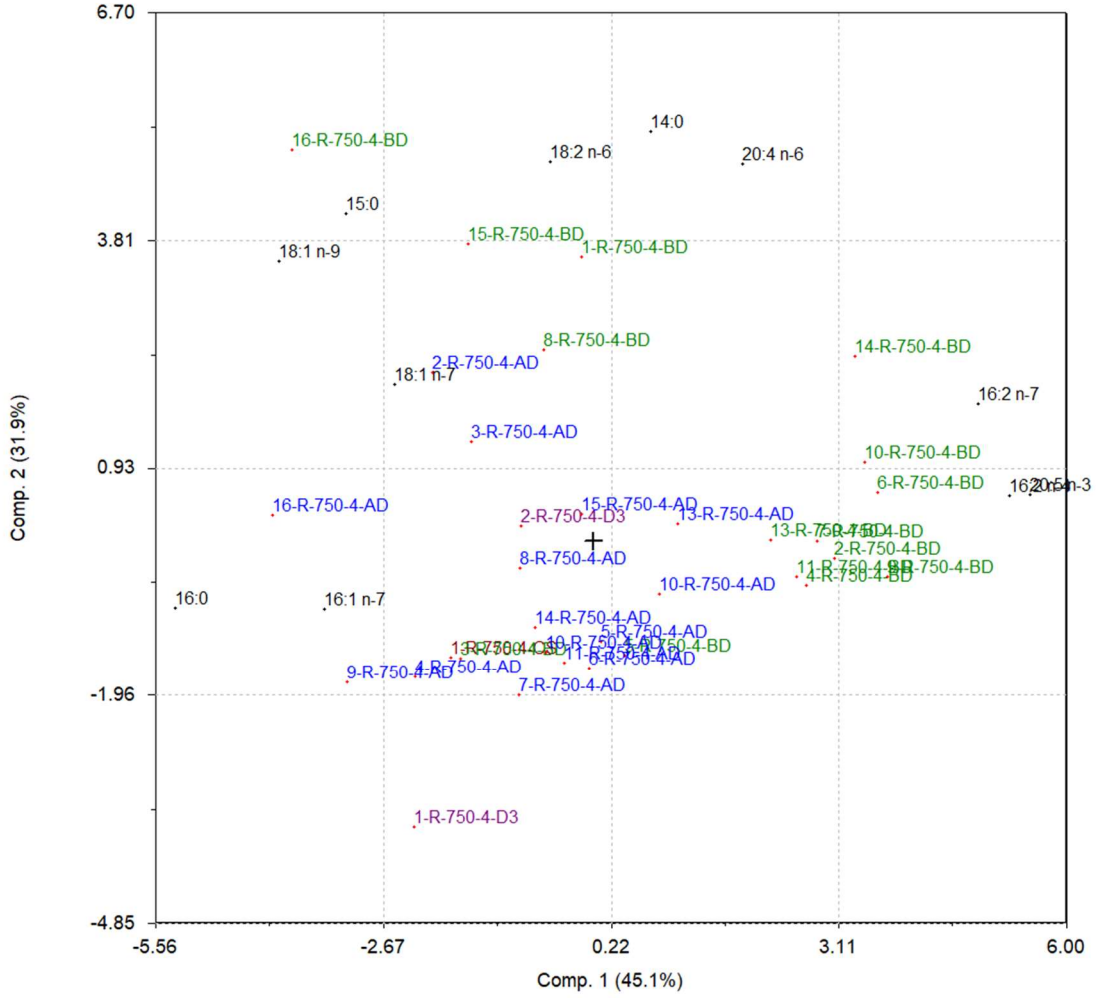

Figure 4. 22: Biplot with scores(samples) and loadings (fatty acid) of the samples in pilot-scale production, reactor R-750-4. The colour green denotes before harvest and dilution (BD), while the colour blue denotes after harvest and dilution (AD). Purple denotes number of days in cultivation after harvest and dilution (Dx). Brown denotes culture start (CS). The fatty acids are named with their short names, where EPA is 20:5 n-3.

In *Figure 4. 23,* a plot of the relative amount of EPA against the optical densities of R-750-4, reveals the relative amount of EPA increases with higher optical density range for cultivation, after which it decreases. This suggests the presence of an optimal optical density range for cultivation. Batch 15 and 16 (BD) had optical densities of 11.2 and 14.1, where their high optical densities may have led to their low %EPA content. However, batches (BD) with similar optical densities displayed high %EPA content, highlighting the influence of multiple factors on EPA content in the reactors.

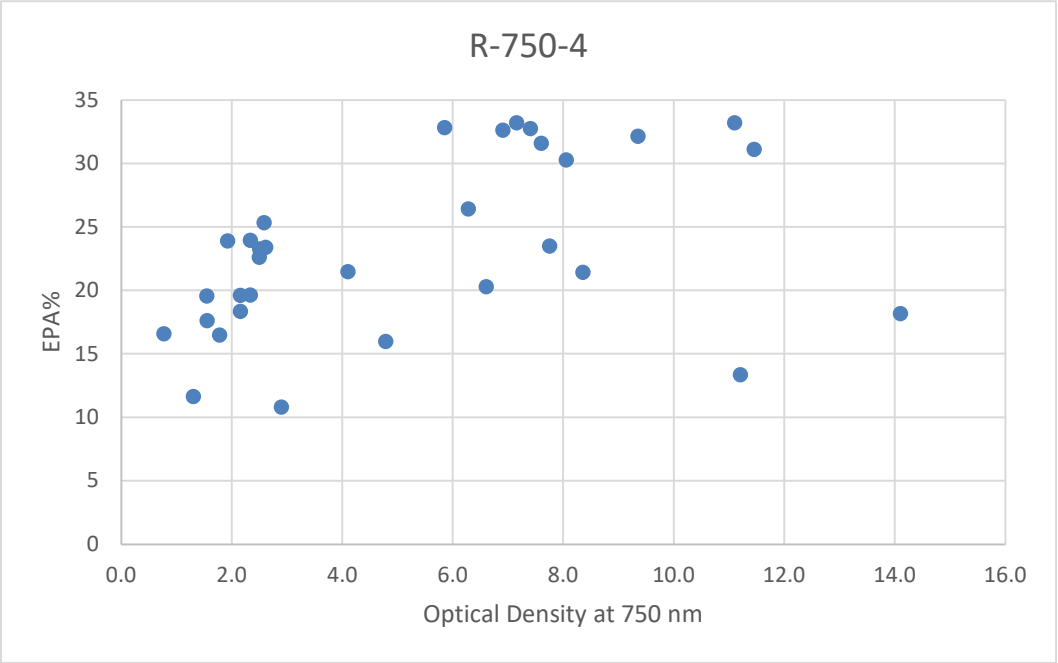

Figure 4. 23: Relative amount of EPA plotted against the optical density shows that the EPA% increases with higher optical densities up until a certain point.

Below, *Figure 4. 24, Figure 4. 25 and Figure 4. 26* illustrates the EPA content in each reactor in both absolute amounts and block normalized and standardized amounts, spanning from culture start, to full harvest. These figures show that the EPA content tends to be high before dilution and harvest and decreases afterwards, consistent with the findings from the earlier biplots. When comparing the patterns between the R-250 and R-750 reactors, they do not exhibit distinct similarities in the development of EPA over time. The R-750-3 and R-750-4, on the other hand, seems to have a slightly more similar pattern. However, the reactors do not have identical development of EPA over time, indicating that there are variations within each reactor, even with the same volume. This could be a result of many factors, like biological variation, contamination, inter-reactor variation etc.

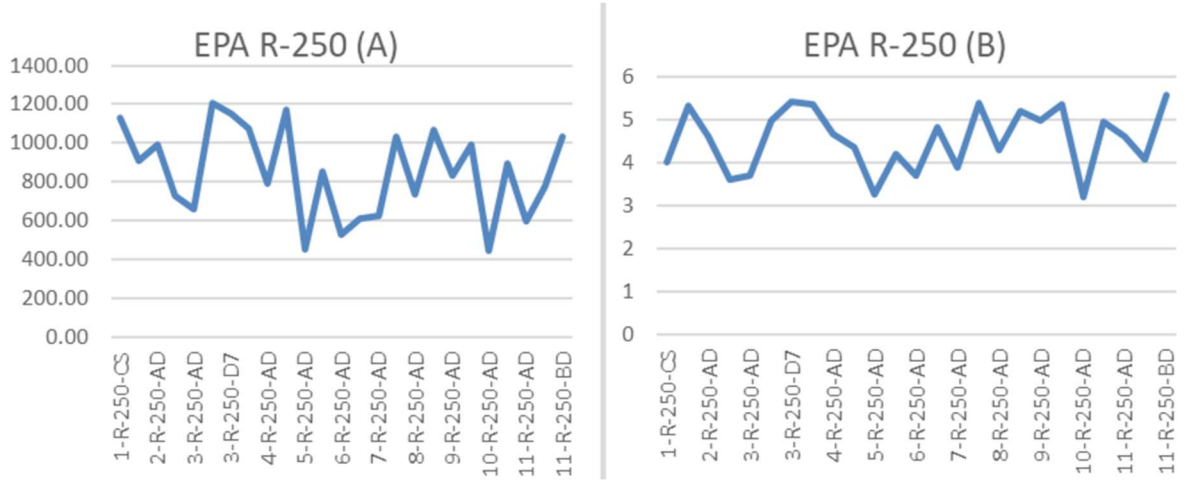

Figure 4. 24: A) Development of absolute amounts of EPA in R-250 from culture start to full harvest. B) Development of block normalized and standardized amounts of EPA in R-250 from culture start to full harvest.

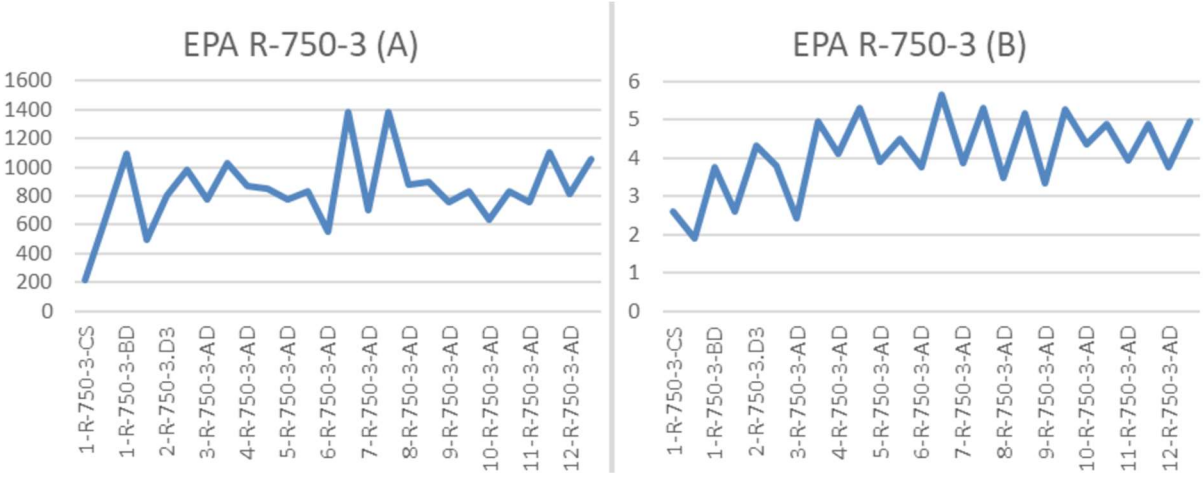

Figure 4. 25: A) Development of absolute amounts of EPA in R-750-3 from culture start to full harvest. B) Development of block normalized and standardized amounts of EPA in R-750-3 from culture start to full harvest.

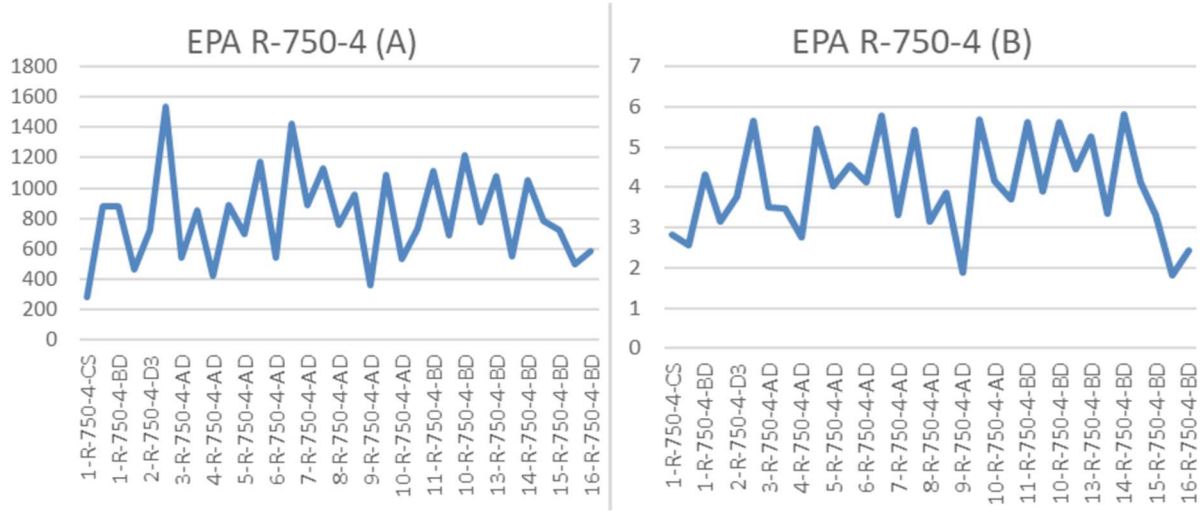

Figure 4. 26: A) Development of absolute amounts of EPA in R-750-4 from culture start to full harvest. B) Development of block normalized and standardized amounts of EPA in R-750-4 from culture start to full harvest.

To assess the significance of changes in fatty acid composition before and after harvest, a t-test was conducted on each of the fatty acid for both absolute amounts and block-normalized and standardized amounts before dilution and harvest and after dilution and harvest.

The t-test results for the absolute amounts indicated significant differences for several fatty acids, including 14:0, 16:2 n-7, 16:2 n-4, 18:2 n-6, 20:4 n-6 and 20:5 n-3. This emphasizes that the fatty acid profile shifts towards being more polyunsaturated before harvest, with EPA showing the most significant difference (*Table 4. 9*).

Table 4. 9: t-test for absolute amounts of fatty acids before and after harvest along with their p-values.

Fatty acid (short name)	p-value
14:0	5.710e-04*
15:0	0.3500
16:0	0.1405
16:1 n-7	0.0334
16:2 n-7	1.013e-06*
16:2 n-4	1.570e-08*
18:1 n-9	0.4974
18:1 n-7	0.4764
18:2 n-6	2.586e-03*
20:4 n-6	7.254e-05*
20:5 n-3	6.312e-11*

To validate these findings, a t-test of the block normalized and standardized data was performed (*Table 4. 10*). This analysis yielded slightly different results, with 16:0, 16:2 n-7, 16:2 n-4, 20:4 n-6 and 20:5 n.3 still showing significant differences before and after harvest. Notably, 14:0 was no longer significant, and 16:0 became significant. Additionally 18:2 n-6 lost is significance. These discrepancies suggest that some information is lost when block-normalizing and standardizing the data. It is important to note that 14:0 and 16:0 could be false positives.

Table 4. 10: t-test for block normalized and standardized amounts of fatty acids before and after harvest along with their p-values.

Fatty acid (short name)	p-value
14:0	0.04558
15:0	0.8517
16:0	8.703e-06*
16:1 n-7	0.01511
16:2 n-7	7.684e-05*
16:2 n-4	4.763e-06*
18:1 n-9	0.06296
18:1 n-7	0.04817
18:2 n-6	0.05369
20:4 n-6	1.012e-04*
20:5 n-3	4.381e-09*

In summary, the pilot-scale experiment revealed that the cultures had higher optical densities before harvest and dilution, likely leading to a stress reaction in the algae resulting in increased PUFA and EPA content. The reactors also exhibited consistent patterns in biplots, with BD samples positively correlating with PUFAs and EPA. Overall, the findings in this experiment emphasized the impact of the harvest process on fatty acid composition and the role of optical density in EPA and PUFA content.

5 Conclusions

Objective 1: GC-FID Method Optimization with Nitrogen as Carrier Gas

The optimal operating conditions for the GC-FID method with nitrogen as carrier gas at a start temperature of 150℃, was a carrier gas velocity of 12 cm/s and a temperature rate of $1℃/min$. These conditions provided similar selectivity and slightly higher efficiency compared to the predefined target values from the original He method, but with the costs of increased analysis time.

Objective 2: Comparative Analysis of Methods (He vs. N_2)

A PCA illustrated that the samples analysed using both methods exhibited substantial similarity regardless of which method was used. One sample (Sample 34) was an exception, likely attributed to integration variations and closely eluting peaks causing interference.

The N_2-method displayed 97% accuracy in quantifying total amount of fatty acids compared to the He-method. The results deviated with an average of 3%. Systematic bias was detected in the N_2-method, primarily affecting lower concentrations of fatty acids with biases up to 80%. Significant differences were established between the methods for most fatty acids in terms of bias and accuracy, although differences were relatively small. The N_2-method provided satisfactory intermediate precision, repeatability and injection repeatability, but poorer repeatability and injection repeatability for most fatty acids than the He-method.

The repeatability study does not seem to give a clear picture of the repeatability since the RSD_R is higher than the RSD_{IR}. This is likely due to the instrument being idle for some time before the tests were conducted.

However, the optimized method shows great potential as an alternative to the helium method for identification and quantification of fatty acids in microalgae.

Objective 3: Investigating Dynamic Changes in Pilot-Scale Production of *Nannochloropsis*

The pilot-scale experiment at the National Algae Pilot at Mongstad revealed dynamic changes in PUFAs and EPA content, with an increase before harvest and a subsequent decrease after harvest and dilution. Optical density was positively correlated with EPA content and PUFA content, likely due to a stress induced response in the microalgae. Fatty acid profiles shifted

towards being saturated and monounsaturated after dilution and harvest to polyunsaturated before harvest. Variation between the reactors was established, even for the rectors with identical volume. There were significant changes, proven by t-test, in amounts of the fatty acids 16:2 n-7, 16:2 n-4, 18:2 n-6, 20:4 n-6 and 20:5 n-3 after dilution and harvest, and before harvest.

Further Perspectives

The optimized GC-FID method with nitrogen as carrier gas should be refined further to reduce bias and enhance accuracy for the fatty acids in low concentrations. Additionally, a new precision test should be conducted for repeatability and injection repeatability when the instrument is in normal use, preferentially as a part of a normal sample sequence. This will help ensure the reliability of results and eliminate trends observed when analysing after idle periods. The trends in response factors and raw areas should also be investigated to reveal any problems with the instruments interfering with the results.

Expanding the range of samples analysed, such as samples from different algae species or using a newer column with the original helium method, can provide insights into the versatility and robustness of the method. This also allows for comparisons under different conditions. Additionally, a temperature rate of 1.351 ℃/min and a carrier gas velocity of 15.43 cm/s gave the closest fit in terms of efficiency (PPC), see *Figure 4. 7*. These settings should be investigated to determine the comparability to the helium method. If deemed appropriate, it could save 20 minutes compared to the optimized method.

Investigate how other parameters (beyond those studied) interact and influence the fatty acid content in pilot-scale production of *Nannochloropsis*. Understanding the multifaced relationships between various parameters can lead to more precise control of the pilot-scale production and a potential for optimizing these.

Exploring the modulation of stress factors on *Nannochloropsis* to enhance lipid production. Stress-induced lipid accumulation is a well-documented phenomenon in microalgae (71, 72), and optimizing this aspect can contribute to more efficient biomass production at the facility at Mongstad.

References

1. Lozano-Muñoz I, Muñoz S, Díaz NF, Medina A, Bazaes J, Riquelme C. *Nutritional enhancement of farmed salmon meat via non-GMO Nannochloropsis gaditana: Eicosapentaenoic acid (EPA, 20:5 n-3), docosapentaenoic acid (DPA, 22:5 n-3) and vitamin D3 for human health.* molecules. 2020;**25**(20):4615.

2. Nogueira N, Nascimento FJA, Cunha C, Cordeiro N. *Nannochloropsis gaditana grown outdoors in annular photobioreactors: Operation strategies.* Algal Research. 2020;**48**:101913.

3. Pignolet O, Jubeau S, Vaca-Garcia C, Michaud P. *Highly valuable microalgae: biochemical and topological aspects*. Journal of Industrial Microbiology and Biotechnology. 2013;**40**(8):781.

4. Ansari FA, Guldhe A, Gupta SK, Rawat I, Bux F. *Improving the feasibility of aquaculture feed by using microalgae.* Environmental Science and Pollution Research. 2021;**28**(32):43234-57.

5. Niemi C, Lage S, Gentili FG. *Comparisons of analysis of fatty acid methyl ester (FAME) of microalgae by chromatographic techniques.* Algal Research. 2019;**39**:101449.

6. Bartle KD, Myers P. *History of gas chromatography*. Trends in Analytical Chemistry. 2002;**21**(9):547-57.

7. Mellor A. *Carrier gases and their differences*. Scion intruments. 2021 [Cited 2023 05.10] Available from: https://scioninstruments.com/us/application-note-carrier-gases-and-their-differences/.

8. HeliumOne. *Helium market, Helium: high-tech, high value applications* Helium.one.com: HeliumOne; [Cited: 2023 05.10] Available from: https://www.helium-one.com/helium/helium-market/.

9. Chromatography Today. *Which carrier gases are most common for an FID?* : Chromatography today; 2022 [updated 19.08.22] [cited 2023 05.10]. Available from: https://www.chromatographytoday.com/news/columns-gc/52/breaking-news/which-carrier-gases-are-most-common-for-an-fid-detector/58499.

10. Mjøs SA, Waktola HD. *Optimizing the relationship between chromatographic efficiency and retention times in temperature-programmed gas chromatography*. Journal of Separation Science. 2015;**38**(17):3014-27.

11. Chhaganlal M, Skartland LK, Mjøs SA. *Transfer of retention patterns in gas chromatography by means of response surface methodology*. Journal of Chromatography A. 2014;**1332**:64-72.

12. Ruane J, Sonnino A, Agostini A. *Bioenergy and the potential contribution of agricultural biotechnologies in developing countries*. Biomass and Bioenergy. 2010;**34**(10):1435.

13. Thoré ESJ, Muylaert K, Bertram MG, Brodin T. *Microalgae*. Current Biology. 2023;**33**(3):R91.

14. Perez-Garcia O, Escalante FME, de-Bashan LE, Bashan Y. *Heterotrophic cultures of microalgae: Metabolism and potential products*. Water Research. 2011;**45**(1):13.

15. Al-Hoqani U, Young R, Purton S. *The biotechnological potential of Nannochloropsis*. Perspect Phycol. 2016;**4**:1-15.

16. Harun R, Singh M, Forde GM, Danquah MK. *Bioprocess engineering of microalgae to produce a variety of consumer products*. Renewable and Sustainable Energy Reviews. 2010;**14**(3):1037-47.

17. Borowitzka MA. *Commercial production of microalgae: ponds, tanks, tubes and fermenters.* Journal of Biotechnology. 1999;**70**(1):313-21.

18. Lee Y-K. *Microalgal mass culture systems and methods: Their limitation and potential*. Journal of Applied Phycology. 2001;**13**(4):307-15.

19. Chisti Y. *Biodiesel from microalgae.* Biotechnology Advances. 2007;**25**(3):294-306.

20. Steinrucken P. *High-value fatty acids from microalgae* [Doctoral Thesis]: University of Bergen; 2018. URL: https://hdl.handle.net/1956/17722

21. Torzillo G, Chini Zittelli G. *Tubular Photobioreactors*. Algal Biorefineries. Springer Internation Publishing, Cham; 2015;**2**: p. 187-212. ISBN: 9783319202006

22. Ugwu CU, Aoyagi H, Uchiyama H. *Photobioreactors for mass cultivation of algae*. Bioresource Technology. 2008;**99**(10):4021-8.

23. Kapoor B, Kapoor D, Gautam S, Singh R, Bhardwaj S. *Dietary polyunsaturated fatty acids (PUFAs): uses and potential health benefits.* Current Nutrition Reports. 2021;**10**(3):232-42.

24. Wasta ZM. *Identifikasjon av fettsyrer i omega-3 produkter ved hjelp av gasskromatografi med masssespektrometisk deteksjon* [Master thesis]. Bergen: University of Bergen; 2012. URL: https://hdl.handle.net/1956/8173

25. Blatti JL, Beld J, Behnke CA, Mendez M, Mayfield SP, Burkart MD. *Manipulating fatty acid biosynthesis in microalgae for biofuel through protein-protein interactions.* PLoS One. 2012;**7**(9):12.

26. Rustan AC, Drevon CA. *Fatty acids: structures and properties*. Encyclopedia of Life Sciences, 1 ed. New York: J.Wiley and Sons. 2005: p 1-7. ISSN: 9780470016176

27. Guiochon G, Guillemin CL. *Gas chromatography. Review of scientific instruments.* 1990;**61**(11):3317-39.

28. Coskun O. *Separation techniques: Chromatography.* Northern Clinics of Istanbul. 2016;**3**(2):156-60. ISSN: 25364553

29. Kuyper B. *An investigation into the source and distribution of bromoform in the southern African and Southern Ocean marine boundary layer* [Doctoral Thesis]. Cape Town: University of Cape Town; 2014. URL: https://core.ac.uk/download/pdf/185418199.pdf

30. Wittkowski R, Matissek R. *Capillary Gas Chromotography in Food Control and Research*: 2020: CRC Press, Hamburg; p. 19-47. ISBN: 1000125130

31. Fowlis IA. *Gas Chromatography*. Analytical Chemistry by Open Learning. **19**. 2 ed. New Jersey: J.Wiley & sons; 1995. Chapter 1. ISBN: 9780471954682

32. Harvey D. *Modern analytical chemistry.* McGraw-Hill Companies. 1 ed. United States of America: 2000. p. 547-62. ISBN: 0071169539

33. Grob RL. *Chapter 1 Basic principles of gas chromatography*. Journal of Chromatogrphy. 1977; **10**: p. 1-21.

34. Snyder LR, Kirkland JJ, Glajch JL. *Practical HPLC method development*: 2 ed. J.Wiley & Sons; New Jersey; 2012. p. 1-20. ISBN: 1118591518

35. Miller JM. *Chromatography: Concepts and contrasts*. 2 ed. New Jersey: J. Wiley & sons; 2009. p. 141-82. ISBN: 9780471472070

36. McNair HM, Miller JM, Snow NH. *Temperature programming. Basic gas chromatography*: J.Wiley & Sons; New Jersey; 2019. p. 87-98. ISBN: 1119450756

37. Alfahmawi RKH. *Gas chromatography-mass spectrometry analyses of fatty acid methyl esters from marine algae* [Master thesis]. Bergen: The University of Bergen; 2019. URL: https://hdl.handle.net/1956/20401

38. van Den Dool H, Dec. Kratz P. *A generalization of the retention index system including linear temperature programmed gas—liquid partition chromatography*. Journal of Chromatography A. 1963;**11**:463-71.

39. Chhaganlal M. *Optimaization and modelling of gas chromatographic retention patterns for analysis of fatty Acids* [Master thesis]. Bergen: University of Bergen; 2012.

40. Wasta Z, Mjøs SA. *A database of chromatographic properties and mass spectra of fatty acid methyl esters from omega-3 products*. Journal of Chromatography A. 2013;**1299**:94-102.

41. Mjøs SA, Waktola HD. *Optimizing the relationship between chromatographic efficiency and retention times in temperature-programmed gas chromatography*. Journal of Separation Science. 2015;**38**(17):3014-27.

42. Ettre LS. *Nomenclature for chromatography (IUPAC Recommendations 1993)*. Pure and Applied Chemistry. 1993;**65**(4):819-72.

43. Zellner BdA, Bicchi C, Dugo P, Rubiolo P, Dugo G, Mondello L. *Linear retention indices in gas chromatographic analysis: a review.* Flavour and Fragrance Journal. 2008;**23**(5):297-314.

44. Skartland LK, Mjøs SA, Grung B. *Experimental designs for modeling retention patterns and separation efficiency in analysis of fatty acid methyl esters by gas chromatography–mass spectrometry.* Journal of Chromatography A. 2011;**1218**(38):6823-31.

45. Waktola HD. *Optimization of separation efficiency in temperature programmed gas chromatography: Application of response surface methodology* [Master thesis]. Bergen: University of Bergen; 2014. URL: https://hdl.handle.net/1956/8028

46. Gritti F, Guiochon G. *The van Deemter equation: Assumptions, limits, and adjustment to modern high performance liquid chromatography.* Journal of Chromatography A. 2013;**1302**:1-13.

47. Knox JH, McLaren L. *A new gas chromatographic method for measuring gaseous diffusion coefficients and obstructive factors*. Analytical Chemistry. 1964;**36**(8):1477-82.

48. Giddings JC. *A new separation concept based on a coupling of concentration and flow nonuniformities*. Separation Science. 1966;**1**(1):123-5.

49. Heseltine J. *Hydrogen as a carrier gas for GC and GC–MS*. LCGC North America. 2010;**28**(1):16–27.

50. Oden K, Burger B, Rigdon A. *Alternative carrier gases for ASTM D7213 Simulated distillation analysis.* Petroleum and Petrochemical. 2017;**5**:1-5. URL: https://gcms.labrulez.com/labrulez-bucket-strapi-h3hsga3/paper/PCAR2269-UNV.pdf

51. Taylor T. *Optimizing gas chromatography using column dimensions: These tips will help you navigate choices about GC column dimensions to achieve significant improvements in resolution.* LC-GC North America. 2020;**38**(12):682-3.

52. Jones S. *GC columns and consumables*. In: Agilent Technologies, editor. Secret of GC columns dimensions; 2008. p. 56. [Cited: 2023 04.10] Available from: https://www.agilent.com/cs/library/slidepresentation/Public/Secrets_GC_Column_Dimensions.pdf.

53. Shantha NC, Napolitano GE. *Gas chromatography of fatty acids*. Journal of Chromatography A. 1992;**62**4(1):37-51.

54. Rahman MM, Abd El-Aty A, Choi JH, Shin HC, Shin SC, Shim JH. *Basic overview on gas chromatography columns*. Analytical separation science. 2015: p. 823-34.

55. Maes C, te Molder M, Luyten W, Herremans G, Winckelmans N, Peeters R, et al. *Determination of nitrogen gas transmission rate (N2GTR) of ethylene vinyl alcohol copolymer, using a newly developed permeation mearurement system.* Polymer Testing. 2021;**93**:106979

56. Sugita K, Sato H. *Sample introduction method in gas chromatography*. Analytical Sciences. 2021;**37**(1):159-65.

57. Poole CF. *Ionization-based detectors for gas chromatography*. Journal of Chromatography A. 2015;**1421**:137-53.

58. Dodds E, McCoy M, Rea L, Kennish J. *Gas chromatographic quantification of fatty acid methyl esters: Flame ionization detection vs. electron impact mass spectrometry.* Lipids. 2005;**40**:419-28.

59. Myers RH, Montgomery DC, Anderson-Cook CM. *Response surface methodology: process and product optimization using designed experiments:* J.Wiley & Sons; New Jersey; 2016; p.1-13. ISBN: 1118916034

60. Mjøs SA. *Two-dimensional fatty acid retention indices.* Journal of Chromatography A. 2004;**1061**(2):201-9.

61. Ferreira SLC, Bruns RE, da Silva EGP, dos Santos WNL, Quintella CM, David JM, et al. *Statistical designs and response surface techniques for the optimization of chromatographic systems.* Journal of Chromatography A. 2007;**1158**(1):2-14.

62. Desalegn SK. *Gas Chromatography optimization using experimental design and surface response methodology* [Master thesis]. Bergen, Norway: University of Bergen; 2018. URL: https://hdl.handle.net/1956/18677

63. Chrombox O Documentation and tutorials [Cited: 2023 08.16] Available from: http://www.chrombox.org/o/doc/index.html#21-theory.

64. Blackwell M. *Multiple hypothesis testing: The F-test. Matt Blackwell Research*. 2008:1-7.

65. Giavarina D. *Understanding Bland Altman analysis*. Biochem Med (Zagreb). 2015;**25**(2):141-51.

66. Froelich P. Nitrogen: *The most cost-effective makeup gas for gas chromatography* Parker Balston: 2014 [Cited: 2023 26.09] Available from: https://grupobiomaster.com/wp-content/uploads/2021/08/14-1.pdf.

67. Kjetland A. *National algae plant opend:* uib.no: UiB; 2016 [Cited: 2023 20.09] [updated 28.11.2016]. Available from: https://www.uib.no/en/news/102924/national-algae-plant-opened.

68. Kleinegris D, Bopple H, Steinrucken P, Erga SR, Kleivdal H. *The National Algaepilot Mongstad: production of microalgae for food and feed.* sureaqua.no; 2018 [Cited: 2023 20.09] Available from: https://www.sureaqua.no/Sureaqua/Events/Dorinde%20-%20Bl%C3%A5BioNorgeSeminar_Microalgae@Mongstad_20181130.pdf.

69. UiB. *National AlgaePARC Mongstad (NAM)* uib.no: UiB; 2019 [Cited: 2023 20.09] [updated 28.09.2019]. Available from: https://www.uib.no/en/bio/122997/national-algaeparc-mongstad-nam.

70. Sá M, Ferrer-Ledo N, Wijffels R, Crespo JG, Barbosa M, Galinha CF. *Monitoring of eicosapentaenoic acid (EPA) production in the microalgae Nannochloropsis oceanica.* Algal Research. 2020;**45**:101766.

71. Sousa S, Freitas AC, Gomes AM, Carvalho AP. *Modulated stress to balance Nannochloropsis oculata growth and eicosapentaenoic acid production.* Applied Microbiology and Biotechnology. 2022;**106**(11):4017-27.

72. Shi TQ, Wang LR, Zhang ZX, Sun XM, Huang H. *Stresses as first-line tools for enhancing lipid and carotenoid production in microalgae*. Front Bioeng Biotechnol. 2020;**8**:610.

6 Appendices

A. Sample preparation

Table A. 1: Volume of IS added to samples and volume of extracts added to 1 mL of isooctane in GC-vial. Red sample numbers are missing samples and were not prepared and analysed.

FA repl1	FA repl2	DW (mg)	IS Vol(µl)	Volume of extract added. to 1 mL isooctane (µl)
1	2	0.2	10	429
3	4	2.54	80	39
5	6	2.6	80	39
7	8	2.62	80	39
9	10	4.11	130	24
11	12	1.96	60	53
13	14	2.01	70	45
15	16	2	60	53
17	18	1.99	60	53
19	20	4.2	130	24
21	22	2.12	70	45
23	24	2.18	70	45
25	26	2.14	70	45
27	28	0.3	10	429
29	30	5.49	170	18
31	32	0.41	20	176
33	34	2.64	80	39
35	36	2.28	70	45
37	38	2.30	70	45
39	40	2.30	70	45
41	42	0.28	10	429
43	44	4.20	130	24
45	46	0.33	10	429
47	48	1.18	40	81
49	50	0.27	10	429
51	52	0.19	10	429
53	54	0.17	10	429
55	56	1.03	40	81
57	58	1.18	40	81
59	60	0.78	30	111
61	62	6.88	210	14
63	64	0.19	10	429
65	66	0.32	10	429
67	68	0.97	30	111
69	70	2.02	70	45
71	72	2.50	80	39
73	74	0.77	30	111
75	76	0.45	20	176
77	78	0.46	20	176
79	80	1.90	60	53

81	82	1.36	50	64
83	84	1.88	60	53
85	86	2.86	90	34
87	88	2.94	90	34
89	90	1.65	50	64
91	92	0.96	30	111
93	94	0.67	20	176
95	96	0.53	20	176
97	98	1.63	50	64
99	100	1.84	60	53
101	102	1.80	60	53
103	104	0.52	20	176
105	106	0.66	20	176
107	108	0.48	20	176
109	110	1.58	50	64
111	112	2.52	80	39
113	114	2.72	90	34
115	116	1.43	50	64
117	118	0.67	30	111
119	120	0.59	20	176
121	122	0.72	30	111
123	124	1.77	60	53
125	126	1.47	50	64
127	128	1.44	50	64
129	130	0.58	20	176
131	132	0.56	20	176
133	134	0.72	30	111
135	136	1.76	60	53
137	138	1.87	60	53
139	140	2.27	70	45
141	142	0.57	20	176
143	144	0.54	20	176
145	146	0.62	20	176
147	148	2.08	70	45
149	150	2.31	70	45
151	152	2.69	90	34
153	154	0.44	20	176
155	156	1.03	40	81
157	158	0.65	20	176
159	160	0.59	20	176
161	162	2.49	80	39
163	164	2.49	80	39
165	166	2.55	80	39
167	168	0.47	20	176
169	170	0.60	20	176
171	172	0.42	20	176
173	174	1.29	40	81
175	176	1.70	60	53
177	178	1.97	60	53
179	180	0.49	20	176

181	182	0.76	30	111
183	184	0.59	20	176
185	186	1.37	50	64
187	188	1.40	50	64
189	190	2.00	60	53
191	192	0.60	20	176
193	194	0.34	20	176
195	196	2.35	80	39
197	198	0.96	30	111
199	200	1.81	60	53
201	202	0.63	20	176
203	204	0.78	30	111
205	206	1.92	60	53
207	208	2.31	70	45
209	210	0.67	30	111
211	212	2.01	70	45
213	214	0.41	20	176
215	216	1.78	60	53
217	218	0.32	10	429
219	220	0.61	20	176
221	222	1.30	40	81
223	224	0.34	20	176
225	226	0.27	10	429
227	228	1.58	50	64
229	230	3.00	100	31
231	232	2.02	70	45
233	234	3.80	120	26
235	236	0.52	20	176
237	238	0.85	30	111
239	240	0.83	30	111
241	242	2.28	70	45
243	244	2.34	80	39
245	246	2.60	80	39
247	248	3.52	110	28
249	250	3.38	110	28
251	252	0.33	10	429
253	254	0.80	30	111
255	256	0.39	20	176
257	258	1.04	40	81
259	260	0.67	30	111
261	262	0.54	20	176

B. Method optimization

Table B. 1: Retention indices calculated for optimal selectivity (18.86 cm/s and 1.702°C/min) and retention indices of target pattern along with their differences for each FAME.

FAME	Calc.	Target	Difference
18:2 n-6	19.06	19.05	0.01
20:2 n-6	21.07	21.07	0
16:1 n-7	16.48	16.48	0
17:1 n-7	17.48	17.48	0
18:1 n-9	18.40	18.40	0
20:1 n-9	20.40	20.40	0
22:1 n-9	22.41	22.41	0
24:1 n-9	24.43	24.43	0
18:3 n-6	19.49	19.47	0.02
18:3 n-3	19.84	19.83	0.01
20:3 n-6	21.50	21.49	0.01
20:5 n-3	22.59	22.59	0
22:5 n-3	24.73	24.74	-0.01
22:6 n-3	24.97	24.99	-0.02

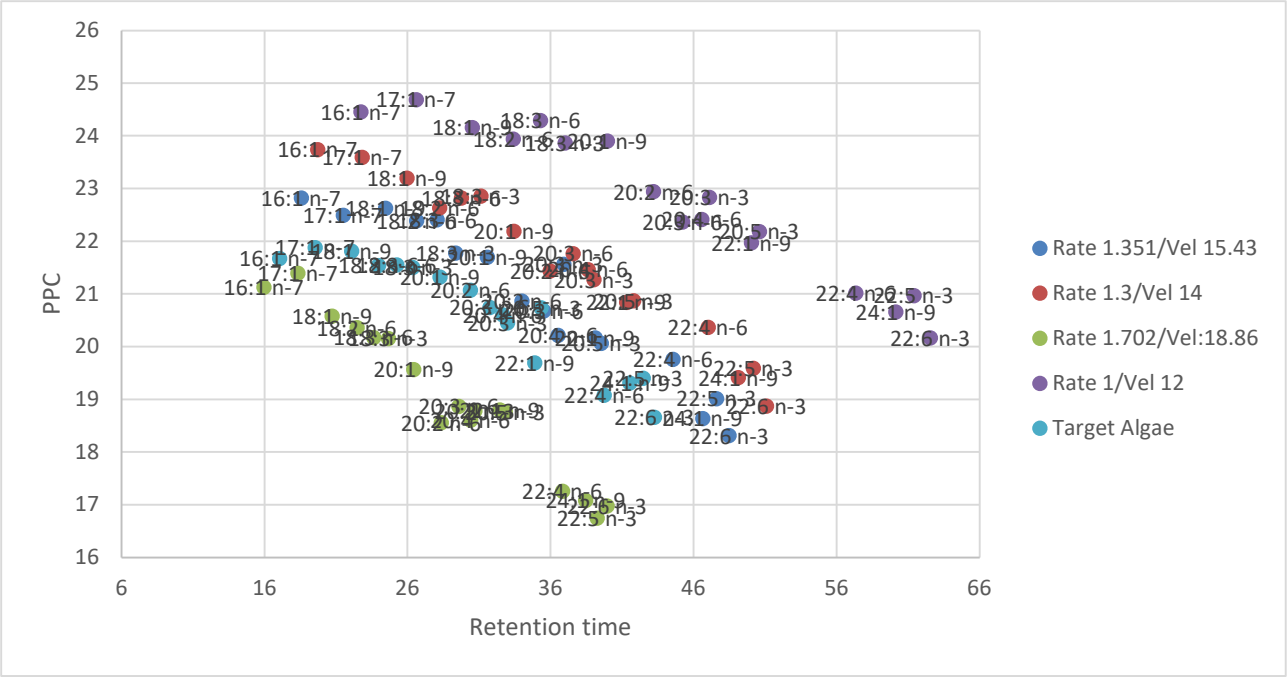

Figure B. 1: Evaluation of efficiency. Retention time and PPC against each other for different temperature rates and mobile phase velocities for a collection of fatty acids. 12:0, 14:0 and 14:1 n-5 is removed due to overlapping peaks.

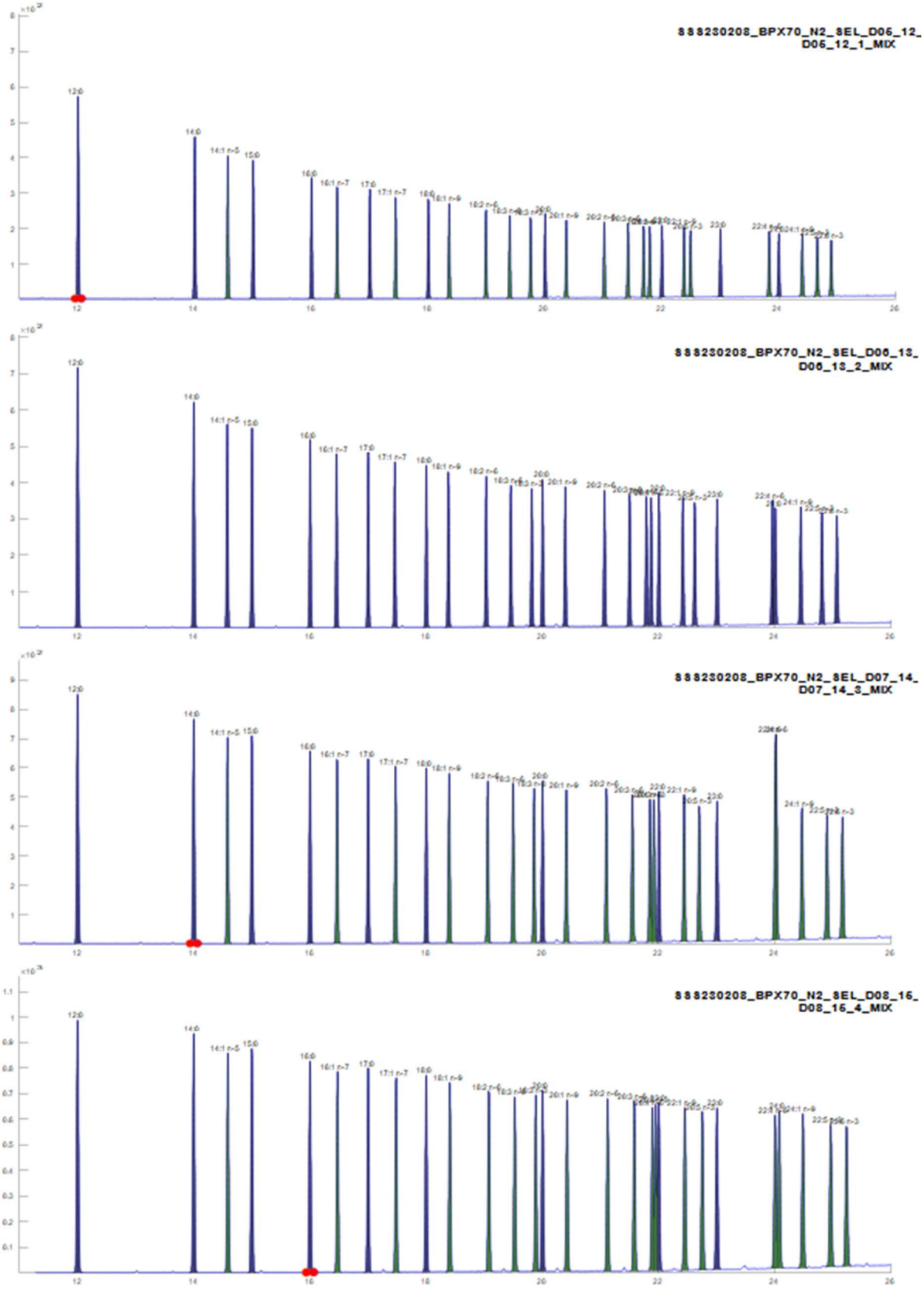
SS230208_BPX70_N2_SEL_D06_12_
D06_12_1_MIX
SS230208_BPX70_N2_SEL_D06_13_
D06_13_2_MIX
SS230208_BPX70_N2_SEL_D07_14_
D07_14_3_MIX
SS230208_BPX70_N2_SEL_D08_15_
D08_15_4_MIX

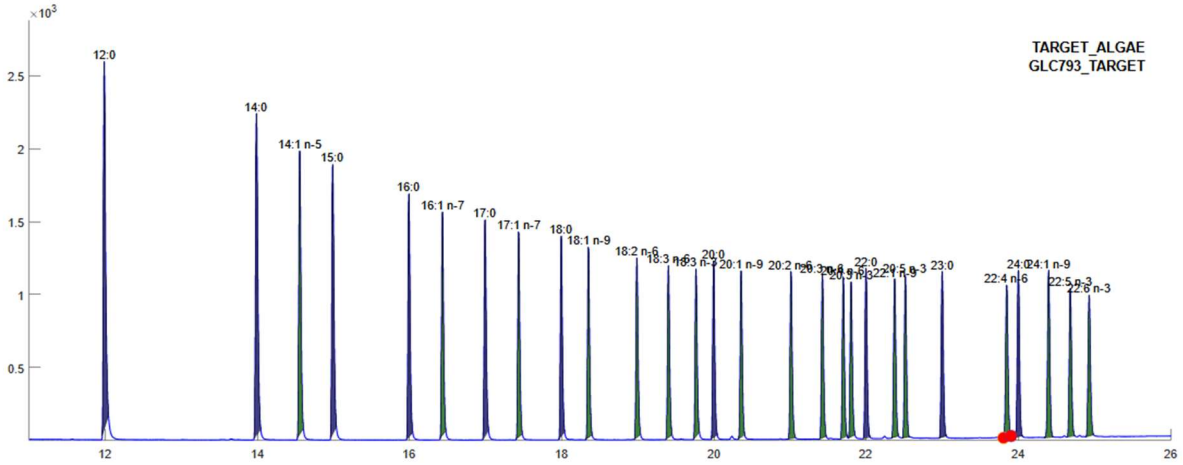

Figure B. 2: RI units, rate/vel, 12/1, 13/2, 14/3, 15/4, target algae. Chromatograms from different temperature programs and mobile phase velocities and the target retention pattern. The chromatograms are on retention index scale.

From the chromatograms above one can see that the separation of the peaks decreases with increasing temperature rate and velocity.

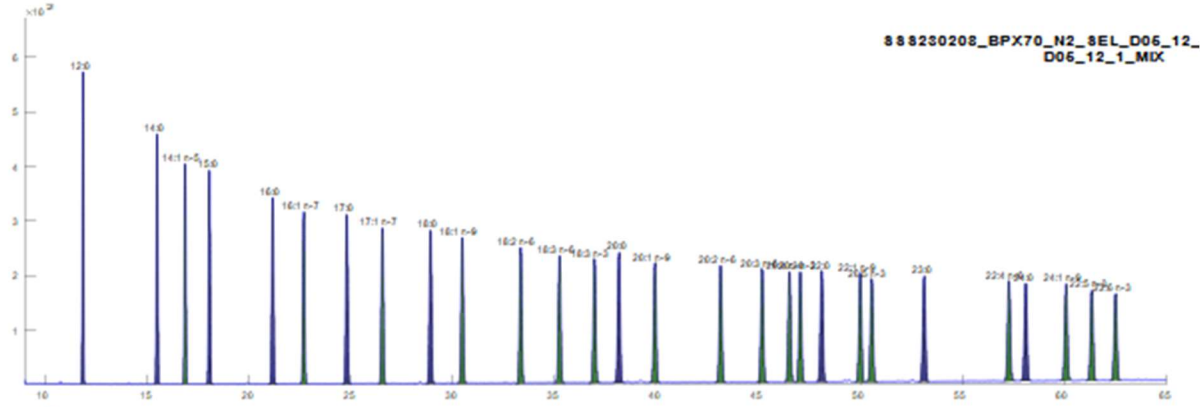
888230208_BPX70_N2_SEL_D06_12_
D06_12_1_MIX

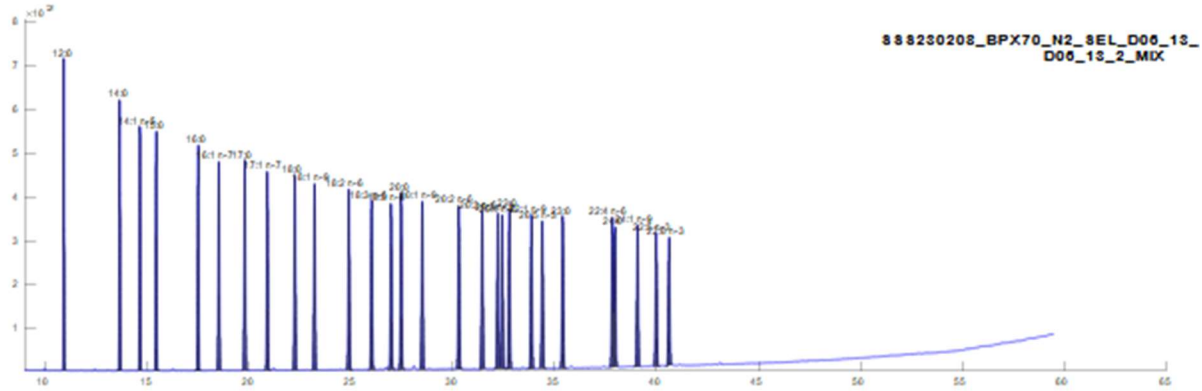
888230208_BPX70_N2_SEL_D06_13_
D06_13_2_MIX

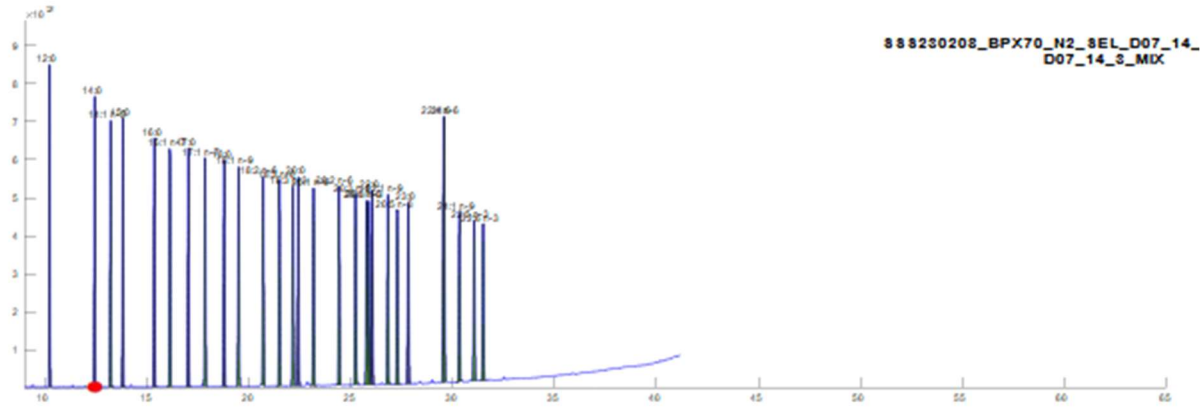
888230208_BPX70_N2_SEL_D07_14_
D07_14_3_MIX

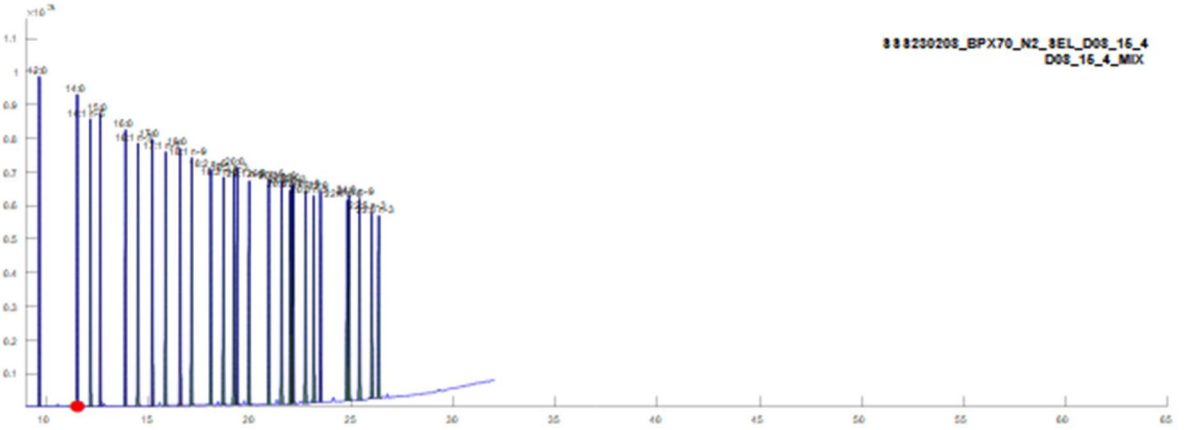
888230208_BPX70_N2_SEL_D08_15_4
D08_15_4_MIX

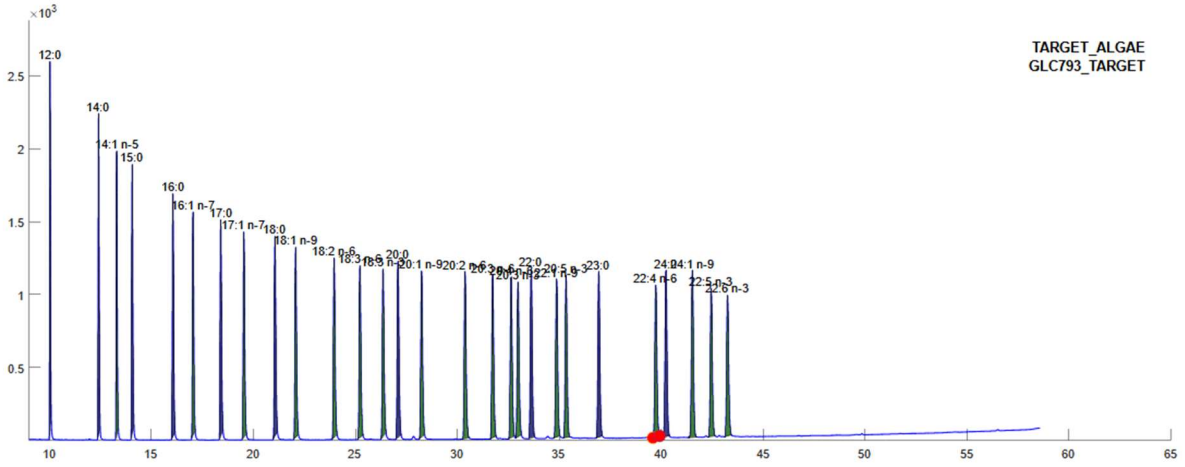

Figure B. 3: RT units. rate/vel, 12/1, 13/2, 14/3, 15/4. Chromatograms from different temperature programs and mobile phase velocities and the target chromatogram. The chromatograms are on retention index scale.

From the chromatograms above one can see that the retention time decreases with increasing temperature rate and velocity.

C. Statistical outputs

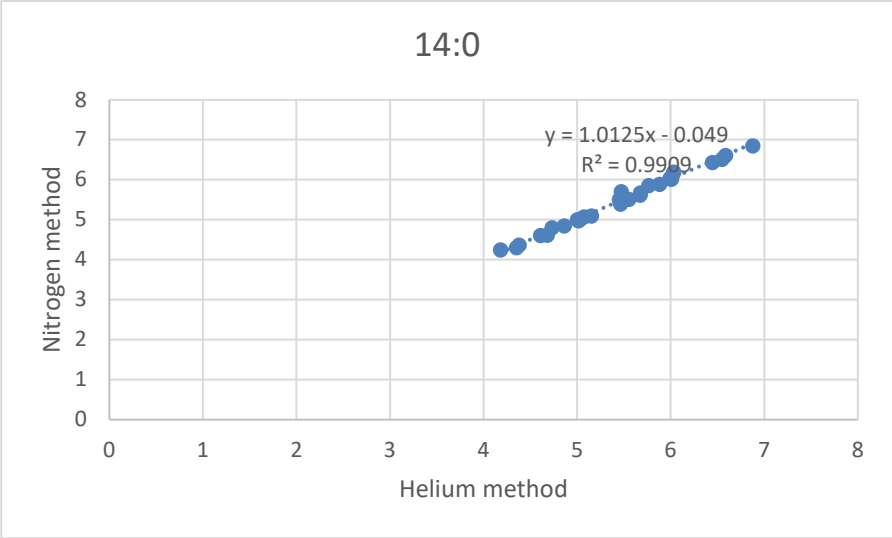

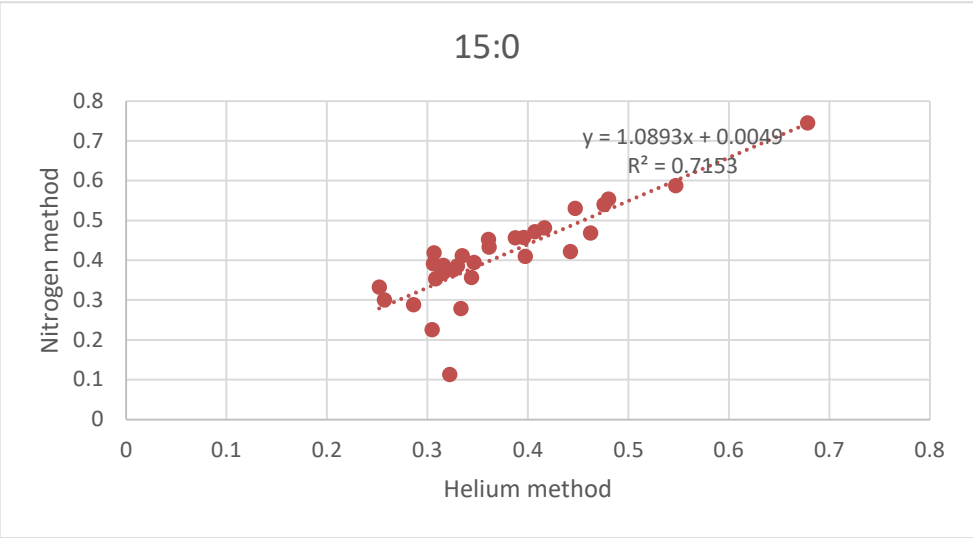

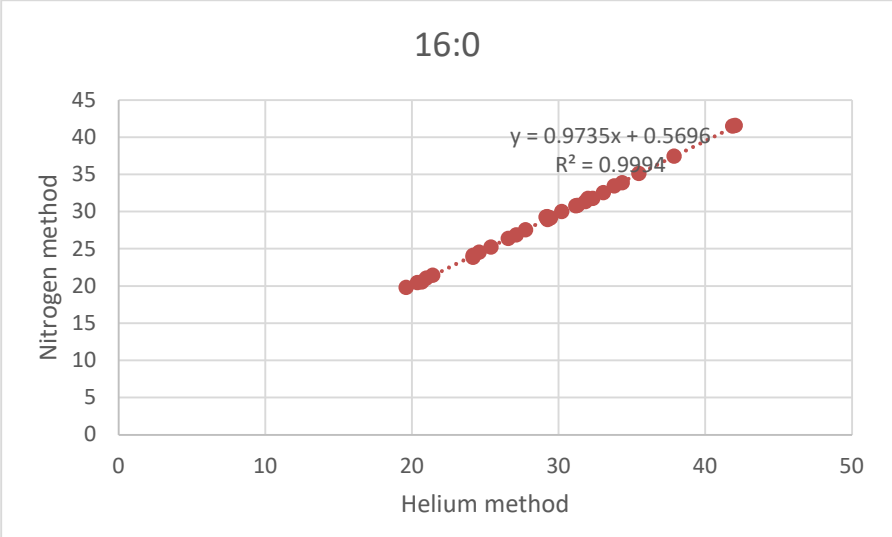

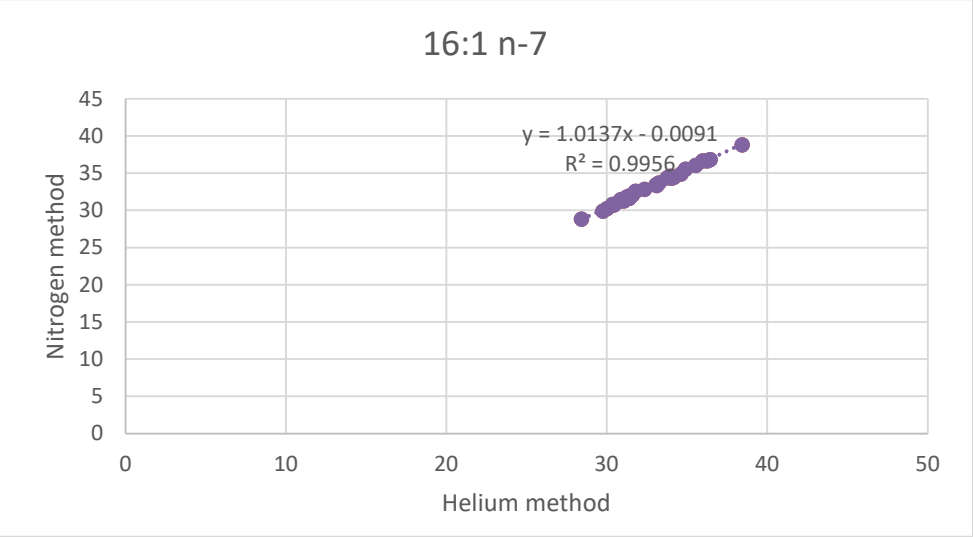

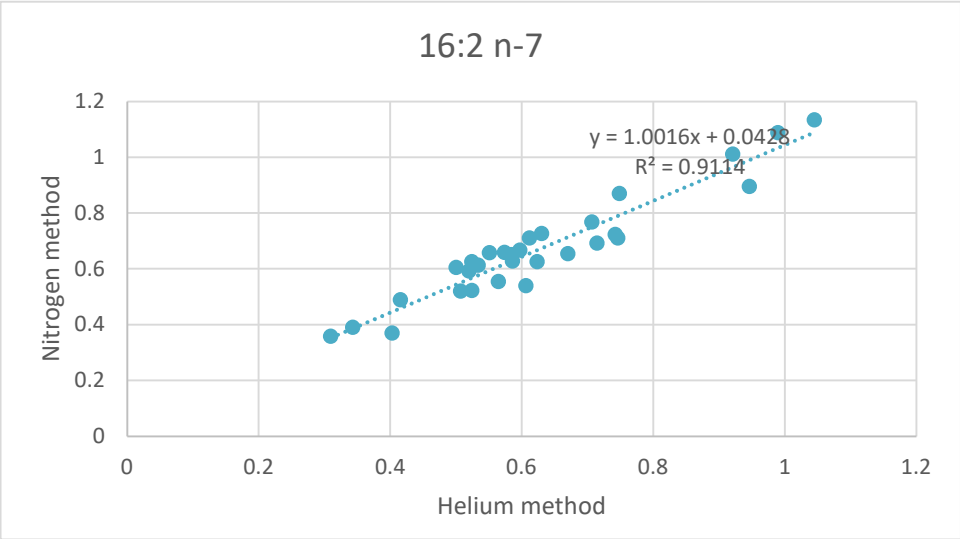
16:2 n-7
y = 1.0016x + 0.0428
R² = 0.9114
Nitrogen method
Helium method
0
0.2
0.4
0.6
0.8
1
1.2

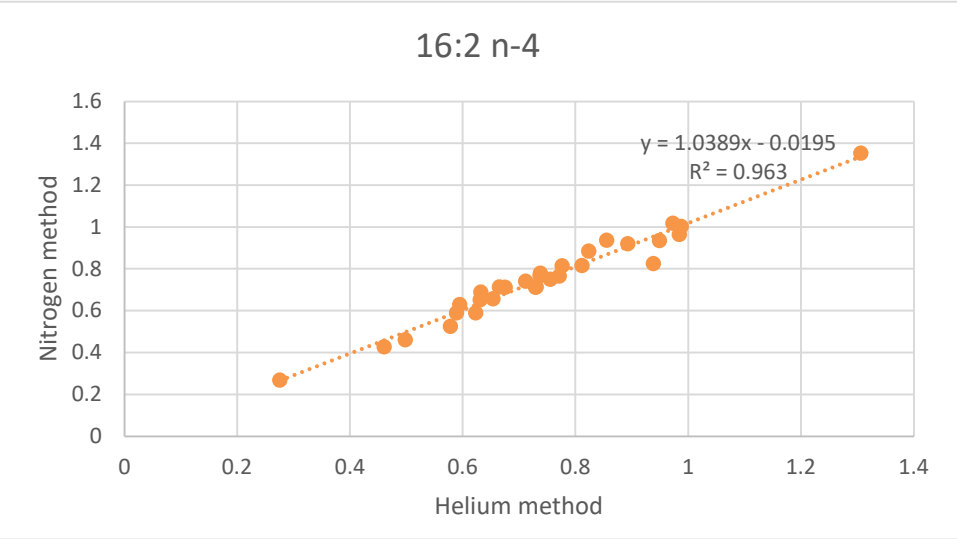
16:2 n-4
y = 1.0389x - 0.0195
R² = 0.963
Nitrogen method
Helium method
0
0.2
0.4
0.6
0.8
1
1.2
1.4
1.6

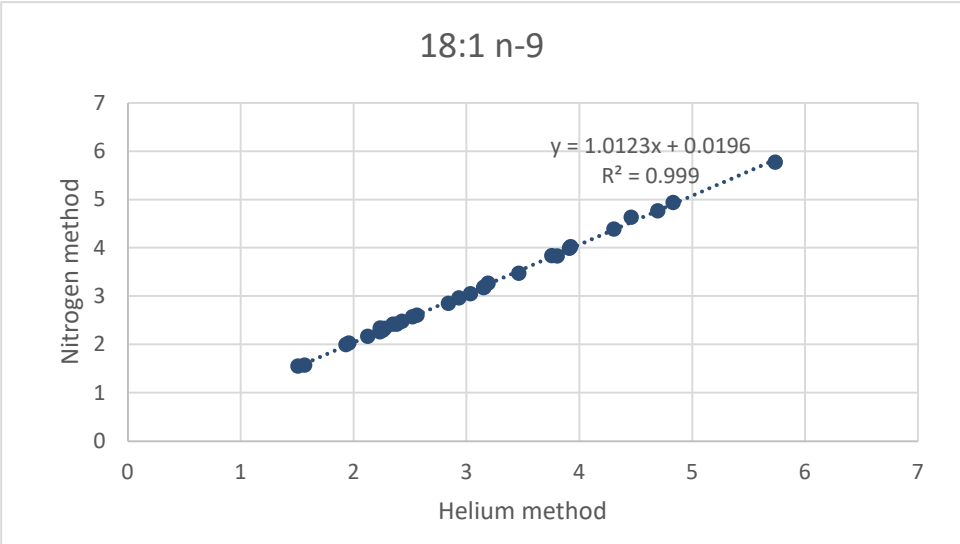
18:1 n-9
y = 1.0123x + 0.0196
R² = 0.999
Nitrogen method
Helium method
0
1
2
3
4
5
6
7

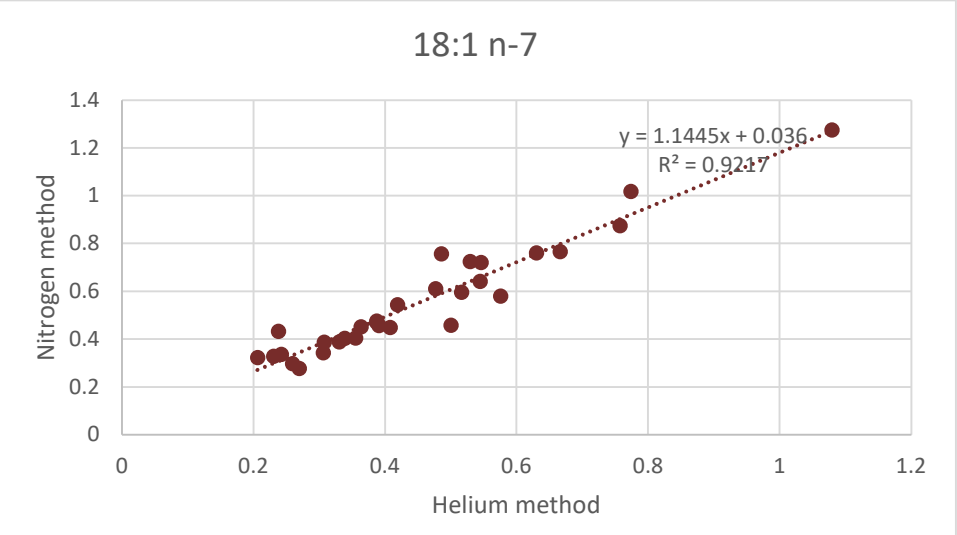
18:1 n-7
y = 1.1445x + 0.036
R² = 0.9217
Nitrogen method
Helium method
0
0.2
0.4
0.6
0.8
1
1.2
1.4

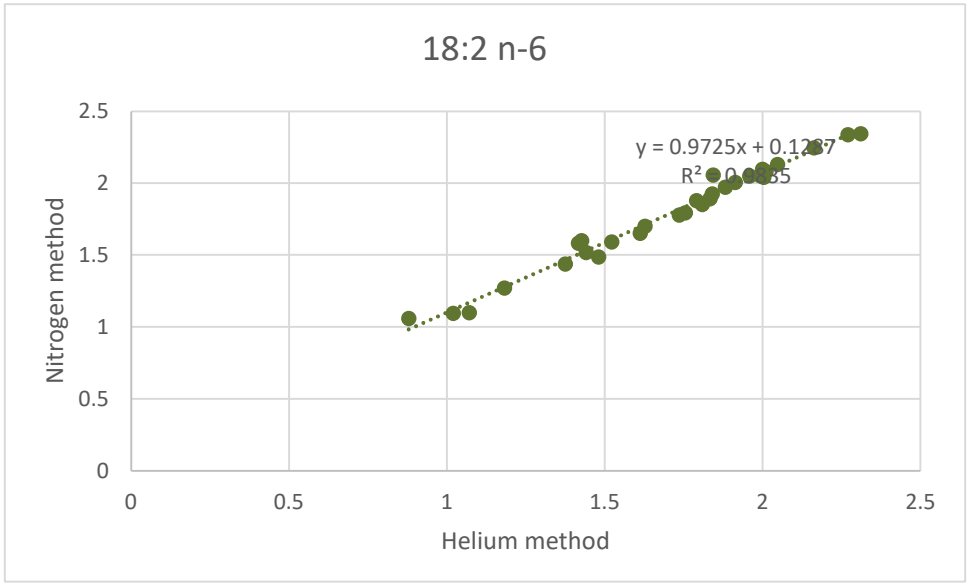

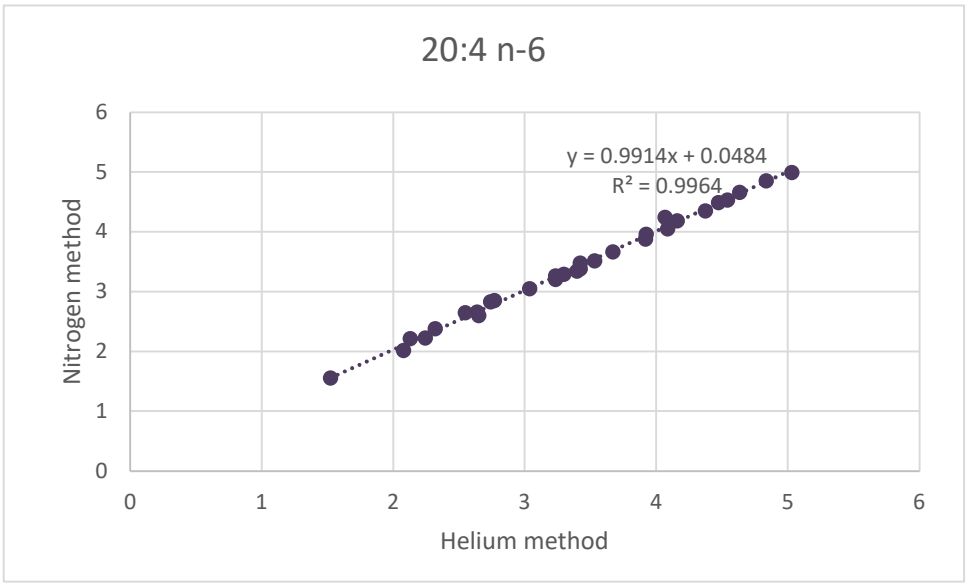

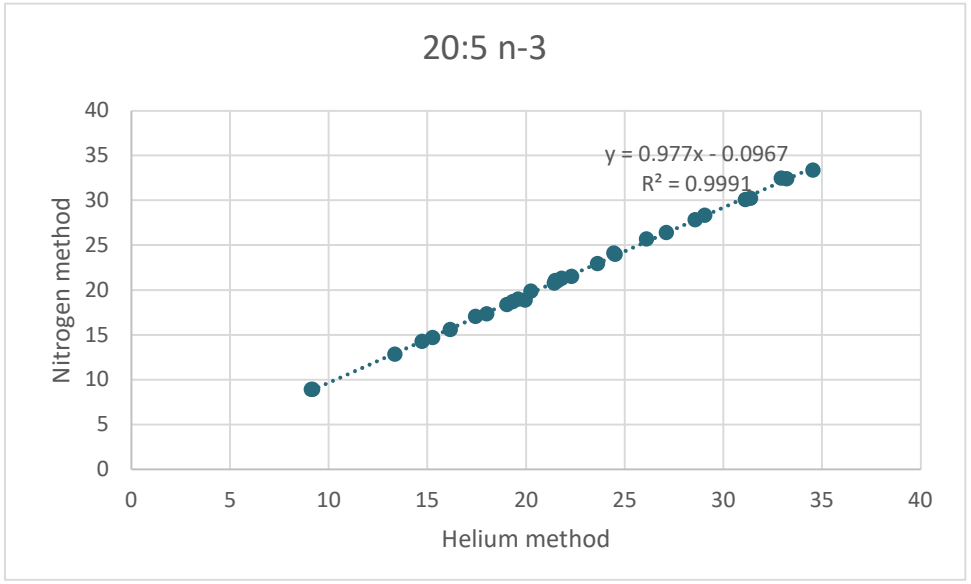

Figure C. 1: Relative amounts of respective fatty acids for nitrogen and helium method plotted against each other.

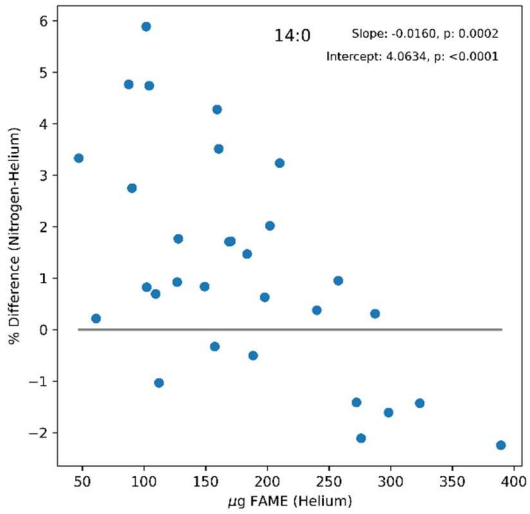
14:0
Slope: -0.0160, p: 0.0002
Intercept: 4.0634, p: <0.0001
% Difference (Nitrogen-Helium)
µg FAME (Helium)

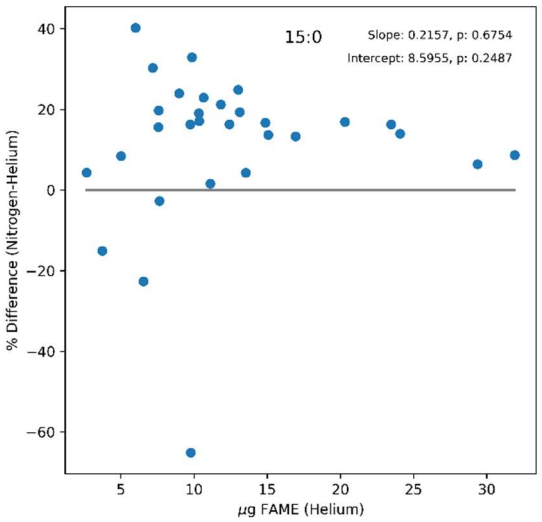
15:0
Slope: 0.2157, p: 0.6754
Intercept: 8.5955, p: 0.2487
% Difference (Nitrogen-Helium)
µg FAME (Helium)

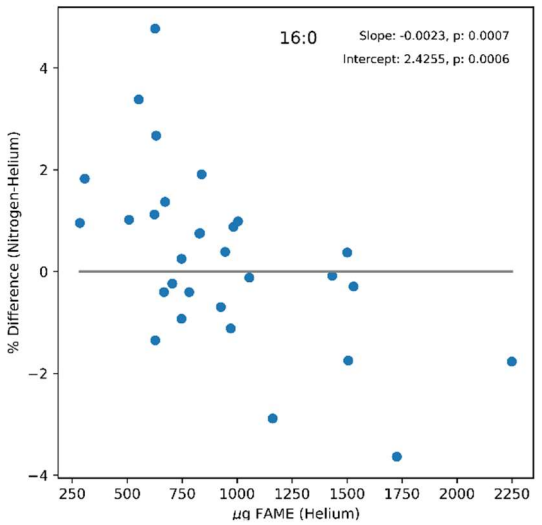
16:0
Slope: -0.0023, p: 0.0007
Intercept: 2.4255, p: 0.0006
% Difference (Nitrogen-Helium)
µg FAME (Helium)

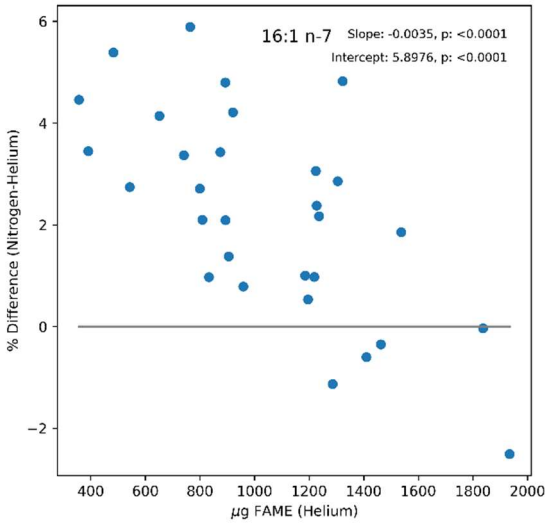
16:1 n-7
Slope: -0.0035, p: <0.0001
Intercept: 5.8976, p: <0.0001
% Difference (Nitrogen-Helium)
µg FAME (Helium)

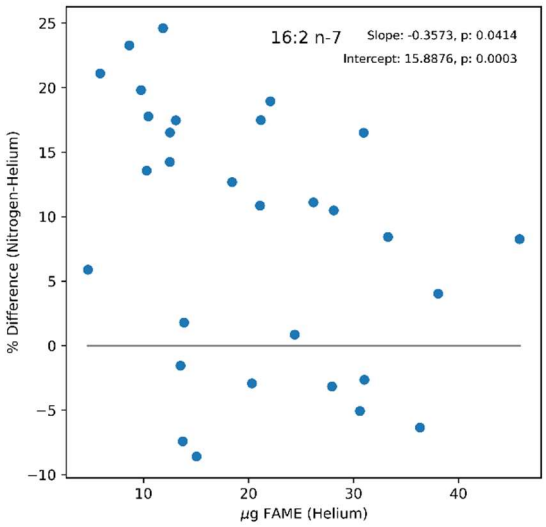
16:2 n-7
Slope: -0.3573, p: 0.0414
Intercept: 15.8876, p: 0.0003
% Difference (Nitrogen-Helium)
µg FAME (Helium)

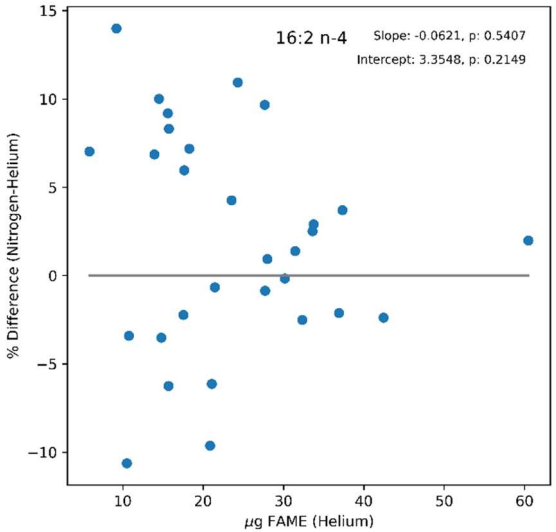
16:2 n-4
Slope: -0.0621, p: 0.5407
Intercept: 3.3548, p: 0.2149
% Difference (Nitrogen-Helium)
µg FAME (Helium)

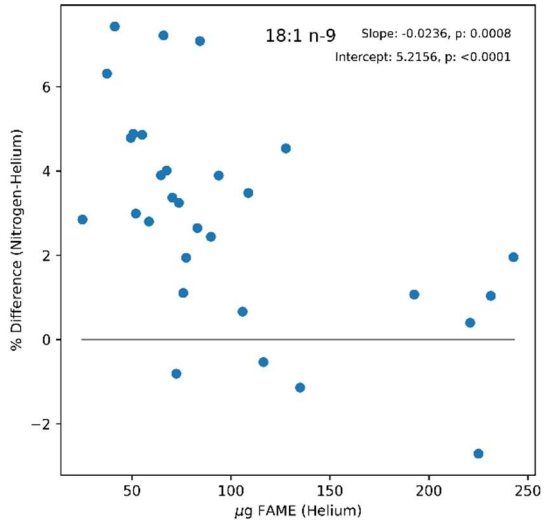

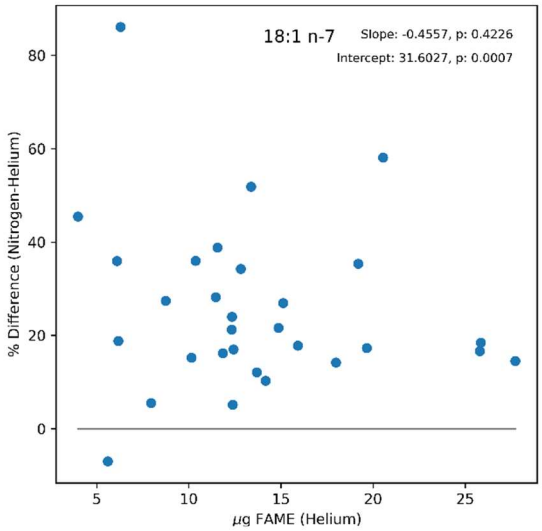

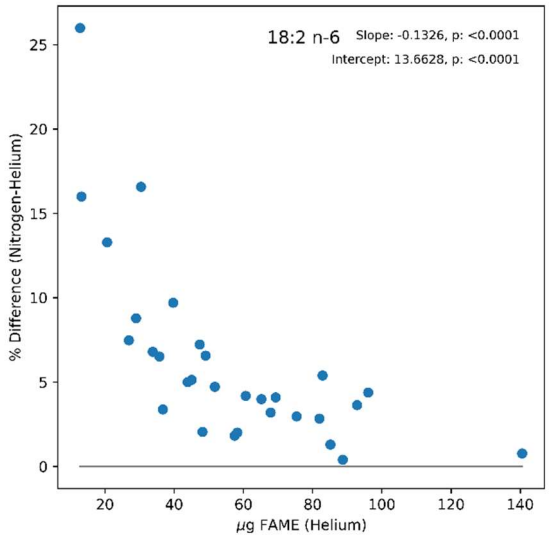

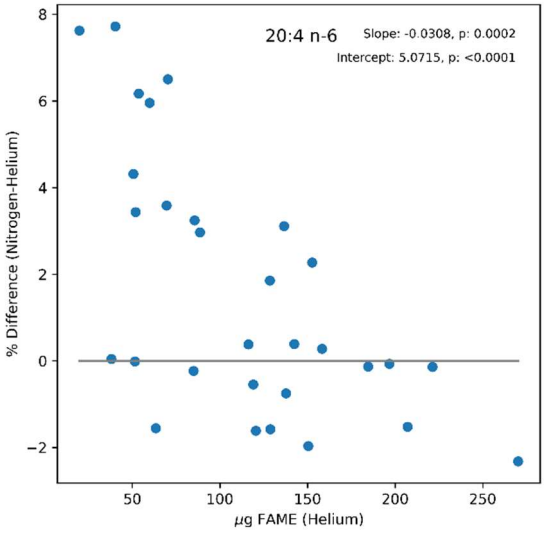

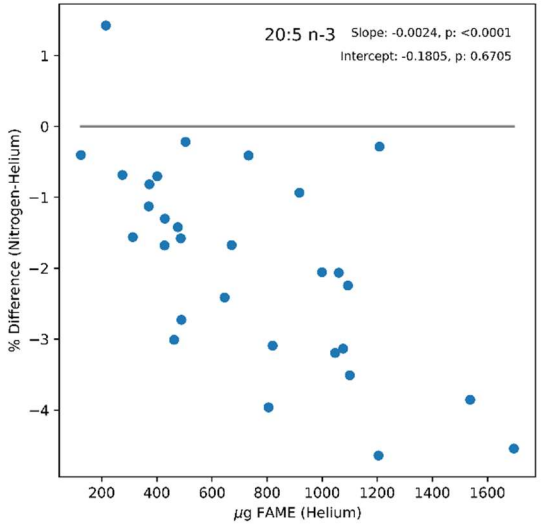

Figure C. 2: Scatterplot of absolute amounts of respective fatty acids of the helium method plotted against the percentage difference between the sum of absolute amounts for both methods.

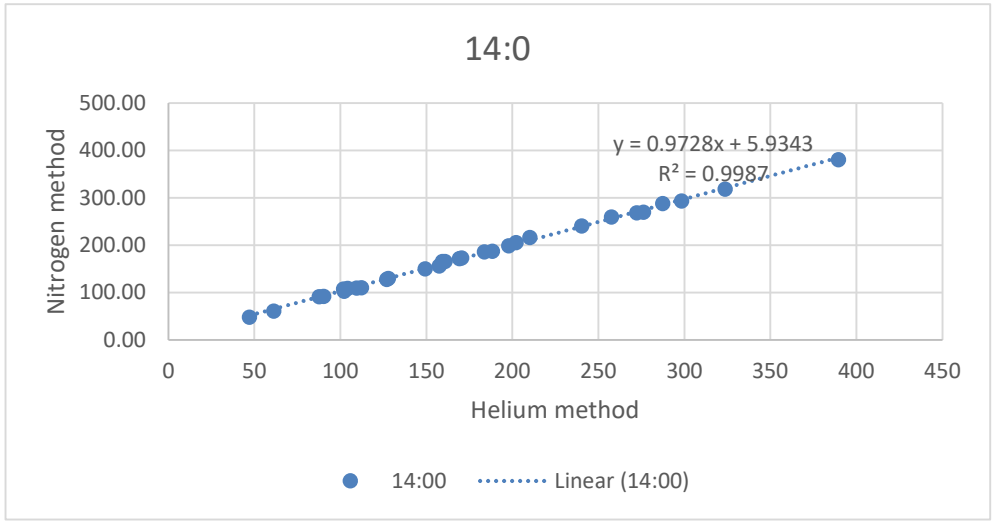
14:0
Nitrogen method
Helium method
y = 0.9728x + 5.9343
R² = 0.9987
14:00
Linear (14:00)

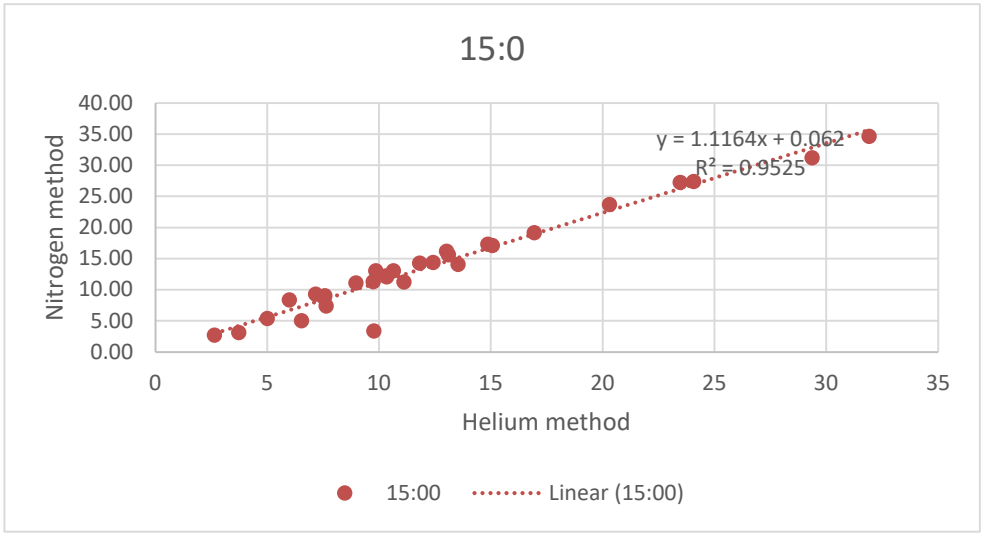
15:0
Nitrogen method
Helium method
y = 1.1164x + 0.062
R² = 0.9525
15:00
Linear (15:00)

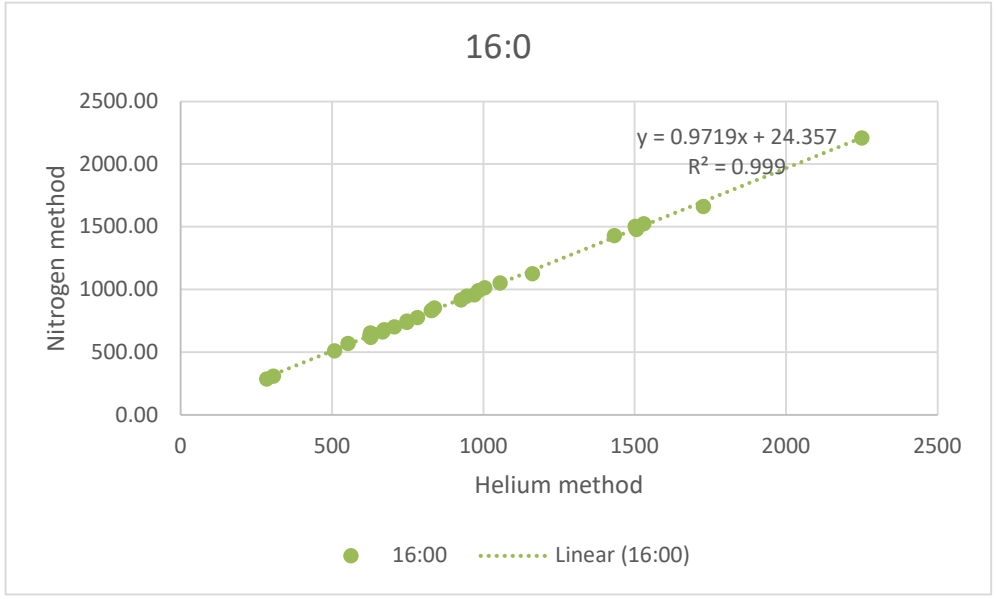
16:0
Nitrogen method
Helium method
y = 0.9719x + 24.357
R² = 0.999
16:00
Linear (16:00)

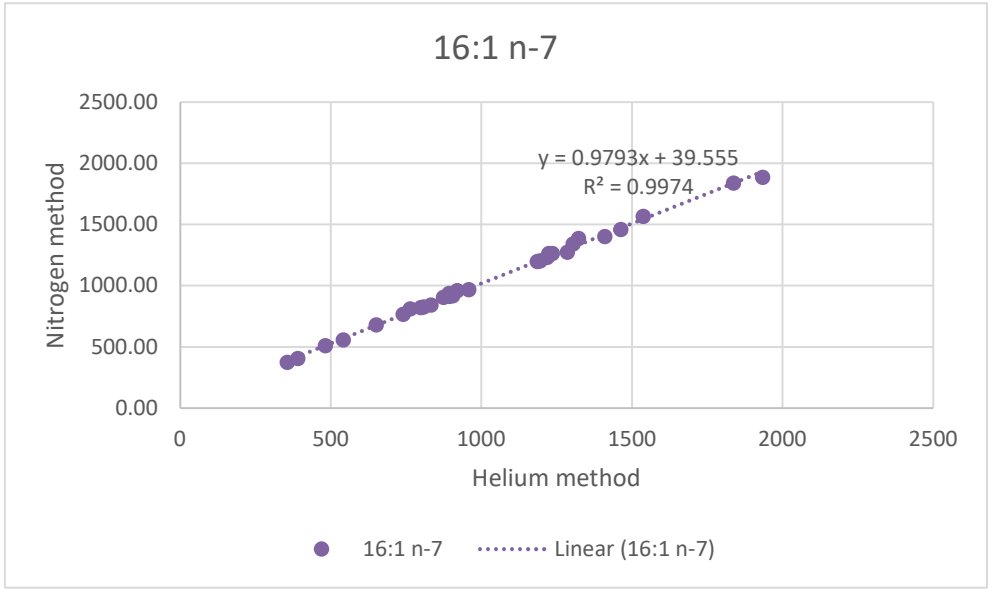
16:1 n-7
Nitrogen method
Helium method
y = 0.9793x + 39.555
R² = 0.9974
16:1 n-7
Linear (16:1 n-7)

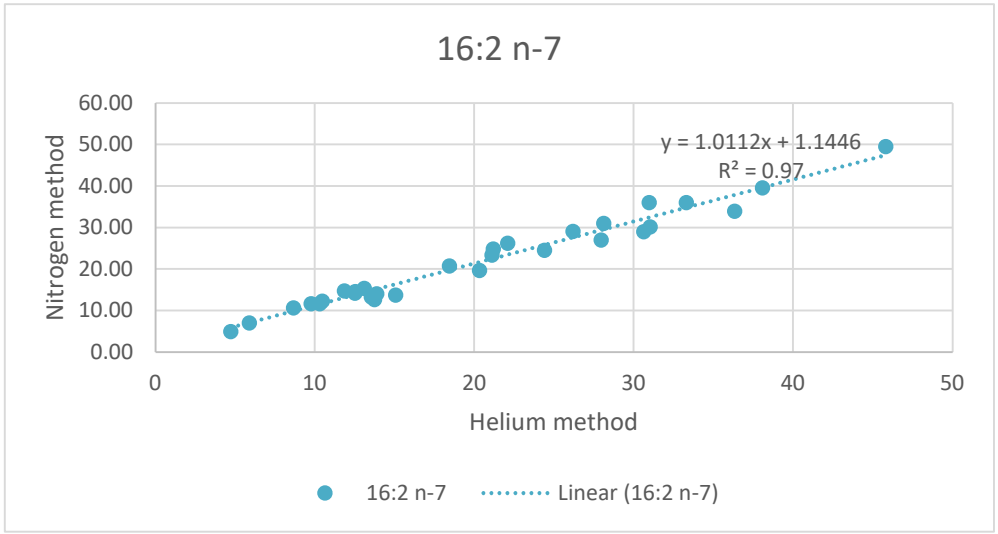
16:2 n-7
Nitrogen method
Helium method
y = 1.0112x + 1.1446
R² = 0.97
16:2 n-7
Linear (16:2 n-7)

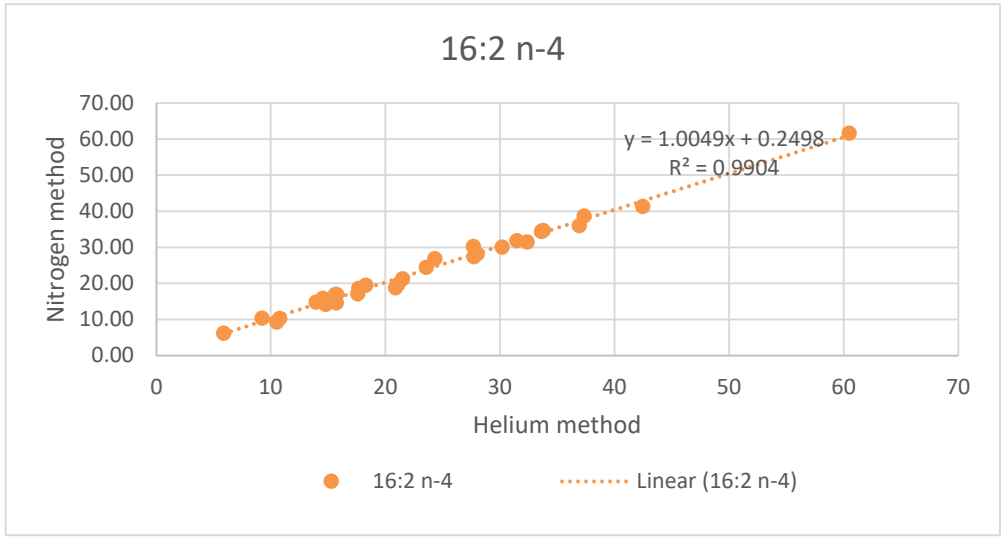
16:2 n-4
Nitrogen method
Helium method
y = 1.0049x + 0.2498
R² = 0.9904
16:2 n-4
Linear (16:2 n-4)

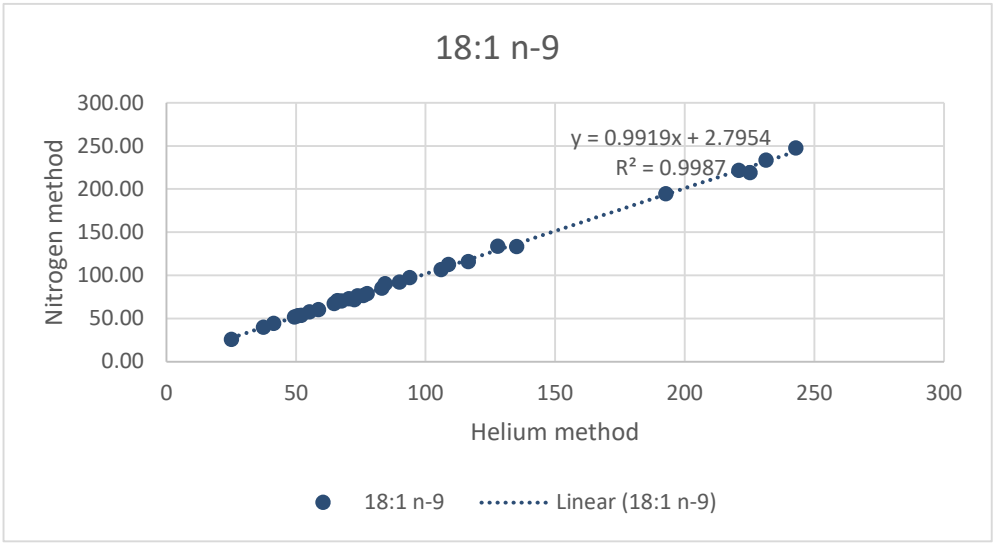
18:1 n-9
Nitrogen method
Helium method
y = 0.9919x + 2.7954
R² = 0.9987
18:1 n-9
Linear (18:1 n-9)

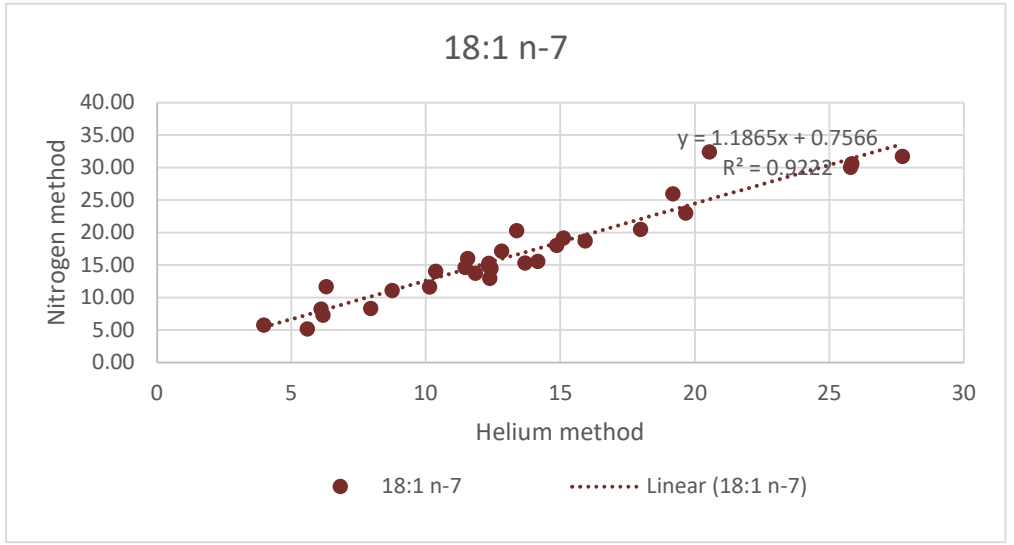
18:1 n-7
Nitrogen method
Helium method
y = 1.1865x + 0.7566
R² = 0.9222
18:1 n-7
Linear (18:1 n-7)

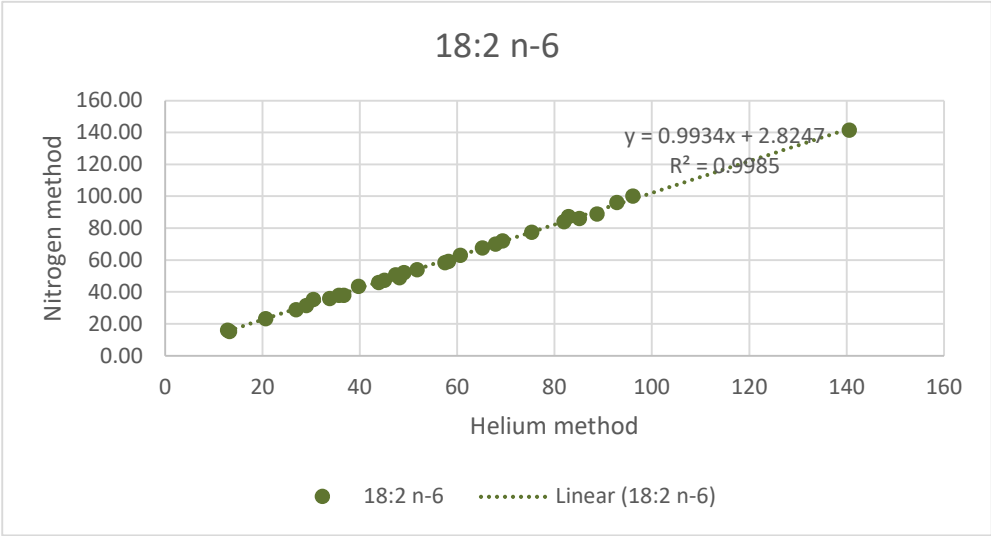

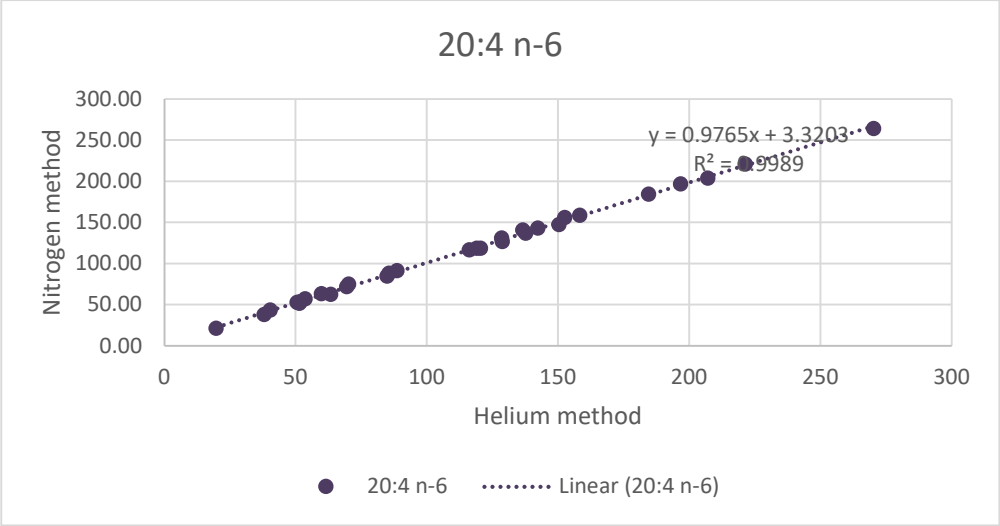

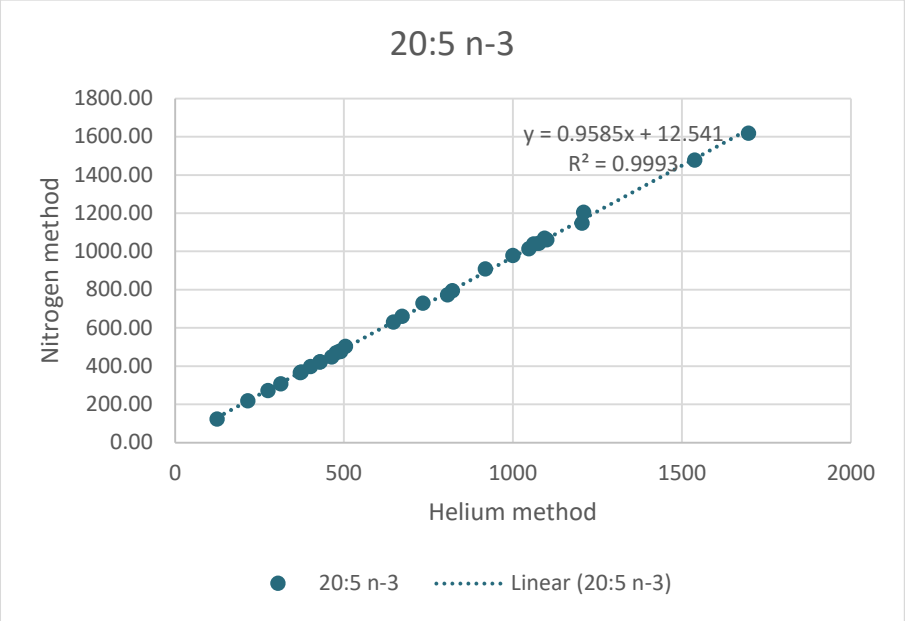

Figure C. 3: Absolute amounts of respective fatty acids for nitrogen and helium method plotted against each other.

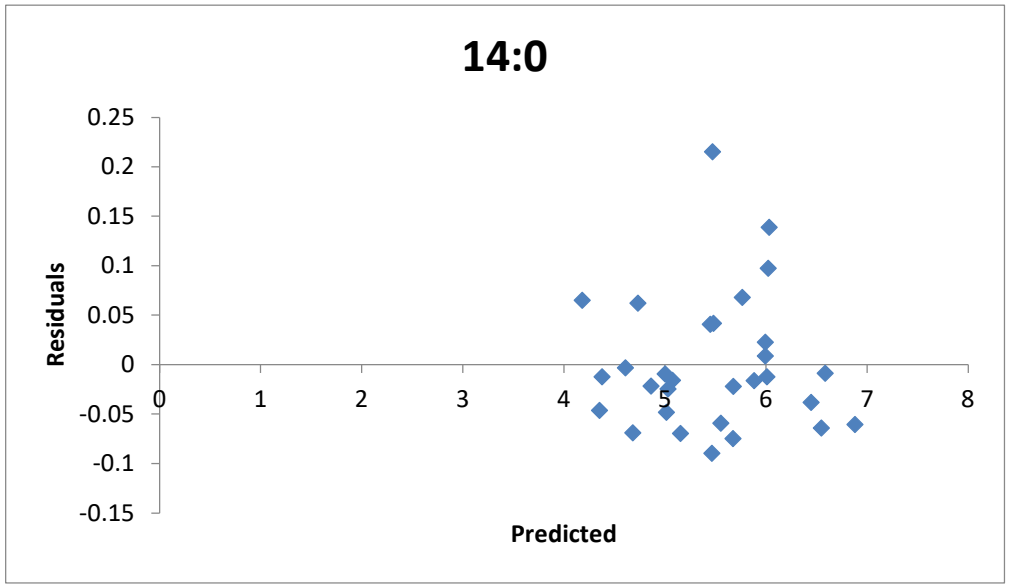
14:0
Residuals
Predicted
0.25
0.2
0.15
0.1
0.05
0
-0.05
-0.1
-0.15
0
1
2
3
4
5
6
7
8

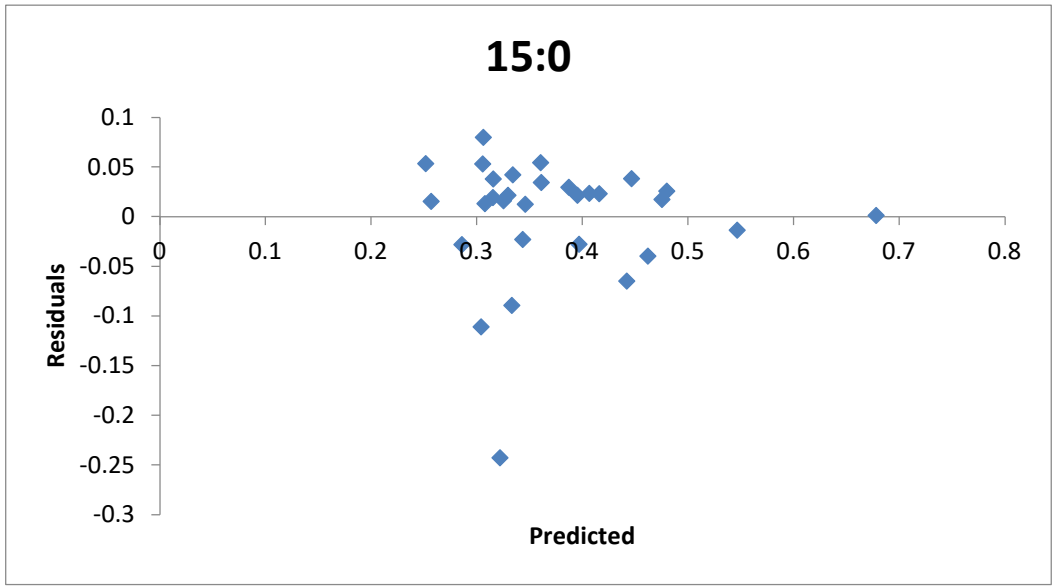
15:0
Residuals
Predicted
0.1
0.05
0
-0.05
-0.1
-0.15
-0.2
-0.25
-0.3
0
0.1
0.2
0.3
0.4
0.5
0.6
0.7
0.8

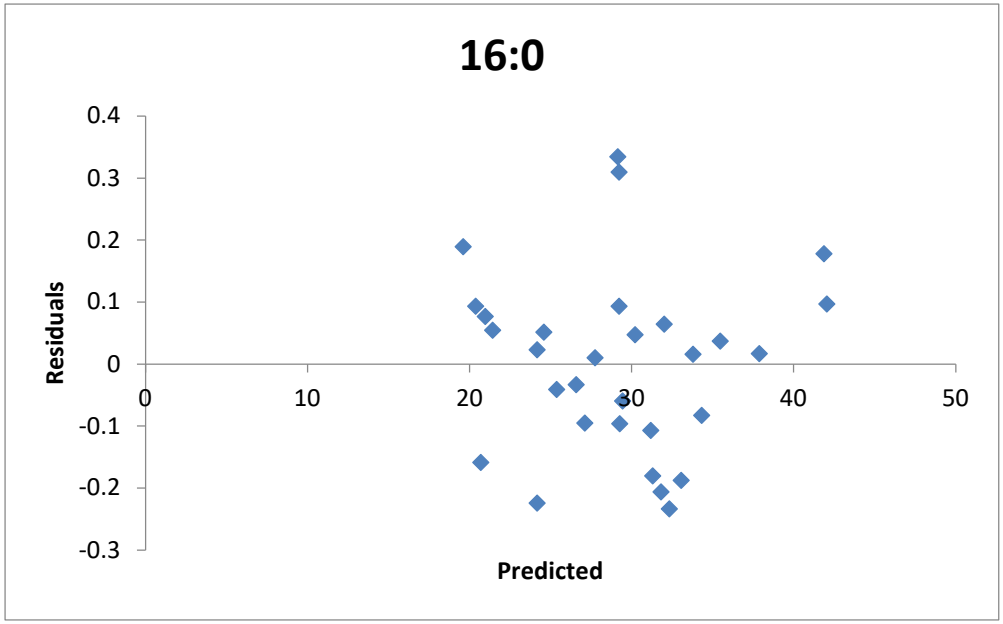
16:0
Residuals
Predicted
0.4
0.3
0.2
0.1
0
-0.1
-0.2
-0.3
0
10
20
30
40
50

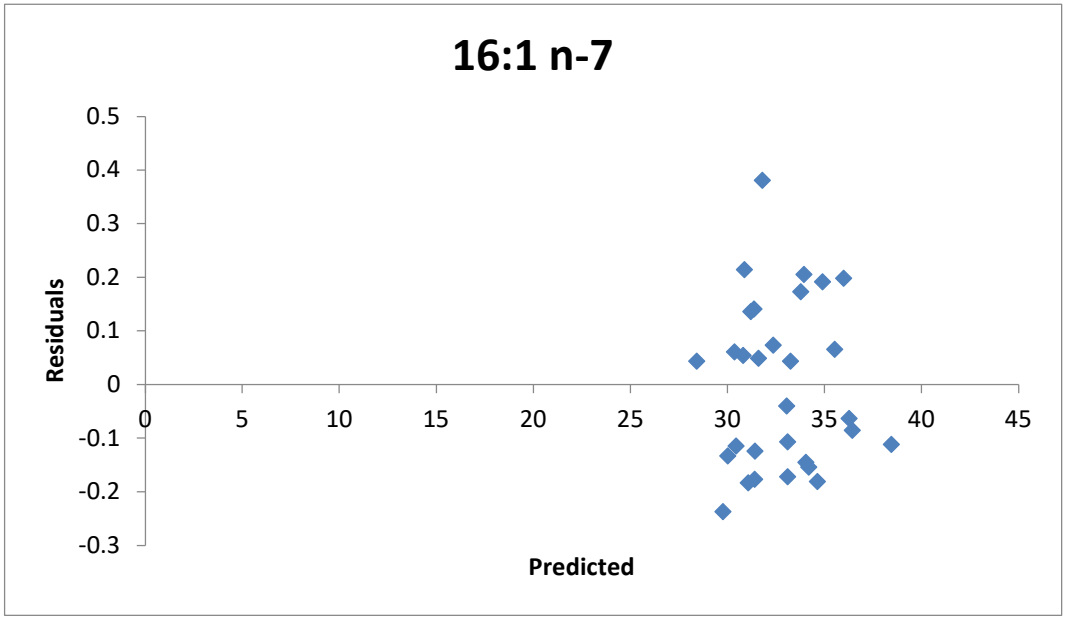
16:1 n-7
Residuals
Predicted
0.5
0.4
0.3
0.2
0.1
0
-0.1
-0.2
-0.3
0
5
10
15
20
25
30
35
40
45

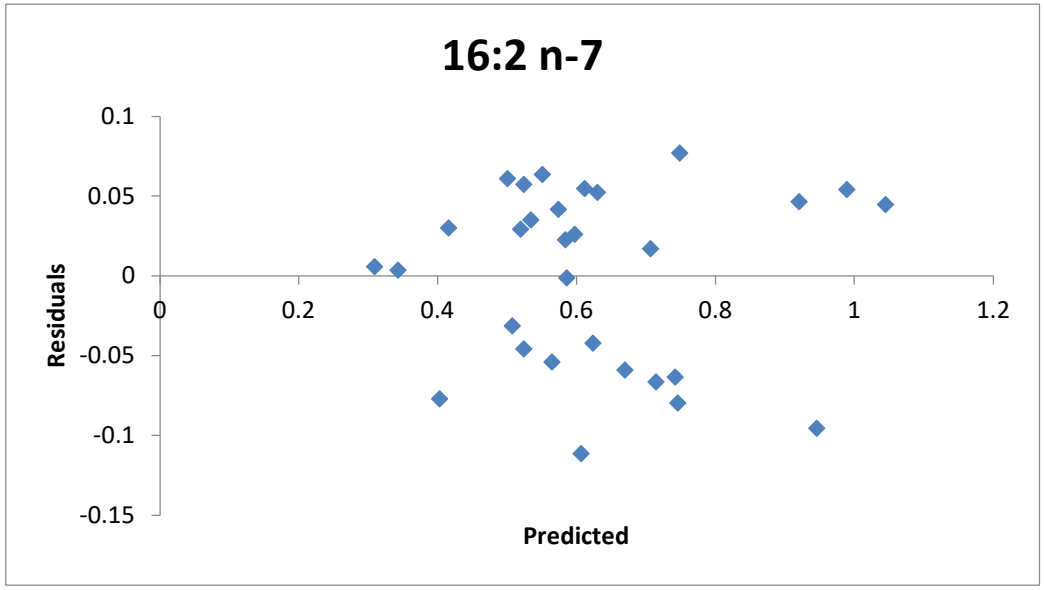
16:2 n-7
Residuals
Predicted
0.1
0.05
0
-0.05
-0.1
-0.15
0
0.2
0.4
0.6
0.8
1
1.2

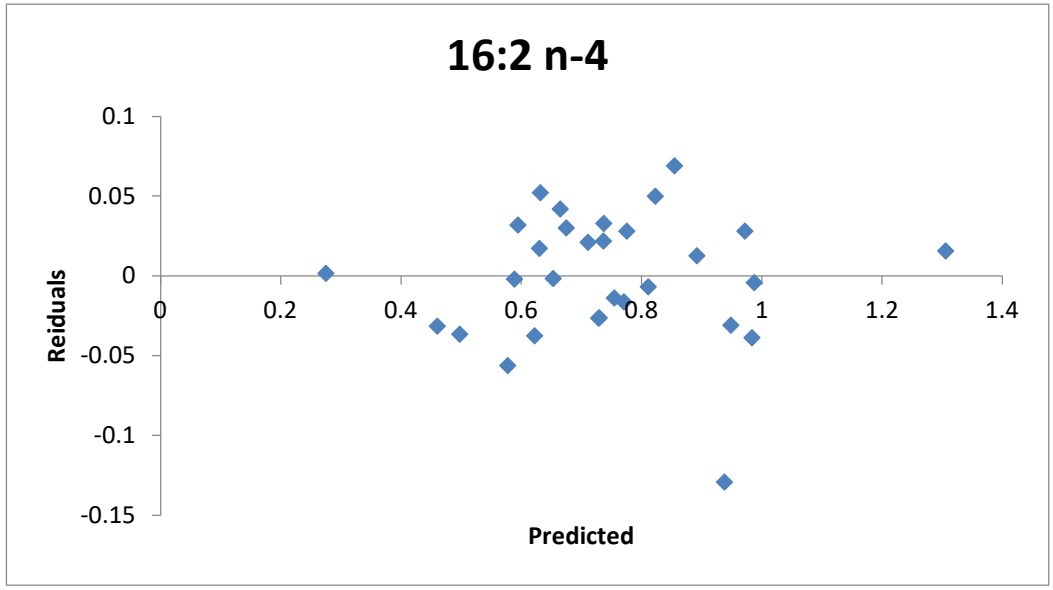
16:2 n-4
Reiduals
Predicted
0.1
0.05
0
-0.05
-0.1
-0.15
0
0.2
0.4
0.6
0.8
1
1.2
1.4

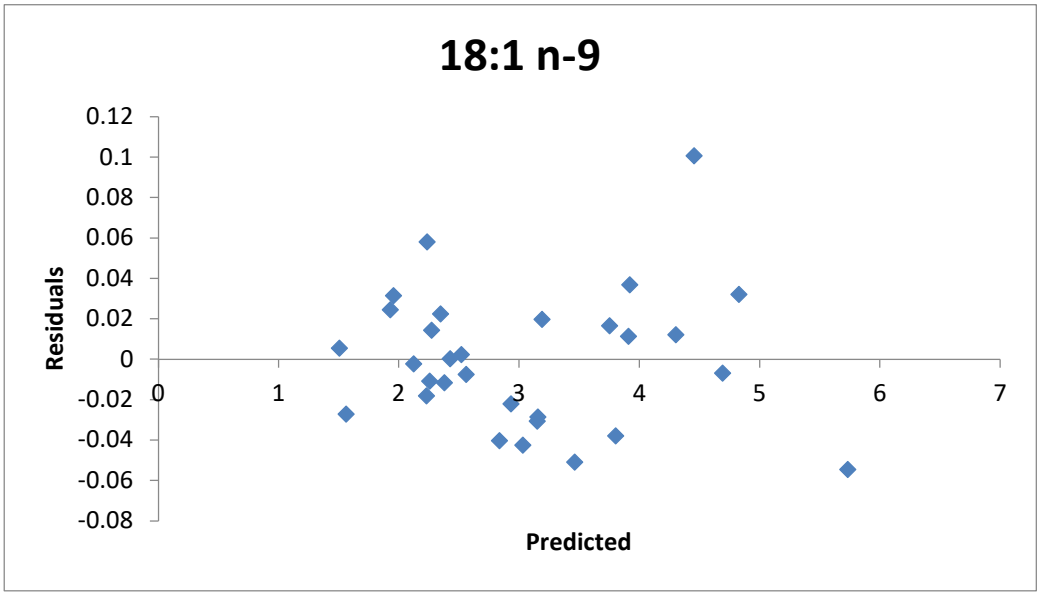
18:1 n-9
Residuals
Predicted
0.12
0.1
0.08
0.06
0.04
0.02
0
-0.02
-0.04
-0.06
-0.08
0
1
2
3
4
5
6
7

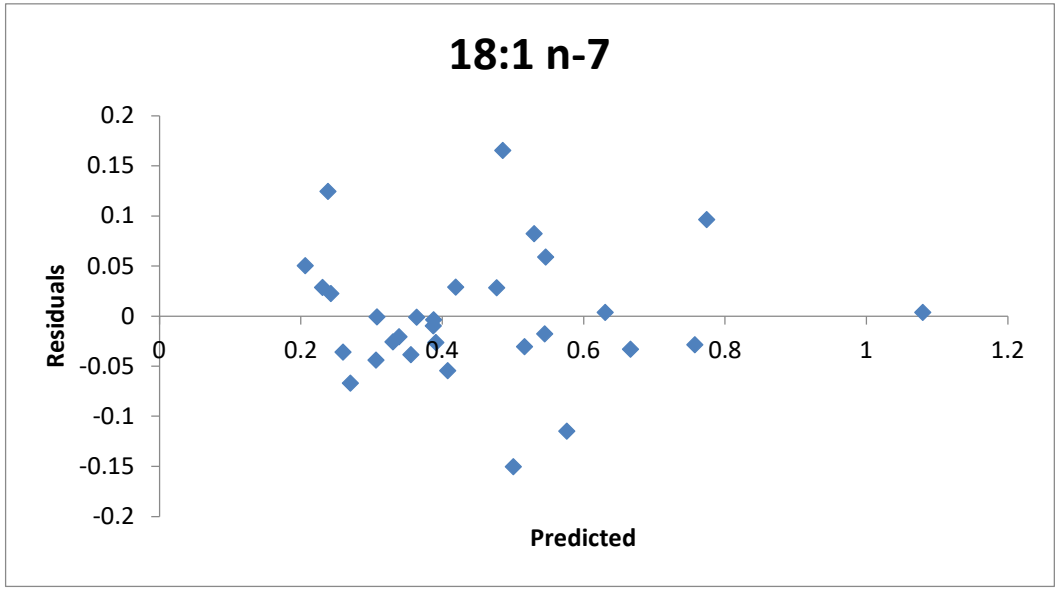
18:1 n-7
Residuals
Predicted
0.2
0.15
0.1
0.05
0
-0.05
-0.1
-0.15
-0.2
0
0.2
0.4
0.6
0.8
1
1.2

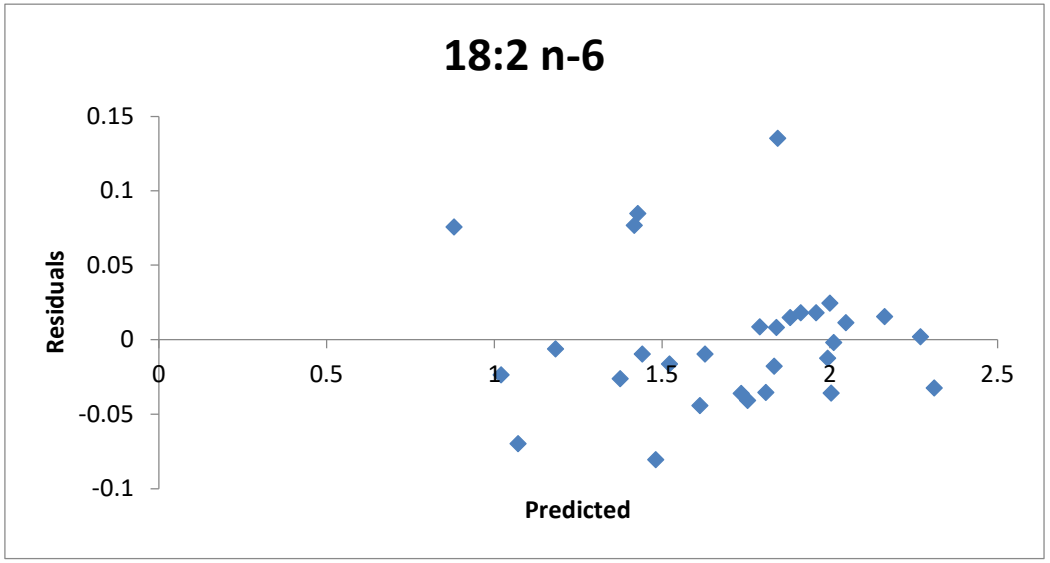

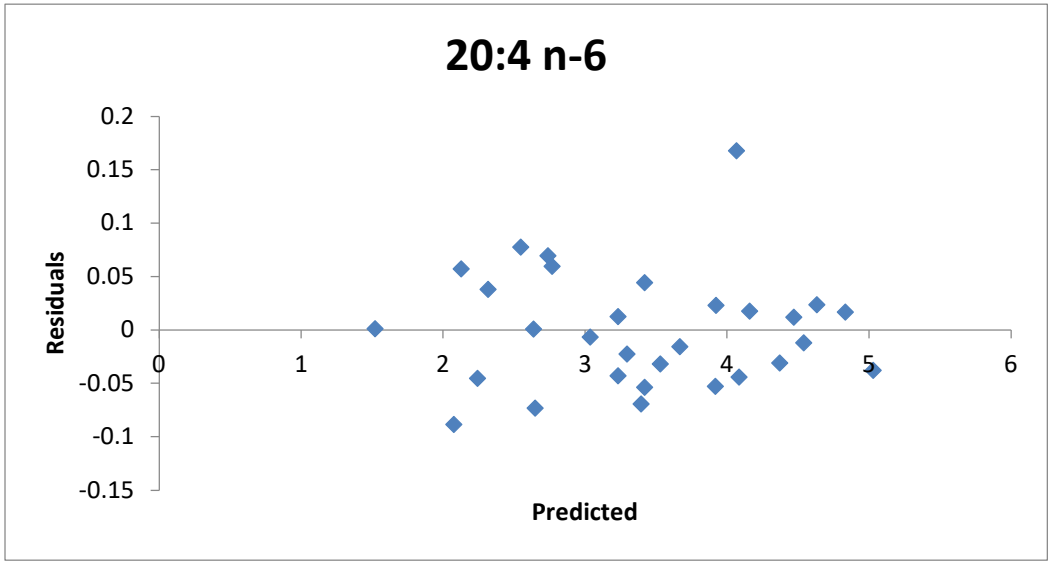

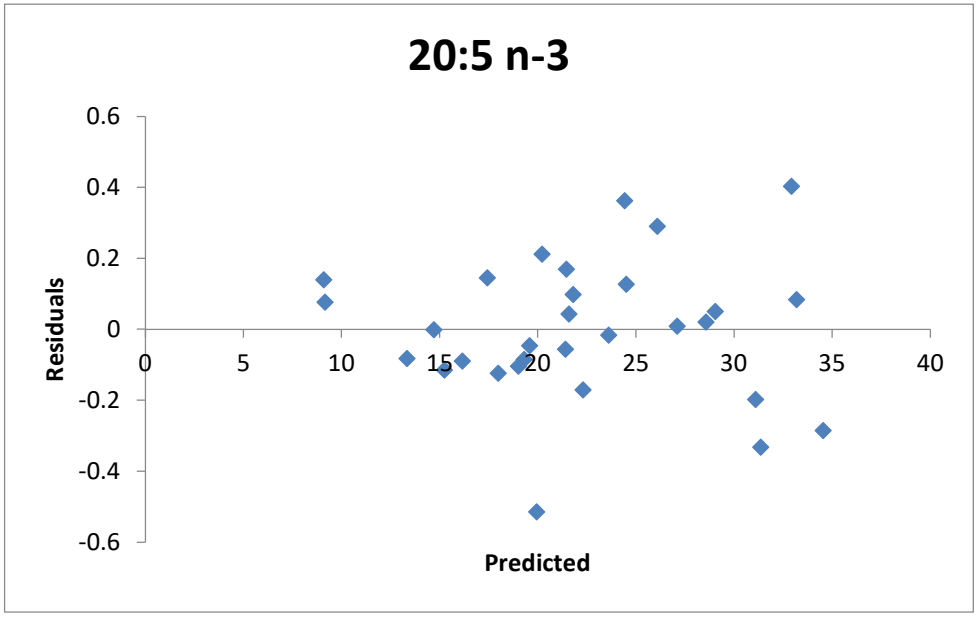

Figure C. 4: Residual plots of relative amounts of all fatty acids from the accuracy study.

Table C. 1: Detailed statistics of absolute amounts. Correlation coefficient (r), R^2 and equations for absolute amounts for each method plotted against each other.

FAME	r	R^2	Slope	Intercept
14:0	0.9993	0.9987	0.9728	5.9343
15:0	0.9760	0.9525	1.116	0.062
16:0	0.9995	0.9990	0.9719	24.357
16:1 n-7	0.9987	0.9974	0.9793	39.555
16:2 n-7	0.9849	0.9700	1.011	1.1446
16:2 n-4	0.9952	0.9904	1.005	0.2498
18:1 n-9	0.9993	0.9987	0.9919	2.7954
18:1 n-7	0.9603	0.9222	1.187	0.7566
18:2 n-6	0.9993	0.9985	0.9934	2.8247
20:4 n-6	0.9995	0.9989	0.9765	3.3203
20:5 n-3	0.9996	0.9993	0.9585	12.541

Table C. 2: Repeatability for second precision test. Repeatability [%] in vials. 10 vials were analysed with the N_2-method.

FAME	Average µg	STD µg	RSD_R%
14:0	136.6	3.861	2.827
15:0	5.087	0.2180	4.285
16:0	424.7	11.66	2.746
16:1 n-7	645.9	16.72	2.589
16:2 n-7	16.21	0.4747	2.928
16:2 n-4	15.04	1.118	7.434
18:1 n-9	38.90	0.8546	2.197
18:1 n-7	6.237	0.3777	6.056
18:2 n-6	38.56	0.7170	1.859
20:4 n-6	99.39	0.3798	0.3821
20:5 n-3	608.0	4.431	0.7288

Table C. 3: Significance test for variance between the methods of respective fatty acids with F-test. Repeatability, second precision test

FAME	F	p-value
14:0	54.34	1.802e-06*
15:0	7.997	4.835e-03
16:0	83.79	2.690e-07*
16:1 n-7	27.50	3.399e-05*
16:2 n-7	2.798	0.1414
16:2 n-4	3.513	0.07520
18:1 n-9	8.456	3.930e-03*
18:1 n-7	1.283	0.7165
18:2 n-6	5.820	0.01503
20:4 n-6	3.091	0.1081
20:5 n-3	1.746	0.4189

Table C. 4: Injection repeatability for second precision test. Injection repeatability [%] in vials. 10 vials were analysed with the N_2-method.

FAME	Average µg	SD µg	RSD_{IR}%
14:0	135.3	3.657	2.703
15:0	5.027	0.1104	2.196
16:0	421.1	10.93	2.596
16:1 n-7	640.8	15.59	2.433
16:2 n-7	16.13	0.4608	2.857
16:2 n-4	14.65	0.7816	5.335
18:1 n-9	38.51	0.9976	2.591
18:1 n-7	6.327	0.3476	5.494
18:2 n-6	38.37	0.7459	1.944
20:4 n-6	99.17	0.3053	0.3079
20:5 n-3	608.7	4.434	0.7284

Table C. 5: Significance test for variance between the methods of the respective fatty acids with F-test. Second precision test, injection repeatability.

FAME	F	p-value
14:0	14.73	4.530e-04*
15:0	14.53	4.780e-04*
16:0	21.86	8.930e-05*
16:1 n-7	19.77	1.36e-04*
16:2 n-7	1.043	0.9516
16:2 n-4	2.326	0.2245
18:1 n-9	12.46	8.85e-04*
18:1 n-7	3.094	0.1078
18:2 n-6	5.872	0.01458
20:4 n-6	4.463	0.03622
20:5 n-3	1.695	0.4439